



**UNIVERSIDADE FEDERAL DE PERNAMBUCO-UFPE
CENTRO DE TECNOLOGIA E GEOCIÊNCIAS-CTG
DEPARTAMENTO DE OCEANOGRAPHIA-DOCEAN
PROGRAMA DE PÓS-GRADUAÇÃO EM
OCEANOGRAPHIA**

**Seasonal variability of the heat and mass transport
along the western boundary of tropical Atlantic**

Marcus André Silva

**Recife/Brasil
2009**

Marcus André Silva

**Seasonal variability of the heat and mass transport
along the western boundary of tropical Atlantic**

Tese apresentada ao Programa de Pós-graduação em Oceanografia da Universidade Federal de Pernambuco como requisito parcial para obtenção do título de Doutor em Ciências, na área de Oceanografia Física.

Orientador: Dr. Moacyr Araújo

**Recife/Brasil
2009**

S586s

Silva, Marcus André

Seasonal variability of the heat and mass transport along the western boundary of tropical Atlantic / Marcus André Silva. - Recife: O Autor, 2009.

xv, 121f.; il., gráfs., tabs.

Tese (Doutorado) – Universidade Federal de Pernambuco. CTG. Programa de Pós-Graduação em Oceanografia, 2009.

Inclui Referências.

1. Oceanografia. 2. Atlântico tropical. 3. Correntes de borda oeste. 4. Bifurcação da CSE. I. Título.

551.46 CDD (22. ed.)

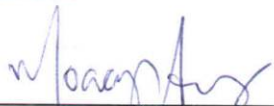
UFPE/BCTG/2009-256

Marcus André Silva

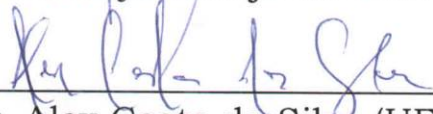
**Seasonal variability of the heat and mass transport
along the western boundary of tropical Atlantic**

Tese apresentada à seguinte banca examinadora em 11/05/2009.


Titulares:



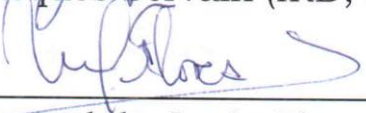
Dr. Moacyr Araújo de Cunha Filho (DOCEAN/UFPE)




Dr. Alex Costa da Silva (UFCE)



Dr. Jacques Servain (IRD, Brest)



Dr. Manuel de Jesús Flores Montes (DOCEAN/UFPE)



Dr. Carmen Medeiros Limongi (DOCEAN/UFPE)

Suplentes:

Dr. Héctor Raúl Montagne Dugrós (DF/UFRPE)

Dr. Sigrid Neumman-Leitão (DOCEAN/UFPE)

**Para minha filha
Mariana.**

Agradecimentos

Aos meus pais, à Renata e minha filhinha Mariana pelo companheirismo, amor e motivação que me dedicaram neste período.

Ao amigo e professor Dr. Moacyr Araújo pela sua orientação, dedicação e principalmente por acreditar sempre no meu trabalho.

Ao Dr. Jacques Servain pelo imenso suporte dado na interpretação dos resultados obtidos neste meu trabalho. Sem o qual este trabalho não seria o mesmo.

Ao Dr. Pierrick Penven pela presteza em colaborar com códigos computacionais bem como, com contribuições importantes na compreensão dos resultados numéricos obtidos.

A todos os professores do Departamento de Oceanografia da UFPE, que sempre me motivaram a seguir na carreira de pesquisador.

À CAPES pela concessão de Bolsa de Pesquisa, sem a qual este trabalho não teria sido possível.

Agradeço aos meus amigos do LOFEC, Dóris, Marcelo, Patrícia, Fabiana, Rodolfo, Isaac e Márcio, pela amizade e companheirismo.

Agradeço a Márcio e Dóris (LOFEC) pelo apoio em diferentes etapas deste trabalho e à Miriam Calland pelo empenho e dedicação na revisão gramatical deste documento.

Agradeço a Christina, Tiago, Pedro, Marcelo, Adilma e todos os amigos dos momentos de descontração, que tornaram esta jornada mais alegre.

A todos os funcionários do DOCEAN, pela presteza e amizade.

E a todos aqueles que, de uma forma ou outra, contribuíram para a realização deste trabalho.

Resumo

O Atlântico tropical compreendido entre 20°N e 20°S apresenta-se hoje como chave para o entendimento das mudanças climáticas na Terra. Duas regiões despertam particular interesse: A banda equatorial do Atlântico onde o sistema de correntes interage com forçantes térmicos superficiais e ressurgência de Ekman, como a área sudoeste do Atlântico tropical (05°S-25°S / 20°W-47°W), onde parte da Corrente Sul Equatorial (CSE) penetra pela borda leste e contribui com muitas das correntes de fronteira oeste ao longo da plataforma continental brasileira. Entretanto, a variabilidade da dinâmica nestas regiões, que se mostra importante por sua contribuição sobre o clima da região nordeste do Brasil, apresenta-se pouco estudada. O presente trabalho investigou estes importantes sistemas do Atlântico tropical utilizando o ROMS (Regional Ocean Model System). A primeira área de estudo compreendida entre 20°S-20°N e 42°W-15°E, com resolução horizontal de 1/6° e 30 camadas sigma (que acompanham o terreno). Variações sazonais do transporte zonal, estrutura das correntes e distribuição da TSM (Março e Agosto) obtidos numericamente foram avaliados e comparados com dados: de literatura, experimentais do PIRATA e observados por satélite. Os resultados desta simulação mostram que o modelo é capaz de reproduzir os principais aspectos da Subcorrente Equatorial (SE), Contra-corrente Norte Equatorial (CNE), Corrente do Golfo (CG) e os ramos central e norte dos sistemas de Corrente Sul Equatorial (cCSE/nCSE), em diferentes seções ao longo do equador. A comparação entre a estrutura térmica nos primeiros 500 m simulada e do Programa PIRATA mostra uma Camada de Mistura (MLD) bem reproduzida, particularmente, a ressurgência que induz uma MLD mais rasa verificada nas boias mais à leste durante o inverno austral até o final da primavera austral. A evolução sazonal do sistema Piscina Quente do Atlântico Sul (SAWP) – Língua Fria (Cold Tongue) foi bem representado, que é importante para futuras previsões de variabilidade climática sobre as fronteiras continentais da parte sudoeste do Atlântico tropical. Do lado sudoeste do Atlântico tropical (05°S-25°S / 20°W-47°W), O ROMS (Regional Ocean Model System) foi utilizado pela primeira vez nesta área para simular a circulação oceânica utilizando uma malha de resolução horizontal de 1/12° com 40 camadas sigma, que acompanham o terreno, para resolução vertical. Para avaliação preliminar da configuração do ROMS adotada foram analisadas as distribuições superficiais e verticais de temperatura, além de calculadas as evoluções sazonais da camada bem misturada e dos balanços, atmosféricos e oceânicos, envolvendo a troca de calor dentro da camada bem misturada. A ordem de grandeza das componentes oceânicas (principalmente a difusão vertical e a advecção horizontal) é da mesma ordem de grandeza dos forçantes atmosféricos e quase sempre opostos entre si, com alguma diferença de fase e transporte dentro das camadas mais superficiais. Resultados de variabilidade interanual foram comparados com os primeiros dois anos de perfis de temperatura observados advindos dos três fundeios do programa PIRATA-SWE (Projeto PIRATA, Extensão Sudoeste). A estrutura térmica simulada nas camadas mais superficiais do oceano está em concordância com os resultados obtidos *in situ*. Resultados de simulação

apontam para uma larga e relativamente fraca CSE, composta por uma sequência de núcleos não bem definidos e próximos a superfície. O transporte que flui para oeste da CSE nos primeiros 400 m de profundidade ao longo da seção que atravessa as boias PIRATA-SWE, calculado para simulação do ROMS entre 2005-2007, apresenta um volume médio transportado de 14,9 Sv, com um máximo observado em JFM (15,7 Sv) e um mínimo durante MJJ (13.8 Sv). Os resultados de simulação indicam que em 2005-2007 o transporte para oeste da CSE foi modulado pela variabilidade da componente zonal do vento. Três seções zonais, posicionadas do continente até a posição da boia PIRATA, confirmam transporte mais intenso da Sub-corrente do Norte do Brasil (SNB), fluindo para norte, e uma diminuição no transporte da Corrente do Brasil (CB), que flui para sul, durante maio de 2006 e maio de 2007, quando a bifurcação do ramo sul da CSE alcança sua posição mais ao sul. Por outro lado, o máximo escoamento da CB foi registrado durante janeiro de 2006, janeiro de 2007 e março de 2007, com um mínimo da SNB fluindo para norte em dezembro de 2005 e outubro/dezembro 2006, correspondendo ao período em que a bifurcação do ramo sul da CSE alcança sua posição mais ao norte (OND). A Elevação da Superfície do Mar (ESM) e a Energia Cinética turbulenta (ECT) superficial calculada a partir das simulações e dos produtos AVISO Rio05 apontam na superfície para os mais altos níveis de energia de meso-escala ao longo do ramo central da CSE e da SNB/CB. Resultados de modelagem ecológica usando o modelo NPZD acoplado com o ROMS confirmam esta região como uma área oligotrófica. Resultados do modelo ecológico são comparados com SeaWifs dataset e a dinâmica e a produção primária são localmente discutidos. Estes resultados preliminares disponibilizam mais informações diante da complexidade da região de divergência da SCE e encoraja-nos a conduzir estudos mais detalhados a respeito da dinâmica e do transporte de massa nessa região utilizando o ROMS. Este trabalho também apresenta a necessidade de continuação, ampliação e extensão vertical para o sistema de observação PIRATA-SWE, especialmente com medidas de salinidade em mais níveis de profundidade, além da instalação de medidores de correntes.

Palavras-chave: Atlântico tropical, modelagem matemática, conteúdo térmico, bifurcação da CSE, correntes de borda oeste.

Abstract

The Tropical Atlantic comprised between 20°N and 20°S presents today an important key to the knowledge of climatic changes in the world. Two areas are of particular interest: the zonal band of the Equatorial Atlantic ocean where the current system interacts with surface thermal forcing and Ekman upwelling, and the Southwestern tropical Atlantic (05°S-25°S / 20°W-47°W), where part of the South Equatorial Current (SEC) enters at its eastern border, feeding many western boundary currents along the Brazilian continental shelf. However, the long-term variability of the dynamics in these regions, which is also important for their contribution to the climate over northeastern Brazil, is largely unknown. This present work investigated these important systems of the South tropical Atlantic using the Regional Ocean Model System (ROMS). The first study area was comprised between 20°S-20°N and 42°W-15°E, with an horizontal grid resolution of 1/6° and 30 vertical sigma (terrain-following) layers. Seasonal variations of zonal transport, current structure and SST distribution (March and August) obtained numerically were evaluated and compared with: literature, PIRATA array and satellite data. Results show that the model is capable of reproducing the mean features of the EUC/NECC/GC and cSEC/nSEC systems, at different sections along the equator. The comparison between the simulated thermal structure, upper 500 m ocean layer, and PIRATA Program dataset shows a very well reproduced Mixing Layer Depth (MLD). In particular, the upwelling induced shallower MLD verified in eastern buoys during austral winter to late spring. The seasonal evolution of the Southwestern Atlantic Warm Pool (SAWP) – Cold Tongue equatorial system was quite represented, which is important for future forecasting of climate variability along the continental boundaries in Southwestern tropical Atlantic. The second part of this work has the first use of ROMS to simulate the ocean circulation in the Southwestern tropical Atlantic. This modelling used a isotropic horizontal grid resolution of 1/12° and 40 sigma layers. For preliminary evaluation of this ROMS configuration, surface and vertical thermal structures were explored. Indeed, seasonal evolutions of the surface mixed layer, atmospheric and oceanic balances involving the mixed layer heat budget were calculated. The magnitude of oceanic components (mainly the vertical diffusion and the horizontal advection) is in the same order as the atmospheric forcing, and practically always opposes to it, with some local and seasonal timing differences and mass transports within the upper levels. Interannual variability results were compared with the first two-year series of observed thermal profiles derived from the three PIRATA-SWE moorings. The simulated thermal structure in the upper ocean layers agrees well with *in-situ* data. ROMS simulations point out a broad and relatively weak SEC flow composed of a sequence of more or less defined near-surface cores. The westward SEC transport for the upper 400 m along the PIRATA-SWE section, calculated from the ROMS simulation for 2005-2007, shows an average volume transport of 14.9 Sv, with a maximum observed in JFM (15.7 Sv), and a minimum during MJJ (13.8 Sv). ROMS results indicate that the 2005-2007 seasonal near-surface westward SEC transport is modulated by the zonal wind variability. Three zonal sections extending from the American

continent to the PIRATA buoy sites confirm that stronger northward NBUC transport and decreasing BC transport were achieved during May 2006 and May 2007, *i.e.* at the time the sSEC bifurcation reached its southernmost position. On the other hand, the maximum southward BC flow was verified during January 2006, January 2007 and March 2007, with a minimum northward NBUC flow in December 2005 and October/December 2006, corresponding to the period when the sSEC bifurcation reached its lowest latitude (OND). Sea Surface Height (SSH) and the surface Eddy Kinetic Energy (EKE) derived from simulations and AVISO Rio05 product point out the highest surface meso-scale activity ($\text{EKE} \geq 50 \text{ cm}^2 \text{ s}^{-2}$) along the cSEC and NBUC/BC patches. Results of an ecological modelling using NPZD model coupled with the ROMS confirm this region as an oligotrophic area. NPZD outputs were compared with SeaWifs dataset and dynamic and primary production are locally discussed. Preliminary results provide additional ingredients in the complexity of the SEC divergence region, and encourages us to conduct a more detailed exploration of the dynamics and mass transport of this region using the ROMS. This also shows the need to continue, extend, and vertically upgrade the observational PIRATA-SWE array system, especially with more levels of salinity measurements and the installation of current measurements.

Keywords: Tropical Atlantic, mathematical modeling, SEC bifurcation, heat content, western boundary current.

Figure List

Figure 1.1. Chart of study area with domain limited by 10°N-40°S and 20°E-60°W with a schematic representation of mean zonal and meridional currents: The upper ocean northward NBUC flow (red solid line), and the deepest southward transport by the DWBC (blue dashed line). The sSEC bifurcation at 100m depth (solid line); between 200m and 500m depth (dashed line); between 500m and 1200m depth (pointed line), according with Stramma and England (1999).	18
Figure 3.1. Region of model integrations, solid lines indicate domain of 1/6° climatological equatorial modelling. Dashed lines indicate southwestern tropical Atlantic domain limits of 1/12° horizontal grid.	31
Figure 4.1. Study area and model integration domain. The sections A, B and C are dashed lines and the squares over the equator line are the PIRATA mooring sites. Bathymetry is represented by gray shading contour.	35
Figure 4.3. Zonal transport (u-component) obtained from model simulation (ROMS) along Section A, 25°W. Dashed lines represent the isotherm 20°C. Monthly-averaged values for March and August.	38
Figure 4.4. Seasonal variability of EUC, NECC, SECc and SECn transports at 25W° section, obtained in simulations.	38
Figure 4.5. Zonal transport (u-component) obtained from model simulation (ROMS) along Section B, 15°W. Dashed lines represent the isotherm 20°C. Monthly-averaged values for March and August.	40
Figure 4.6. Seasonal variability of EUC, NECC, SECc and SECn transports at 15W° section, obtained in simulations.	41
Figure 4.7. Zonal transport (u-component) obtained from model simulation (ROMS) along Section C, 5°W. Dashed lines represent the isotherm 20°C. Monthly-averaged values for March and August.	42
Figure 4.8. Seasonal variability of EUC, NECC, SECc and SECn transports at 5W° section, obtained in simulations.	43
Figure 4.9. Comparison of the vertical temperature distribution provided by ROMS (black dashed contours) with the three PIRATA buoys (colour shading) extending from surface down to 500 m. Monthly-averaged distributions for the PIRATA period 1997-2007.	44
Figure 4.10. Monthly-averaged SST obtained from ROMS model (above) and from satellite observations (AVHRR-NOAA) (below) for March and August. .	45
Figure 5.1. Model domain (dashed lines) with the PIRATA-SWE locations (filled triangles) and three sites located along the western boundary region closer to the Brazilian edge (filled circles). Near shore 100m and 1000m isobaths are plotted.	48
Figure 5.2. Horizontal distribution of SST obtained from ROMS in mid-September (a) and mid March (b). PIRATA-SWE locations (filled triangles) and three sites located along the western boundary region closer to the Brazilian edge (filled circles).	50
Figure 5.3. Horizontal distribution of SST obtained from observed satellite data on 15 September 2005 (a) and 15 March 2006 (b). PIRATA-SWE locations (filled triangles) and three sites located along the western boundary region closer to the Brazilian edge (filled circles).	51
Figure 5.4. Comparison of the monthly mean vertical temperature	

distribution ($^{\circ}\text{C}$) provided by ROMS (black dashed contours) with monthly mean for the period of September 2005 to February 2008 of the three PIRATA-SWE buoys (colour shading and white lines) extending from surface down to 500m. The four vertical black thin lines correspond to September 15th, December 15th, March 15th and June 15th,. (a) 8°S - 30°W ; (b) 14°S - 32°W ; (c) 19°S - 34°W53

Figure 5.5. September (a), December (b), March (c) and June (d) monthly averaged vertical profiles of temperature 0-500m at the three PIRATA-SWE sites provided by climatic ROMS and by PIRATA monthly averaged profiles from September 2005 to February 2008.....55

Figure 5.6. Comparison of temporal evolution of seasonal heat content in the mixed layer at 8°S - 30°W (a), 14°S - 32°W (b) and 19°S - 34°W (c), provided by PIRATA in-situ observations (dashed line) and ROMS (solid line) for the period of September to August.57

Figure 5.7. Seasonal evolution of SST ($^{\circ}\text{C}$) (black dashed line), atmospheric (red line) and oceanic (blue line) contributions to the local change of SST ($^{\circ}\text{C}/\text{Month}$) (black continuous line) provided by ROMS at 8°S - 34°W (a), 8°S - 30°W (b), 14°S - 38°W (c), 14°S - 32°W (d), 19°S - 38°W (e) and 19°S - 34°W (f) locations.....61

Figure 5.8. Mean annual volume transport averaged across three zonal sections at 8°S (a), 14°S (b) and 19°S (c), and across the section along the PIRATA-SWE array (d). Positive (negative) values indicated by solid (dashed) white lines correspond to northward (southward) currents (panels 8a, 8b, and 8c), while positive (negative) values indicated by solid (dashed) white lines for the section along the PIRATA array correspond to eastward (westward) currents (panel 8d). The three horizontal solid black lines indicate the 24.5, 26.8 and 32.15 sigma-t values (in kg.m^{-3}).63

Figure 6.1. Comparison between ROMS-derived SST (a and c) and GHRSSST-PP-derived SST (b and d) for September 15th 2005 and March 15th 2006....67

Figure 6.2. Comparison between simulated and observed temperature ($^{\circ}\text{C}$) variations for the upper 500m from September 2005 to June 2007 for the three PIRATA-SWE locations at (a) 08°S - 30°W , (b) 14°S - 32°W and (c) 19°S - 34°W . Model-derived temperature is represented by black contours and the PIRATA-SWE observed temperature appears as white contours and shaded colors.71

Figure 6.3. Comparison of monthly averaged vertical profiles of temperature for the first 500m between the PIRATA-SWE in-situ observations (dashed line) and the ROMS simulation (solid line) for: (a) September 2005, (b) December 2005, (c) March 2006 and (d) June 2006. Colours are associated to each PIRATA-SWE buoy: 08°S - 30°W (blue), 14°S - 32°W (black) and 19°S - 34°W (red).73

Figure 6.4. Comparison of temporal evolution of seasonal mixed layer depth (MLD) at: (a) 8°S - 30°W , (b) 14°S - 32°W and (c) 19°S - 34°W , provided by PIRATA-SWE in-situ observations (dashed line) with ROMS (solid line) for the period of September 2005 to June 2007.....75

Figure 6.5. Averaged (2005-2007) SSH and EKE comparisons between ROMS simulations and AVISO Rio05 data: (a) ROMS - SSH (cm), (b) ROMS - EKE ($\text{cm}^2 \text{s}^{-2}$), (c) RIO05+AVISO - SSH (cm) and (d) AVISO - EKE ($\text{cm}^2 \text{s}^{-2}$)..77

Figure 6.6. Transport function (Sv) for the modelled seasonal averaged

(three months, 2005-2007) currents integrated from 600 m to the sea surface for a) MJJ and b) OND. The 1000 m isobath is represented by a red line.....	78
Figure 6.7. Model simulation of meridional current and transport values averaged from September 2005 to July 2007 along zonal sections (0-1500 m) at: (a) 8°S, (b) 14°S and (c) 19°S. Positive (negative) values indicated by solid (dashed) lines correspond to northward (southward) currents.	80
Figure. 6.8. Annual averaged (2005-2007) meridional current (cm s-1) and transport (in Sv) obtained by ROMS for: (a) the along zonal section (0-1500 m) at 7°S. Positive (negative) values indicated by solid (dashed) lines correspond to northward (southward) currents, (b) the depth averaged range 200-1000 m, where CFLOW is stronger.....	83
Figure. 6.9. Interannual variability of the North Brazil Undercurrent (NBUC) transport along 8oS (from the surface to 400 m), and Brazil Current (BC) transport along 19oS (from the surface to 400 m), obtained from ROMS simulations for the period of September 2005 to July 2007. Positive (negative) values indicated by the black (gray) line correspond to northward (southward) transports.	85
Figure. 6.10. Seasonal averaged (three months, 2005-2007) meridional velocity (m s-1) obtained from the ROMS simulation for a) MJJ and b) OND. The velocities are averaged within a 1° longitude band off of the Brazilian coast. The white line is the contour of zero velocity that represents the bifurcation of the sSEC. The white areas represent the Vitoria-Trindade Ridge and Abrolhos Bank.	87
Figure 7.1. Model domain (dashed gray lines) with the PIRATA-SWE locations (filled triangles). Section along three PIRATA-SWE sites (solid lines). Thin dashed lines are 100m and 1000m isobaths, respectively.	94
Figure 7.2. Chlorophyll a distribution on surface to SeaWifs on: a) November b) July and ROMS results on: c) November d) July.....	95
Figure 7.3. Vertical salinity distribution of ROMS along PIRATA-SWE sites on: a) November b) July.	97
Figure 7.4. Vertical nitrate distribution of ROMS along PIRATA-SWE sites on: a) November b) July.	99

List of Abbreviations

AABW	Atlantic Antarctic Bottom Water
AAIW	Atlantic Antarctic Intermediate Water
AC	Agulhas Current
ACC	Antarctic Circumpolar Current
ACM	Acoustic Current Meter
ADCP	Acoustic Doppler Current Profile
AMSR-E	Advanced Microwave Scanning Radiometer
BC	Brazil Current
Brazilian CHM	Brazilian Navy Hydrographic Center
CC	Coefficient of Correlation
CLIVAR	Climate Variability and Predictability Program
COADS	Comprehensive Ocean-Atmosphere Data Set
cSEC	central band of the South Equatorial Current
CTW	Coastal Trapped Wave
CW	Central Water
CW	Coastal Water
DMSP	Defense Meteorological Satellites Program
DWBC	Deep Western Boundary Current
EOF	Empirical Orthogonal Functions
ERA-40	Reanalysis of the Global Atmosphere for 45 years
ERS	European Remote Sensing Satellite
ETOPO-2	Digital Terrain Data with 2" resolution
EUC	Equatorial Undercurrent
Guinea C.	Guinea Current
GC	Gulf Current
GEOSAT	Geodetic Satellite
GFDL	Geophysical Fluid Dynamics Laboratory
GLOSS/IOC	Global Sea Level Observing System
GOES	Geostationary Operational Environmental Satellites
HDF-EOS	Hierarchical Data Format - Earth Observing System

IBGE	Institute of Geography and Statistics
IO/USP	Institute of Oceanography of São Paulo University
IRD	Institut de recherche pour le développement
ISV	Intraseasonal Variability
ITCZ	Intertropical Convergence Zone
IWBC	Intermediate Western Boundary Current
MLD	Mixed Layer Depth
MOC	Meridional Overturning Cell
MODIS	Moderate-resolution Imaging Spectroradiometer
MOM	Modular Ocean Model
MSLA	Mean Sea Level Anomaly
MSW	Maximum Salinity Water
NADW	North Atlantic Deep Water
NBC	North Brazil Current
NBUC	North Brazil Undercurrent
NCAR	National Center for Atmospheric Research
NCEP	National Centers for Environmental Prediction
NEC	North Equatorial Current
nSEC	northern band of the South Equatorial Current
NOAA	National Oceanic and Atmospheric Administration
OCCAM	Ocean Circulation and Climate Advanced Modeling Project
PCA	Principal Component Analysis
POD	Proper Orthogonal Decomposition
POP	Parallel Ocean Program
QuikSCAT	Quick Scatterometer
RCM	Recording Current Meter
RMPG	Geodetic Permanent Tide Gauge Network
ROMS	Regional Ocean Modeling System
SAC	South Atlantic Current
SACW	South Atlantic Central Water
SACZ	South Atlantic Convergence Zone
SASH	South Atlantic Subtropical High

SBB	Southeast Brazil Bight
SCF	Squared Covariance Fraction
SEC	South Equatorial Current
SECC	South Equatorial Countercurrent
SEUC	South Equatorial Undercurrent
SICC	Southern Intermediate Countercurrent
SMW	Salinity Maximum Water
SODA	Simple Ocean Data Assimilation
sSEC	southern band of the South Equatorial Current
SSM/I	Special Sensor Microwave
SST	Sea Surface Temperature
STC	Subtropical Cell
Sv	Sverdrup
SVD	Singular Value Decomposition
TMI	Microwave Imager
TOGA-TAO	Tropical Ocean Global Atmosphere - Tropical Atmosphere Ocean
TRMM	Tropical Rainfall Measuring Mission
TSW	Tropical Surface Water
TW	Tropical Water
uCDW	upper Circumpolar Deep Water
WOA	World Ocean Atlas
ZCAS	Convergence Zone of the South Atlantic

Contents

AGRADECIMENTOS	III
RESUMO	IV
ABSTRACT	VI
FIGURE LIST	VIII
LIST OF ABBREVIATIONS	XI
CONTENTS	XIV
CHAPTER 1	16
1. MOTIVATION AND OBJECTIVE	16
CHAPTER 2	23
2. OBSERVATIONAL AND DERIVED DATA	23
CHAPTER 3	29
3. THE MODELLING TOOLS	29
CHAPTER 4	34
4. THE PATHWAYS AND THERMAL STRUCTURE OF SURFACE CURRENTS IN THE EQUATORIAL ATLANTIC OCEAN.....	34
CHAPTER 5	46
5. NEAR SURFACE TRANSPORT AND HEAT BUDGET IN THE SOUTHWESTERN TROPICAL ATLANTIC USING A HIGH-RESOLUTION NUMERICAL MODELLING SYSTEM	46
CHAPTER 6	65
6.1. THE HIGH-RESOLVED INTERANNUAL ROMS APPROACH	66

CHAPTER 7	92
7. REGIONAL BIOGEOCHEMICAL MODELLING IN THE SOUTHWESTERN TROPICAL ATLANTIC	92
CHAPTER 8	100
8. CONCLUSIONS AND PERSPECTIVES	100
REFERENCES	108

Chapter 1

1. Motivation and objective

The equatorial Atlantic Ocean is a very complex area where zonal currents and counter-currents coexist with strong ocean-atmosphere heat exchanges as well as local upwelling of cold waters. It is not surprising that several research programs have been proposed to study the transport and heat variability in this area, as for example the Global Atmospheric Research Program (GARP), the Atlantic Tropical Experiment (GATE), the Francais Ocean Climat Atlantique Equatorial (FOCAL), and the Pilot Research Moored Array in the Tropical Atlantic (PIRATA). Most of these efforts focus on air-sea interaction processes related to climate change investigations.

The importance of sea surface temperature (SST) variability in the tropical Atlantic, for example, as a response to the seasonal varying winds has been the subject of numerous studies. SST in the tropics is largely determined by upper ocean dynamics including advection. Therefore, it is necessary to understand and model its influence in climate, as well as, to know the surface currents and their variability (Lumpkin and Garzoli, 2005).

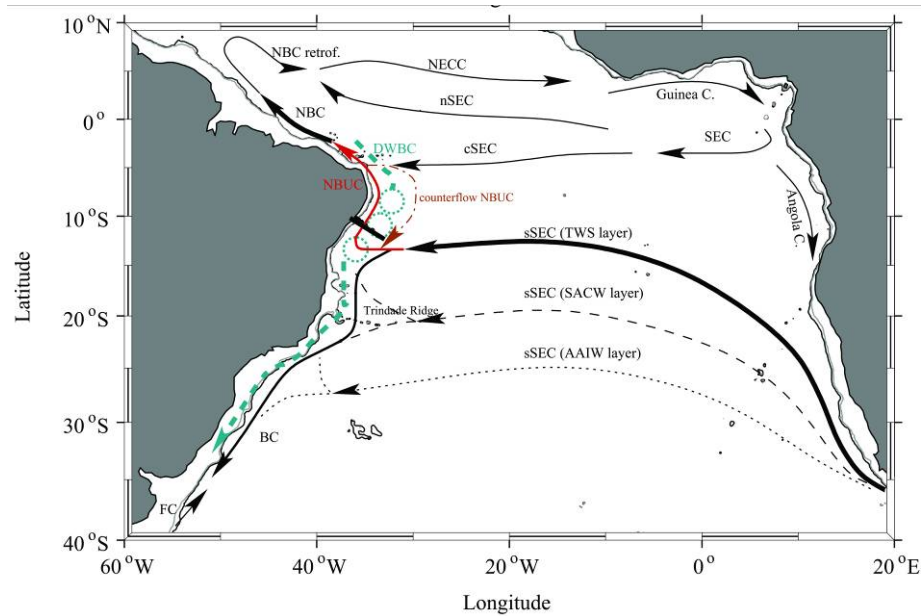
Different work-groups have presented results from modeling and

observations confirming that the tropical Atlantic is a critical region for processes associated to the Meridional Overturning Circulation (MOC), such as cross-equatorial exchanges, and sea surface temperature variability that impacts on climate variability of the coupled tropical ocean/atmosphere system - see Stramma and Schott (1999), Lee and Csanady (1999a,b), Stramma et al. (2003), for an overview. In the tropical ocean, cold thermocline waters of non-equatorial origin from both hemispheres are transformed into warm water masses via entrainment and subsequent surface heat flux, and then escape from this region northward as well as southward, although the net heat transport is northward. The tropical Atlantic warm water pool stores heat during May-October and permits heat escape in November-April.

The warm component of the “conveyor belt” in the equatorial Atlantic is sensitive to this global circulation cell, but also to smaller horizontal scale movements related to the subtropical subduction and to the equatorial recirculation cell, for which Ekman divergence partially compensates geostrophic convergence (Blanke et al, 1999). According to Stramma and Schott (1999), the water mass exchange, including net northward meridional heat transport across the equator, occurs on three layers (surface, central and bottom). In the surface layer, it is accomplished by warm Tropical Surface Water (TSW). In the central layer, Antarctic Intermediate Water (AAIW) and upper Circumpolar Deep Water (uCDW) move northward in the upper 1200 m and is compensated by cold North Atlantic Deep Water (NADW), which moves southward between 1200 and 4000 m. In the bottom layer, the northward transport of Antarctic Bottom Water (ABW) also carries a small amount of cold water into the northern hemisphere.

The main zonal currents that act on the equatorial surface layer are the North Equatorial Current (NEC), the North Equatorial Countercurrent (NECC), the South Equatorial Current (SEC), and the Equatorial Undercurrent (EUC) near the equator. These standards were more recently detailed from drifter observations as analyzed by Lumpkin and Garzoli (2005). In the South tropical Atlantic, the SEC flows westward on the upper ocean circulation. Molinari (1982) described the SEC as divided into three

bands in the tropical Atlantic. The northern branch of SEC was called northern SEC (nSEC), the flow between the SEUC and the SECC is known as central SEC (cSEC), and finally, flowing south of the SECC, the southern SEC (sSEC). On the western boundary of the tropical Atlantic, the sSEC bifurcates into the North Brazilian Undercurrent (NBUC) that flows northward, and the Brazilian Current (BC) that flows southward along the Brazilian coast. In the beginning of the northern Brazilian shelf, near 4°S, the NBUC joins the cSEC to form the shallower NBC. After crossing the equator, a part of NBC retroflects and contributes to eastward flows of the NECC and EUC. Therefore the west border of the tropical Atlantic, near 35° W, has particular importance for the mixture of water masses because it contains a large portion of the Atlantic Meridional Overturning Circulation (MOC) passing through it (Schott et al., 2003).



(Veleda, 2008)

Figure 1.1. Chart of study area with domain limited by 10°N-40°S and 20°E-60°W with a schematic representation of mean zonal and meridional currents: The upper ocean northward NBUC flow (red solid line), and the deepest southward transport by the DWBC (blue dashed line). The sSEC bifurcation at 100m depth (solid line); between 200m and 500m depth (dashed line); between 500m and 1200m depth (pointed line), according with Stramma and England (1999).

Inside the southwestern border of the tropical Atlantic, the Northern Atlantic Deep Water (NADW), originated by the cold water plunged from the North Atlantic, which runs towards the South Atlantic, are relatively well-

known (Arhan et al., 1998; Stramma et al., 2005). However, in the southern hemisphere, the formation of shallow warm water by subduction, and its northward transfer, to close the heat budget of MOC across the equator, is less understood. The southern Atlantic Ocean presents prime importance for global climate change due to the number of key zones where oceanic signals, on various scales (from intra-seasonal to decadal), crosses through. In the southern subtropical Atlantic basin, mainly subjected to both cyclonic and anticyclonic gyres strongly controlled by the surface wind (Stramma and Schott, 1999; Lumpkin and Garzoli, 2005), the following key zones can be listed, from South Africa to South America successively:

- (i) The Agulhas Current off South Africa, coming up from the Indian Ocean and propagating northwards while skirting the African coast;
- (ii) The Benguela Current system, including the continuation towards the north of the previous current, and the regional cyclonic circulation within the Angola Dome region;
- (iii) The south subtropical Atlantic gyre (15°S-20°S, 40°W-20°W), corresponding to an important area of warm-salted water formation by subduction, and feeding the South Equatorial Current (SEC), which is itself formed by at least three easterly branches separated by narrow regions of less evident counter-currents (Stramma, 1991);
- (iv) And finally, more to the west, near South America, the zone of divergence of the southern SEC while approaching the Brazilian edge.

This last region is in part at the origin of the feeding of numerous current systems bordering the Brazilian coast, either towards the north or south. Towards the north, the northern branch of the SEC termination forms the North Brazilian Current-North Brazilian Under Current (NBC-NBUC) system, one of the most powerful western boundary currents in the world. This system participates in the feeding of a few other currents (Stramma et al.,

2005); among them, the northward Guyana Current, the eastward North Equatorial Counter Current with its associated complex retroflexion system (Goes et al., 2005), and finally the eastward Equatorial Under Current (EUC). It is believed that NBC accounts for approximately one-third of the net warm-water transported across the equatorial tropical gyre boundary into the North Atlantic, compensating for the southward export of NADW (Stramma, 1991; Stramma and England, 1999) as previously cited. More to the south, the southern branch of SEC forms the Brazil Current (BC) propagating southward along the coast of Brazil meeting the Malvinas Current (Gordon and Greengrove, 1986) at about 35°S, which is itself fed partially by cold water coming from the Pacific Ocean via the Drake's passage. The latitude where the SEC bifurcation occurs is not yet very well known, although it has been demonstrated that the North Brazil Under Current (NBUC) originates south of 10°S (Stramma et al., 2003, 2005; Schott et al., 2002, 2005), where a branch of the SEC flows northward and merges within the NBUC. The BC, which flows southwesterly, merges into the Atlantic Meridional Overturning Cell (MOC) system (Silveira et al., 1994; Stramma et al., 1990, 1995; Schott et al., 1998) in the vicinity of the Brazil-Malvinas confluence (Olson et al., 1988; Garzoli and Garraffo, 1989).

The interactions between sea surface temperature (SST) and the easterly atmospheric circulation may play a significant role in local climate fluctuations of Northeast Brazil, a region affected by intermittence of severe droughts and floods (Moura and Shukla, 1981; Rao et al., 1993).

In the oligotrophic regions of the ocean, the supply of inorganic nutrients to the euphotic layer may limit the concentration of microalgal biomass, the rate of phytoplankton growth, or both (Marañón et al., 2000). Several Mechanisms have been proposed to explain the formation and maintenance of the deep chlorophyll maximum (DCM), that is a oceanographic feature of tropical and subtropical oceans. Higher in-situ growth at the nutricline than in the upper mixed layer, and acclimation of phytoplankton to low irradiance, has been suggested (Cullen, 1982) as cause of DCM formation at subtropical gyres.

Very early reports of low productivity in the subtropical gyres

(Steeman-Nielsen and Jansen, 1957; Thomas, 1970; Eppley et al., 1973) have been considered to be in error due to methodological inadequacies (Fitzwater et al., 1982). Nevertheless, recent work carried out in oligotrophic regions, using new techniques (Malone et al. 1993; Letelier et al. 1996), presents a large range in the rates of phytoplankton production and growth inside these areas. In fact, this controversy will be maintained, while the lack of knowledge about temporal and spatial variability in the biology of open ocean is being kept (Marañón et al., 2000). Consequently, any uncertainties in the productivity estimates in these areas will have significant effects on the prediction of global biogeochemical models (Marañón et al., 2000). In other hand, there are few studies about the physical processes related with DCM formation inside the southwestern tropical Atlantic. Montes (2003) suggests that the support of nutrient inside euphotic zone, in the southwestern tropical Atlantic, is maintained by diffusion process in nutricline basis.

Supported by the ideas stated above, the goal of this work is to investigate the seasonal and intraseasonal variability of the western boundary regime of the South tropical Atlantic. I will conduct this research following these pathways:

- (a) The use of a numerical model in the Tropical Atlantic to investigate the seasonal and intraseasonal variability of main currents and SST along equatorial band.
- (b) The investigation of the near surface ocean heat budget in the Southwestern tropical Atlantic from high resolved modelling results.
- (c) The investigation of the zonal wind stress variability as an important forcing for the intraseasonal variability of the southern branch of SEC regime.
- (d) The influence of sSEC on the distribution of phytoplankton biomass along the southwestern boundary of the tropical Atlantic.

This manuscript is organized as follows: the next chapter brings an

overview of the study area and the used datasets. The main characteristics of ROMS and conditions of the simulations are presented in Chapter 3. Chapter 4 shows illustrations of the tropical Atlantic simulation, where, simulated and observed thermal structures in upper ocean layer are compared. Also in Chapter 4, intensities of simulated oceanic currents, as well as the mass transport across three zonal sections along the equator are presented. Chapter 5 presents simulated and observed thermal structures in the upper layer to improve the climatological high resolved simulation of Southwestern tropical Atlantic. Chapter 5 also provides a simulated seasonal evolution of oceanic components that compound the heat content in the mixed layer, as well as mass and heat transport across three zonal sections and a fourth section along the PIRATA-SWE sites. Chapter 6 presents the results of an interannual simulation in the same region of the Southwestern tropical Atlantic (seen in chapter 5). In Chapter 6 the ROMS evaluation is performed by comparing outputs of the model with observed high-frequency SST fields estimated by satellite, thermal structures and mixed layer depths provided by the PIRATA-SWE dataset. As a first dynamical application of ROMS, it shows examples of simulated variation of mass transports across three zonal transects, and a section along the PIRATA-SWE sites. In Chapter 7, results of biogeochemical modelling of the oligotrophic zone in the Southwestern tropical Atlantic are presented. The last Chapter presents the conclusion and perspectives.

Chapter 2

2. Observational and derived data

This thesis concentrates on the tropical Atlantic with specific focus at the upper layer of the western boundary of the Southern tropical Atlantic along the Brazilian shelf. The purpose here is to introduce the data necessary to feed surface and open boundaries of the modelling package chosen, The Regional Ocean Model system (ROMS). The data presented in this chapter can describe the seasonal and intraseasonal mechanisms of the coupling ocean and atmosphere variability. Thus, results from the ROMS simulation were obtained to evaluate this modelling tool representing these regions.

2.1. Surface forcing datasets

2.1.1. Comprehensive Ocean-Atmosphere Data Set (COADS)

The Comprehensive Ocean-Atmosphere Data Set (COADS) is a extensive and widely used set of sea surface data. The COADS is maintained by U.S. inter-agency cooperation since January of 1981, formed by NOAA's Environmental Research Labs. (ERL), Cooperative Institute for Research in Environmental Sciences (CIRES), NCDC and NCAR. The COADS data is actually composed by observational data from a variety of ship cruises, drifting and moored buoys from Canada's Marine Environmental Data Service (MEDS) and Pacific Marine Environmental Laboratory (PMEL) and the National Data Buoy Center (NDBC) (Wooddruff et al., 1998)

The basic observed variables in COADS include sea surface and air temperatures, wind, humidity (dew point or wet bulb temperature), barometric pressure, cloudiness weather, and wave and swell fields. The observations have been quality controlled, and monthly statistics calculated for the period of 1854 to 1995, for resolution of $2^{\circ} \times 2^{\circ}$ boxes and $1^{\circ} \times 1^{\circ}$ from 1960 to 1993 (Wooddruff et al., 1998; daSilva et al., 1994).

2.1.2. QuikSCAT daily wind data

The wind stress data were obtained from the CERSAT/IFREMER (Centre ERS d'Archivage et de Traitement/Institut Français de Recherche pour l'Exploitation de la Mer) available on line at <http://www.ifremer.fr/> using OPENDAP tool (<http://www.opendap.org>), to be used in interannual runs. The scatterometer winds are retrieved from Quick Scatterometer (QuikSCAT) the version 3 (Penven et al., 2008, Liu, 2002). It consists of daily averaged gridded values of scalar wind speed, meridional and zonal components of the wind velocity and wind speed squared. The grid has 1.8° latitude x 1.6° longitude resolution (Tsai et. al., 2000).

2.2. PIRATA data set

Entering now in its permanent phase, PIRATA is an ocean-meteorological observing system which contributes to the operational climate survey of the global ocean (Servain et al., 1998; Bourlés et al., 2008). PIRATA is the result of an international scientific cooperation gathering Brazil, France and the United States of America. Its main scientific motivation is to monitor, describe and understand the two main modes of climatic variability over the tropical Atlantic which are the equatorial and the meridional modes (Servain et al., 1998). Based on this rationale, the original array configuration is presently composed by 10 ATLAS moorings (Hayes et al., 1991) along the equatorial line (35°W, 23°W, 10°W and 0°E) and two meridional lines, one along the 38°W meridian (4°N, 7°N, 12°N and 15°N), and the other along the 10°W meridian (0°N, 6°S and 10°S). Brazil and France are responsible for the yearly sea maintenance of the array, while USA provides the ATLAS material and process the raw data. Daily transmissions of the first 500m of ocean temperature (11 levels) and salinity (4 levels), and the meteorological main variables at the sea surface, are ensured thanks to the ARGOS satellite system, and immediately available on the Web after first validation (<http://www.pmel.noaa.gov/pirata/>).

Once assured the success of the PIRATA original array (Bourlés et al., 2008), and in order to complete the necessary set of observations to understand more in details the seasonal and inter-annual variability over specific areas in the tropical Atlantic, it was decided to extend the original mooring array. Three extensions were proposed: a first one over the southwest tropical basin (along the Brazilian coast), a second one over the southeast basin (along the African coast, south of the Equator), and a third one over the northern and northeast basin (again along the African coast). Brazil took alone the responsibility of implementing the south-western extension. Obviously, the main goal of this project, the PIRATA South West Extension (PIRATA-SWE), is primarily to help in the forecasting of the Brazilian climate, especially over the Northeast Brazilian region.

Three sites for the ATLAS mooring were chosen for the PIRATA-SWE (Figure 5.1) according to scientific arguments (Nobre et al., 2005, 2008): (i)

8°S-30°W in connection with the 0°N-10°W site of the PIRATA's backbone, (i.e. the equatorial Atlantic warm pool vs. the cold tongue complex); (ii) 14°S-32°W in connection with the SEC flow (properties and heat flux transport variability); (iii) 19°S-34°W in connection with the SACZ (relations to the oceanic heat flux changes). Obviously, the PIRATA-SWE array only addresses the changes in the thermohaline structure within the SEC's flow into the bifurcation region. The understanding of changes in the partition between the NBC and the BC at the SEC bifurcation is out of the PIRATA-SWE objectives.

The three ATLAS buoys of the PIRATA-SWE were launched during the second half of August 2005, thus the time series analysed here cover the first year of dataset, from September 2005 to August 2006. With the exception of a four-month interruption of the 8°S-32°W site due to anchoring problems (the buoy's nylon cable sheared off after ten months of deployment), the buoys reported daily with nearly 100% of data return. In this study we are using the daily observed PIRATA-SWE data for temperature (0m, 20m, 40m, 60m, 80m, 100m, 120m, 140m, 180m, 300m, 500m) operationally obtained on the Web at the PMEL/NOAA address (<http://www.pmel.noaa.gov/pirata/>).

2.3. Hydrology and biogeochemical datasets

2.3.1. WOA2005 data

The World Ocean Atlas (WOA2005) is a data product of the Ocean Climate Laboratory of National Oceanographic Data Center (NODC). The WOA consists a climatology with global grids at 1° spatial resolution of three-dimensional fields (Conkright et al., 2002). The data are normally interpolated onto 33 vertical layers from surface to seafloor. WOA fields include eight ocean properties (temperature, salinity, dissolved oxygen, apparent oxygen utilization, percent oxygen saturation, phosphate, silic acid and nitrate). WOA fields are produced for annual, seasonal and monthly time-scales. This data product is distributed with ROMSTOLS (Penven et al., 2008) package version used in this thesis.

2.3.2. ECCO interannual model data

The ECCO Ocean Data Assimilation is a project which study seasonal to interannual changes in ocean circulation from assimilating observations with a global circulation model. The model assimilates altimetric data provide from TOPEX/POSEIDON data, CTD and XBT's profiles, current meter, drifters, floats and air sea-flux from NCEP reanalyses. The ECCO model domain has 46 vertical levels and a telescopic horizontal grid of 1° covering the globe (80°N to 80°S) and $1/3^\circ$ within 20° of the equator. Hydrology ECCO results from 2000 to 2007 were obtained through the use of OPENDAP tool (<http://www.opendap.org>) to feed the boundary and initial conditions of interannual run of high resolution ROMS simulation of the southwestern tropical Atlantic.

2.3.3. SeaWifs data

The SeaWifs chlorophyll a data is a derived product from images from SeaWifs scanner and algorithms (O' Reilly et al., 1998). The processed data can be obtained at different time-scales (monthly, 8-day, daily). It is available in http://las.pfeg.noaa.gov/OceanWatch/ocean_watch_safari.php with horizontal resolution of 0.1° . The Climatological run of biogeochemical model used seasonal Seawifs data of Chlorophyll a to build boundary and initial conditions is seasonal and was obtained with ROMSTOOLS (Penven, et al., 2008).

2.4. MLD Criteria

Most criteria used to determine the MLD in the ocean require that the deviation of the temperature T (or density, σ_t) from its surface value be smaller than a certain fixed value (Sprintall and Tomczak, 1990; Brainerd and Gregg, 1995). The MLD is estimated as the depth at which density is equal to the sea surface value plus an increment $\Delta\sigma_t$ equivalent to a desired net decrease in temperature. For instance, Miller (1976) and Spall (1991) use $\Delta\sigma_t = 0.125 \sigma_t(0)$ to determine the mixed layer depth, while Sprintall and Tomczak (1992) and Ohlmann et al. (1996) adopt $\Delta\sigma_t = 0.5^\circ\text{C}(\partial\sigma_t/\partial T)$, where $\partial\sigma_t/\partial T$ is the coefficient of thermal expansion. Following Sprintall and Tomczak (1992), we evaluate the MLD in terms of temperature and density steps ($\Delta T = 0.5^\circ\text{C}$ and $\Delta\sigma_t = 0.5^\circ\text{C}(\partial\sigma_t/\partial T)$) from the SST and density ($T(0)$ and $\sigma_t(0)$) obtained from the PIRATA and ROMS profiles:

$$\text{MLD} = z \left(\sigma_t = \sigma_t(0) + \frac{\partial\sigma_t}{\partial T} \Delta T \right) \quad (\text{A.1})$$

where $\partial\sigma_t/\partial T$ is calculated as a function of the surface temperature and salinity (Blanck, 1999).

Chapter 3

3. The modelling tools

To evaluate interactions between ocean and atmosphere, its variability, and distribution transport, inside a study area, a numerical modelling related to low operational cost and to the possibility of studying large geographic areas were chosen. Based on the use of a numerical modelling tool, the focus of this work is to investigate a seasonal and intraseasonal variability of the main transport systems, heat budget and biogeochemical cycles. In this chapter, the Regional Ocean Modeling System (ROMS) is presented, with more details on definitions of grids, boundary and stability conditions.

3.1 The Regional Ocean Modeling System - ROMS

ROMS is an ocean model (Shchepetkin and McWilliams, 2005) previously adapted to different regions of the world (Haidvogel et al., 2000; Malanotte-Rizzoli et al., 2000; She and Klinck, 2000; Penven et al., 2000, 2001a,b; McCreedy and Geyer, 2001; Lutjeharms et al., 2003). The model solves the free surface primitive equations in an Earth-centered rotating environment based on the classical Boussinesq approximation and hydrostatic vertical momentum balance. ROMS is discretized in terrain-following vertical coordinates. The model grid, forcing, initial and boundary conditions were built using the ROMSTOOLS package developed by the Institut de Recherche pour le Développement (IRD) (Penven et al., 2008). Upstream advection is treated with a third-order scheme that enhances the solution by generating steep gradients as a function of a given grid size (Shchepetkin and McWilliams, 1998). Unresolved vertical subgrid-scale processes are parameterized by an adaptation of the non-local K-profile planetary boundary layer scheme (Large et al., 1994). A complete description of the model can be found in Haidvogel et al. (2000) and Shchepetkin and McWilliams (2005).

3.2 Model Grids

Reproducing ocean features along the Equatorial band required a horizontal regular grid of 341 x 245 cells with a resolution of $1/6^\circ$ in an area that goes from 20°S to 20°N and between 42°W and 15°E (Figure 3.1). The vertical discretization used had 30 sigma levels (terrain-following). For application in the Southwestern tropical Atlantic, near the NE Brazilian coast, the integration domain used was from 25°S to 5°S and from 47°W to 20°W (dashed line in Figure. 3.1), with a isotropic $1/12^\circ$ horizontal grid with 323 x 249 horizontal mesh cells and a vertical discretization of 40 levels.

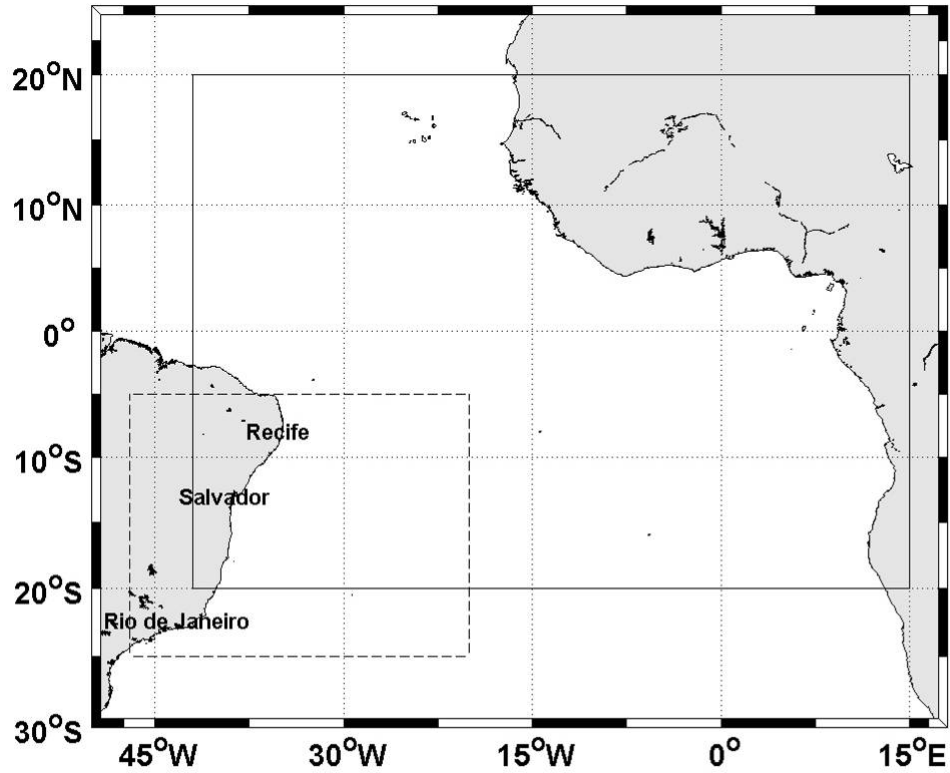


Figure 3.1. Region of model integrations, solid lines indicate domain of $1/6^\circ$ climatological equatorial modelling. Dashed lines indicate southwestern tropical Atlantic domain limits of $1/12^\circ$ horizontal grid.

At both presented cases, bottom topography was derived from a $2'$ resolution database ETOPO2 (Smith and Sandwell, 1997). A slope parameter $r = \nabla h/h < 0.20$ was used to prevent errors in the computation of the pressure gradient (Haidvogel et al., 2000).

3.3 Boundary Conditions

At the open boundaries, an active, implicit, upstream-biased radiation condition connects the model solution to the surrounding ocean (Marchesiello et al., 2001). Horizontal Laplacian diffusivity inside the integration domain is zero, and 1 degree relaxation scheme is imposed (up to $10^4 \text{ m}^2 \text{ s}^{-1}$) in the sponge layers near the open ocean boundaries. The model equations are subjected to no-slip boundary conditions along the coastline.

The oceanic circulation was forced on sea surface by monthly-averaged winds, heat and fresh water fluxes derived from COADS (daSilva et al., 1994) for the climatological simulations (Chapters 4, 5 and 7). For the interannual run (Chapter 6) a daily-mean (2005-2007) wind stress by QuikSCAT (Liu, 2002) replaces the COADS wind dataset. To compose the lateral forcing of climatological run, hydrography and geostrophic velocities derived from WOA2005 (Conkright et al., 2002) were used. On the other hand, a basin-scale daily-mean (2005-2007) hydrography and currents derived from OGCM-ECCO (<http://ecco.jpl.nasa.gov/>) was used to infer thermohaline properties and water volume exchanges at the open horizontal boundaries.

3.3 Biogeochemical model coupled to ROMS

The ROMS version used in this thesis presents the possibility of being coupled with a biogeochemical model NCPZD (Moore, 2002). This model is based on limitant nutrient. Its hypothesis considers twelve variables of state: nitrate, ammonia, Chlorophyll a, phytoplankton, zooplankton, micro and macro detritus (for nitrogen and carbon), oxygen, inorganic dissolved carbon and pH. These variables are balanced during each time step according to biogeochemical reactions and to horizontal and vertical advectives transport, as well as to vertical diffusion transport calculated by the physical model.

More details about equations can be found in ROMS documentation (<http://roms.mpl.ird.fr/documentation.html>).

3.4 Model Simulation

The climatological simulations ran from a state of rest during 10 years. After a spin-up period of one year, the model had achieved a statistically steady state. All the numerical results from these runs examined correspond to the last year of simulation (year 10).

The interannual simulation was performed in two steps. First, the

rested ocean was gradually forced by applying ramp functions to the boundary conditions for the period Jan.-Dec. 2001. After this, the full sets of forcing conditions for 2001-2007 were considered for the interannual simulation. Only results from 2005-2007 were used.

Chapter 4

4. The pathways and thermal structure of surface currents in the equatorial Atlantic Ocean

This chapter aims to use a regional well-solved circulation model to investigate the subsurface zonal currents and the thermal structure of the upper 500 m equatorial ocean layer. The simulations were performed with the Regional Ocean Modeling System (ROMS), which improves the numerical resolution of strong currents and counter-currents systems like those observed in equatorial Atlantic.

Nowadays, the knowledge of the pathways and the dynamics of the oceans through prediction models can contribute to solve many questions on climate and oceanography sciences. Modeling constitutes an essential tool for evaluation of the standings and variations presented in a complex hydrodynamic regime, just like the equatorial Atlantic Ocean. Using the available records of observed PIRATA data, Foltz et al. (2003) showed that the latent heat loss and the absorbed shortwave radiation represent the largest contributions for the seasonal SST variability in the northwest and southeast tropical Atlantic basin. Over the equator, however, the authors

suggest that the contributions from the latent heat loss are less important than the horizontal temperature advection and the vertical entrainment. Chaves and Nobre (2004) by observational and numerical modeling results suggest that atmospheric variability over the southwest tropical Atlantic also influences the SST variability locally, thus forming a coupled system with multiple feedback processes.

4.1 The ROMS Approach

The simulation performed here consists in a meso-scale scenario that reproduced the equatorial currents system. The model domain results in 341 x 245 horizontal mesh cells in a regular horizontal grid with a resolution of $1/6^\circ$ covering an ocean area from latitude 20°S to 20°N and from 42°W to 15°E of longitude. The vertical discretization used had 30 levels. Bottom topography was derived from a 2' resolution database ETOPO2 (Smith and Sandwell, 1997). At the three open boundaries (north, west and south) an active, implicit, upstream biased radiation condition connects the model solution to the surrounding ocean (Marchesiello et al., 2001).

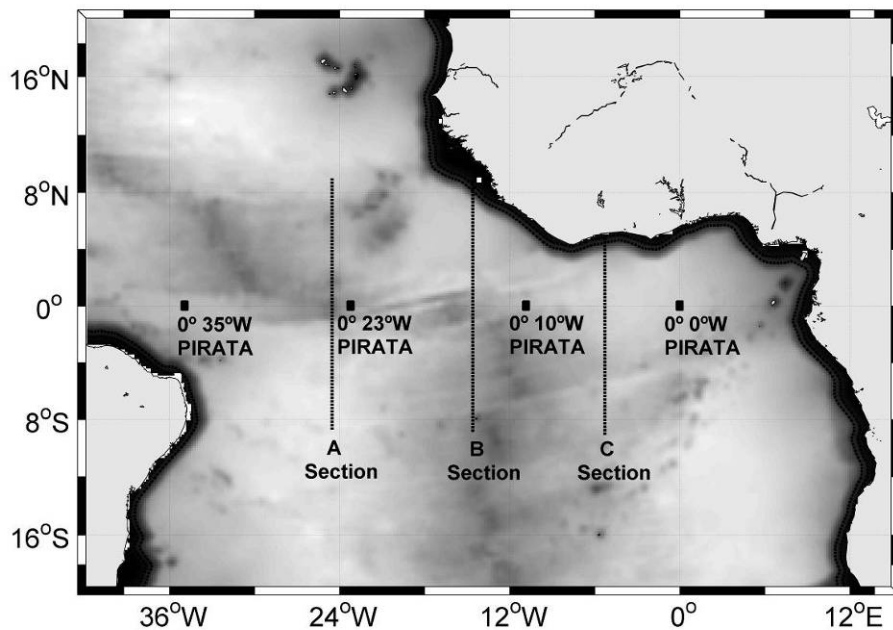


Figure 4.1. Study area and model integration domain. The sections A, B and C are dashed lines and the squares over the equator line are the PIRATA mooring sites. Bathymetry is represented by gray shading contour.

Horizontal Laplacian diffusivity inside the integration domain is zero, and a 5-point smooth increasing is imposed (up to $800 \text{ m}^2\text{s}^{-1}$) in sponge layers near open ocean boundaries. The model domain was forced at the sea surface by winds, heat and fresh water fluxes derived from the Comprehensive Ocean-Atmosphere Data Set (COADS) monthly fluxes data at $0.5^\circ \times 0.5^\circ$ resolution (da Silva et al., 1994). The database World Ocean Atlas 2001 (WOA2001), monthly climatology at $1^\circ \times 1^\circ$ resolution (Conkright et al., 2002), is used to infer thermodynamics (temperature and salinity) and geostrophic currents at the open boundaries.

4.2 Experimental dataset

The horizontal distributions of monthly-averaged Sea Surface Temperature (SST) obtained in simulations were compared to satellite observations. The Advanced Very High Resolution Radiometer (AVHRR) aboard the National Oceanic Atmospheric Administration (NOAA) satellite was employed in comparisons. The data set from AVHRR-SST has a $1/18^\circ$ resolution and the observation period was 1985-2006. This dataset is available on <<http://dods.jpl.nasa.gov/>>.

4.3 ROMS Simulation Results

Using the forcing boundary conditions presented in previous section 4.1, the model ran from a state of rest during 10 years. Figure 4.2 shows a time series of the integration domain kinetic energy (KE) from the model. It indicates that after a spin-up period of two years, the model has achieved a statistically steady state. After stabilization, the model had only small oscillations, standing a mean kinetic energy around $1,4 \text{ J.m}^{-3}$. These oscillations represent the seasonal changes in each year. All the numerical results correspond to the last year of simulation (year 10).

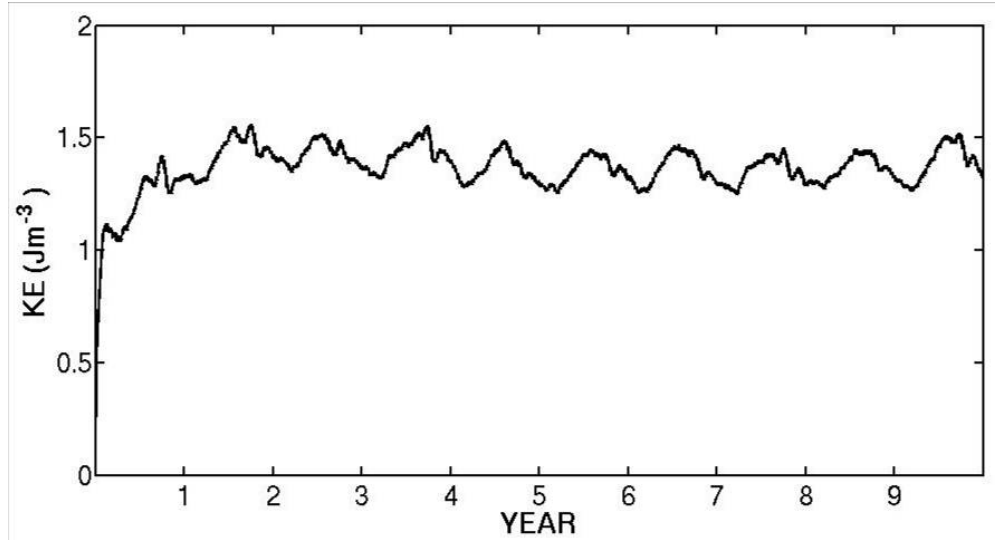


Figure 4.2. Mean kinetic energy ($J.m^{-3}$) of model (ROMS) during 10 simulation years.

4.3.1 Current structure and zonal transport

The equatorial currents obtained in numerical simulations were identified and characterized along the three sections located at 25°W, 15°W and 5°W (see Figure 4.1). According to Lumpkin and Garzoli (2005), the SEC system is part of the equatorial gyre. This flow is clearly divided in two westward jets, the SECc and the SECnc, separated at 0-2°S by a band of weak southward flow, which is induced by the equatorial divergence. Numerical results confirm these observations, with the westward SECc flow occurring between 1°S–8°S, as well as the westward SECn transport near surface in the range ~1°N–4°N, between the equator and the NECC (Figure 4.3 to 4.7).

Model results show that the eastward flow of NECC occurs at ~4°N–8°N, with an indistinct core in function to the time of the year (Figure 4.3 to 4.7). These results corroborate with the description of Richardson and McKee (1984). They found an eastward NECC flow close to surface in latitudes 3°N–10°N with velocities reaching up to 0.5 m.s⁻¹.

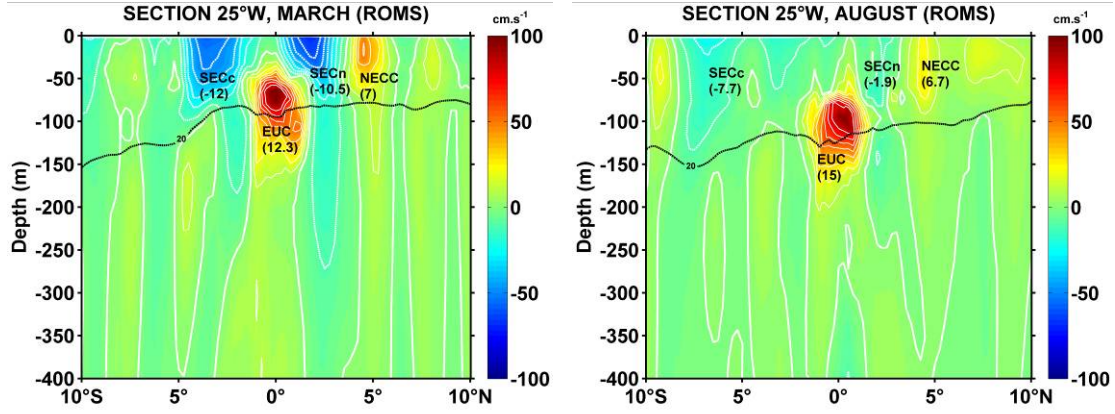


Figure 4.3. Zonal transport (u -component) obtained from model simulation (ROMS) along Section A, 25°W. Dashed lines represent the isotherm 20°C. Monthly-averaged values for March and August.

The EUC was present in simulations below the equator line on all ocean basin. These results agree with the findings of Stramma and Schott (1999), which state that the EUC crosses the entire Atlantic, feeding more or less the equatorial upwelling.

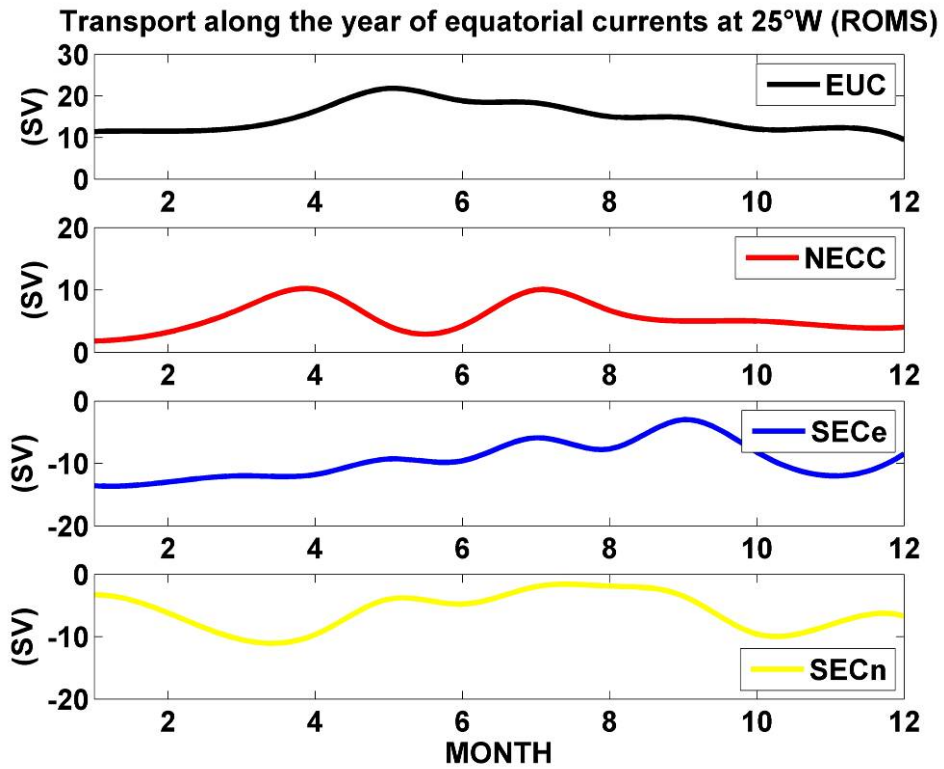


Figure 4.4. Seasonal variability of EUC, NECC, SECc and SECn transports at 25W° section, obtained in simulations.

Numerical results presented in Figure 4.3 show at 25°W (section A, Figure 4.1) a core of the EUC located closer to sea surface in March (~80 m, velocity of 0.8 m.s⁻¹) than in August (~100m, velocity of 1.0 m.s⁻¹). Giarolla et al. (2005) pointed out that the EUC is shallower during January to May and deeper in other parts of the year. By the same time, the sea measurements of Stramma et al (2003), obtained during March-April 2000 in a 23°W section show a EUC core velocity of 0.75 m.s⁻¹ at ~80 m depth. Simulation results are also in good agreement with the recent analysis of Brandt et al. (2006). These authors measured a EUC core (0.7 m.s⁻¹) positioned at 85 m along the 26°W section. The associated EUC transport calculated from model results also presented a good fit to values estimated from sea measurements. While Brandt et al. (2006) found 13.8 Sv (1 Sv \equiv 10⁶ m³.s⁻¹) in the section 26°W, ROMS model pointed out 12.3 Sv (March) and 15 Sv (August) at the 25°W section (Figure 4.3).

The two main equatorial SEC branches were sharply defined in simulations, separated by the EUC. Numerical velocities of SECc reach -0.5 m.s⁻¹ and SECn reach -0.6 m.s⁻¹ in March. In August the SECc and the SECn were more extended, with velocities reaching -0.2 m.s⁻¹. Measurements (Brandt et al., 2006) at 26°W furnished westward transports of -4.9 Sv (SECc) and -3.5 Sv (SECn). Model issues show good agreement with these estimations, especially for the central SEC.

Simulations showed that the NECC is more defined during March, with a core velocity of 0.4 m.s⁻¹ located near 5°N. In August, a deeper current core was present in this same latitude (Figure 4.3), with velocities of 0.3 m.s⁻¹. According to Richardson and McKee (1984), the NECC responds strongly to seasonal variations on atmospheric forcing. Around March, when the Intertropical Convergence Zone (ITCZ) is at its southernmost position, the equatorial trade-winds are weakest while in August, when the ITCZ is at its northernmost position, the equatorial winds are strongest (Weisberg, 1985).

The seasonal variability of the transport close to equator due to main zonal currents at 25°W (section A) is presented in Figure 4.4. In general one may say that the transport along the 25°W section did not show strong seasonal variability. EUC presented maximum values during April–August

(21.8 Sv), and lowest transport in the period September to March. The NECC variability shows two maxima in April and July, 10.1 Sv and 10 Sv, respectively. These numerical results mismatch with Richardson and McKee (1984) contributions, which found that NECC has peaks of transport at 25°W-30°W profiles during July-September. The equatorial branches of the SEC (SECc and SECn) presented minimum westward transports between May and September, which is in contrast to the period of maximum eastward transport by EUC.

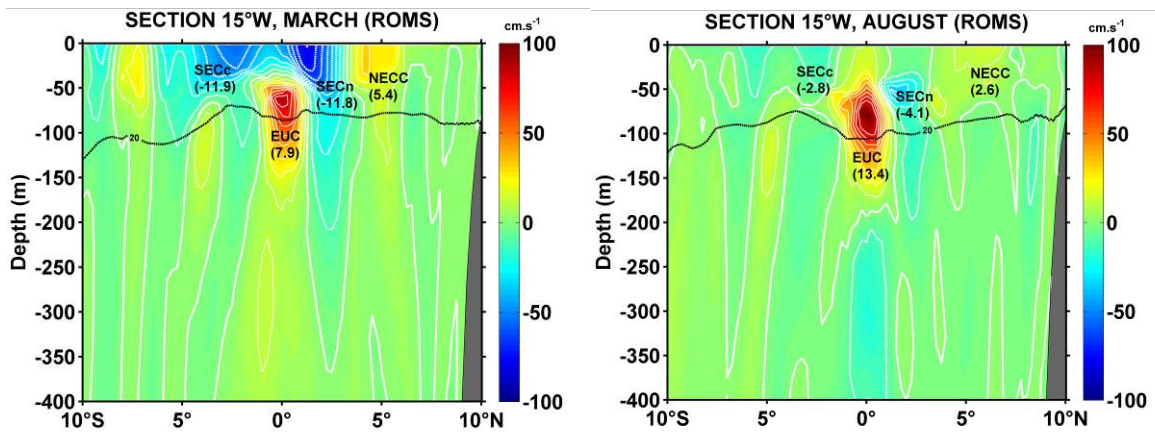


Figure 4.5. Zonal transport (*u*-component) obtained from model simulation (ROMS) along Section B, 15°W. Dashed lines represent the isotherm 20°C. Monthly-averaged values for March and August.

The comparison between mean zonal current structures obtained numerically for March and August at 15°W (section B) is shown in Figure 4.5. The seasonal variability of the zonal transport at this longitude is presented in Figure 4.6. At 15°W the SECn core is deeper than the SECc core, although both westward currents are sharply in March when compared to the weaker and sparser structures found in August. The SECc reaches velocities of -0.5 m.s^{-1} during March and drops to -0.15 m.s^{-1} in August. The SECn showed velocity core of -0.7 m.s^{-1} in March, which is reduced to -0.4 m.s^{-1} during August. Figure 4.5 shows that both currents have almost the same mean net transport in March (-11.8 Sv, SECn) and August (-11.9 Sv, SECc). During the austral winter (August), weakest westward transports are verified in simulations, when the SECn drops to -4.1 Sv and SECc to -2.8 Sv (Figure 4.5 and 4.6).

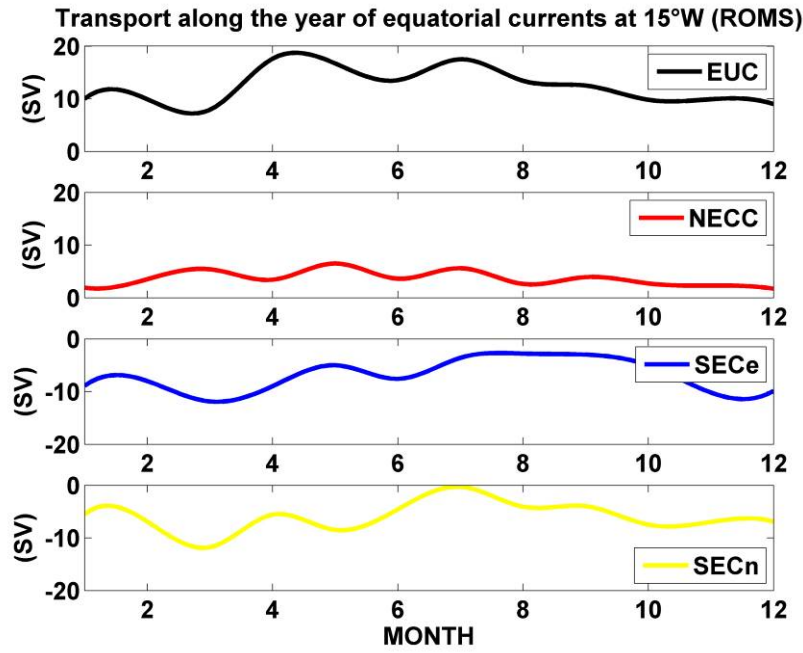


Figure 4.6. Seasonal variability of EUC, NECC, SECc and SECn transports at 15W° section, obtained in simulations.

Numerical results indicate that the EUC core at 15°W has the same maximum velocity (0.8 m.s^{-1}) in both months of comparison, but it presents an increase in transport flow that rises from 7.9 Sv in March to 13.4 Sv in August (Figure 4.5). Simulations also indicate that month-averaged NECC transport of 5.4 Sv in March is reduced to 2.6 Sv in August. The EUC presented the highest values of transport in the period April–September. The SEC branches have the highest values of flow during the months of October to April, always in phase with the period of reduced values of EUC transport.

The velocity structure, core position and zonal transports at the 5°W cross-equatorial transect (section C, Figure 4.1) are presented in Figures 4.7 and 4.8. In Figure 4.7 it is possible to identify the Guinea Current (GC), the equatorial SEC branches and the EUC. The NECC merges with GC near the Africa Coast and flows into the Guinea Gulf.

Simulations also indicated that although the core velocities reach almost the same maximum intensity (0.8 m.s^{-1} , not shown here) in both periods, the EUC core is deeper in August (80–110m depth) than in March (50–70m depth). In contrast, the SEC branches were more defined in March. During this period the SECc at 5°W is shallower and more extended than

SECn, both with cores velocity of -0.5 m.s^{-1} . In August, the SECc and SECn present the weakest values along the last simulated year, with core velocities around -0.1 m.s^{-1} and -0.3 m.s^{-1} , respectively. Model results showed more important GC velocities in March, although the overall transport had been superior in August (3.8 Sv). In March (1.6 Sv) the GC was pushed against the continent due to the enlargement of the SECn. Due to reduction of the current area, in March, the GC gains on velocity, but loses in transport (Figure 4.7). The simulations show that the mean SECc transport was sensible reduced in August when compared to March, dropping from -8.2 Sv to -4 Sv. The contribution of EUC to equatorial mean eastward transport did not show important differences for both compared periods (March 11.3 Sv and August 10.3 Sv). As verified in 25°W and 15°W sections, the EUC core is slightly deeper during August when compared to its position in March (Figure 4.7).

The seasonal variation of the equatorial transport along the 5°W section presented in Figure 4.8 shows highest values of the EUC and GC in the period April–August, and lowest values occurring in the period September–March. In opposition, the SEC seasonality presents inverse standards, with weakest SECc and SECn transports in April–August and strongest westward flows from September to March.

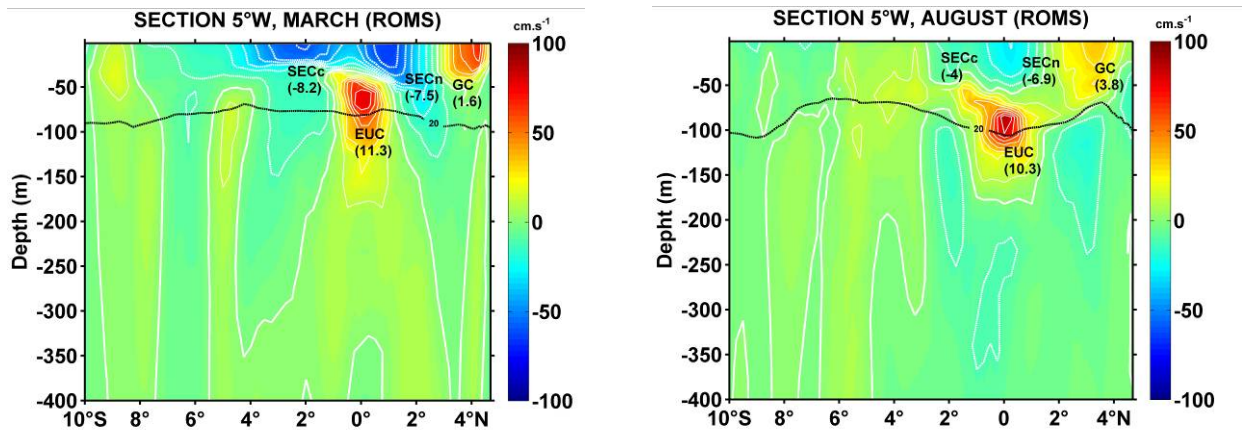


Figure 4.7. Zonal transport (u -component) obtained from model simulation (ROMS) along Section C, 5°W . Dashed lines represent the isotherm 20°C . Monthly-averaged values for March and August.

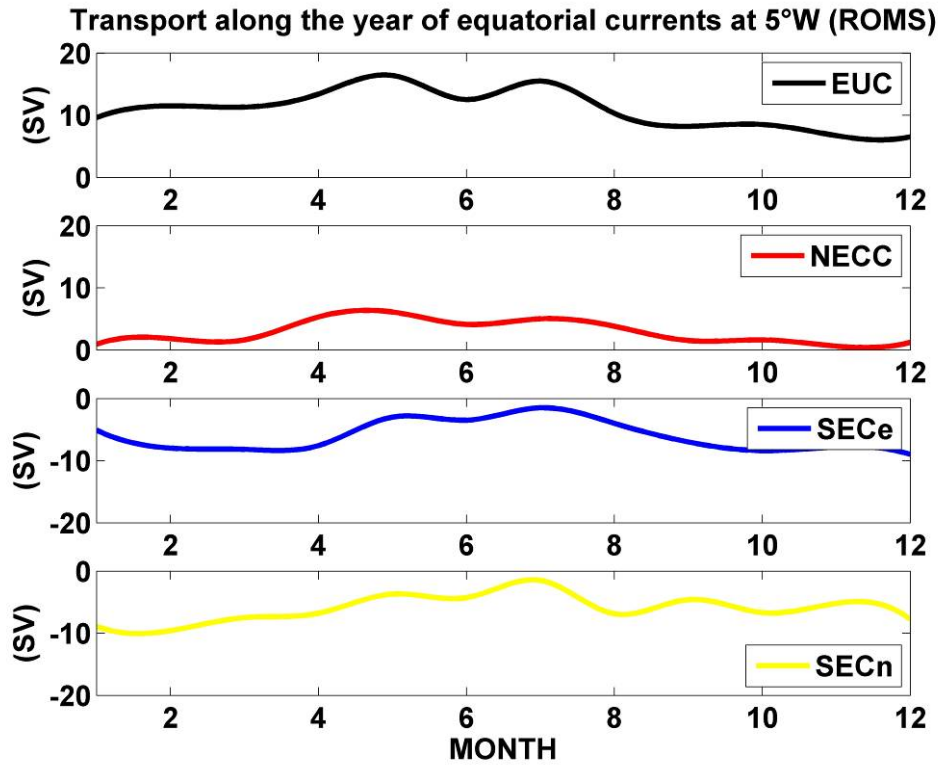


Figure 4.8. Seasonal variability of EUC, NECC, SECc and SECn transports at 5W° section, obtained in simulations.

4.3.2 Thermal structure

The vertical thermal structure of surface layers in Equatorial Atlantic obtained from ROMS simulations is compared with observations of the PIRATA Program. Monthly-averaged temperature profiles from these moorings (1997-2007, 500 m depth) and climatological model results were used to construct the Hovmöller diagrams presented in Figure 4.9. The vertical distribution of the simulated temperature fairly agrees with the field measurements. In subsurface ($z > 100$ m) the best resemblance ($\Delta < |0.5^\circ\text{C}|$) occurs for the western PIRATA sites (35°W and 23°W). Such weak difference between model and observed data is noted in March for those sites in the shallow (0-100 m) and deeper (300-500 m) waters. Larger differences (~ 1 to 3°C), noted between 100 and 300 m for eastern PIRATA sites (10°W and 0°W) in austral winter continue to be acceptable considering that the ROMS is running here according to a climatic forcing. Of special interest is the very well reproduced MLD for the equatorial PIRATA sites, in particular the

upwelling induced shallower MLD verified in eastern buoys during austral winter and late spring (Figure 4.9).

SST results obtained from the climatological run are compared in Fig. 10 with satellite observations for both months, March and August. SST values provided by the model are close to the satellite observation, especially taking in consideration that results from ROMS were obtained with $1/6^\circ$ horizontal resolution while the AVHRR images are generated with a $1/18^\circ$ grid.

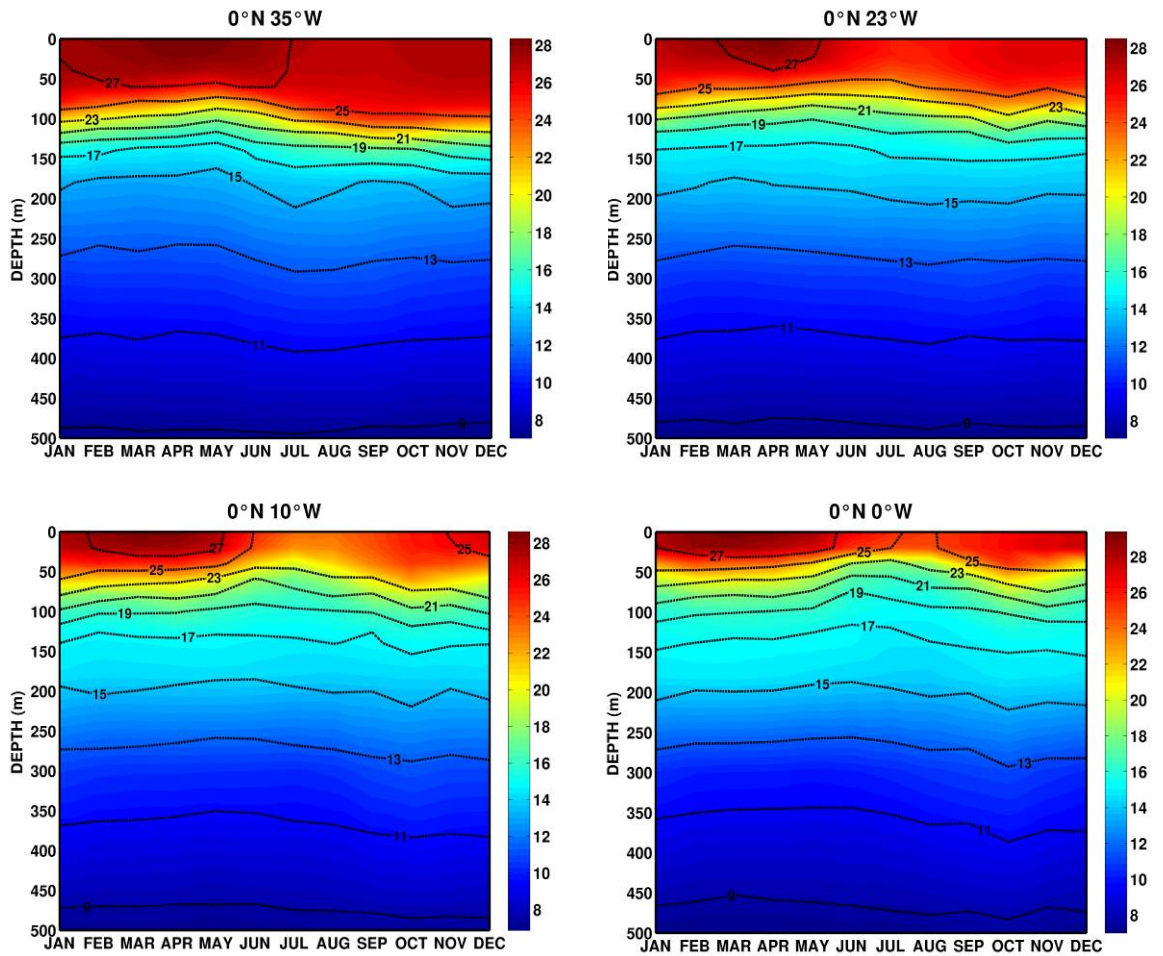


Figure 4.9. Comparison of the vertical temperature distribution provided by ROMS (black dashed contours) with the three PIRATA buoys (colour shading) extending from surface down to 500 m. Monthly-averaged distributions for the PIRATA period 1997-2007.

The warm belt on equatorial region observed in March is well reproduced numerically, as well as the meridional loss of ocean surface heat in North/South directions. In particular, one may see the presence of a well defined pool of warm waters on the southwestern equatorial Atlantic, which is also observed in August. This so-called Southwestern Atlantic Warm Pool (SAWP), is marked by high SST values ($> 27^{\circ}\text{C}$), that extends off the coastline from the equator to about 12°S during austral winter. According to Huang et al. (1995), the SAWP is one of the regions of warm waters accumulation. In contrast to these warm waters a Cold Tongue region can be defined as a region of relatively cold water ($< 24^{\circ}\text{C}$) that enters the tropical mixed layer west of 30°W in the Atlantic in late boreal spring in response to intensified winds and a shallowing of the thermocline (Figure 4.9 and 4.10).

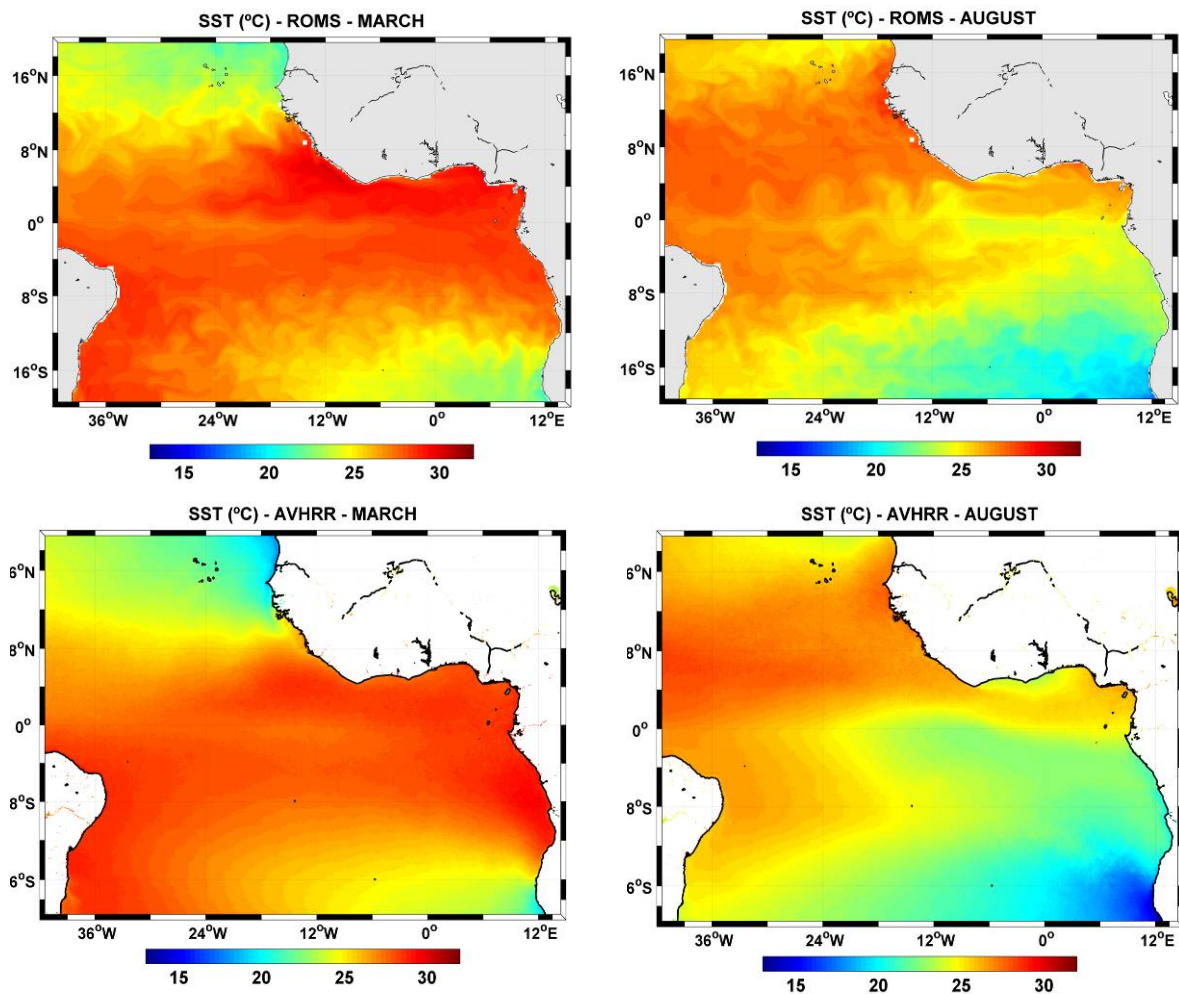


Figure 4.10. Monthly-averaged SST obtained from ROMS model (above) and from satellite observations (AVHRR-NOAA) (below) for March and August.

Chapter 5

5. Near surface transport and Heat budget in the Southwestern Tropical Atlantic using a high-resolution numerical modelling system

The Southwestern tropical Atlantic is an interesting ocean area, acting as a cradle of multiple oceanic-weather forcings of great importance. In this region, part of the South Equatorial Current (SEC) feeds many western boundary currents along the eastern Brazilian edge, thus contributing to the climatic variability over Northeast Brazil. In this chapter, thermal structures, heat budget in the surface mixing layer and mass transports were obtained from climatological ROMS ocean simulations, and analyzed in connection with scarce available long-term observations of PIRATA-SWE dataset.

5.1 The near surface current system along the area

The South Equatorial Current (SEC) divergence occurs in the Southwestern tropical Atlantic, producing a northern and a southern branch along the Brazilian coastline. Towards the north, the northern branch of the SEC termination forms the North Brazil Under Current-North Brazil Current (NBUC-NBC) system (Silveira et al., 1994; Stramma et al., 1995; Rodrigues et al., 2007), one of the most powerful western boundary current in the world. This is the preferential way of connecting the subduction regions of the subtropical South Atlantic, the eastern equatorial and off-equatorial undercurrents, as part of the Atlantic Subtropical Cell (STC), which in turn feeds the equatorial upwelling systems (Malanotte-Rizolli et al., 2000; Schott et al., 2005). This region is also an important highway for the Atlantic Meridional Overturning Circulation (MOC), where the southward flow of deeper North Atlantic Deep Water (NADW) is compensated by the northward transfer of near surface warm and intermediate waters, as well as by the Antarctic Bottom Water (Lumpkin & Speer, 2003; Ganachaud, 2003).

After the bifurcation close to the Brazilian shelf, the SEC also supplies the Brazil Current (BC) propagating southward along the coast of Brazil (Stramma, 1991; Peterson & Stramma, 1991; Stramma et al., 1995). Being in the region of the southeast trade winds and the South Atlantic Convergence Zone (SACZ), interactions between sea surface temperatures (SST) and the easterly atmospheric circulation may play a significant role in local climate fluctuations of Northeast Brazil, a region affected by intermittence of severe droughts or floods (Moura & Shukla, 1981; Rao et al., 1993).

5.2 The ROMS approach

The study case presented here involves the open ocean area near the Brazilian coast. The integration domain is comprised between 5°S and 25°S, 20°W and 47°W (Figure 5.1). An isotropic 1/12° horizontal grid results in 323 x 249 horizontal mesh cells. Vertical discretization has 40 levels. Bottom topography was derived from a 2' resolution database ETOPO2 (Smith &

Sandwell, 1997), and a slope parameter $r = \nabla h/h < 0.20$ is used to prevent errors in the computation of pressure gradient (Haidvogel et al., 2000).

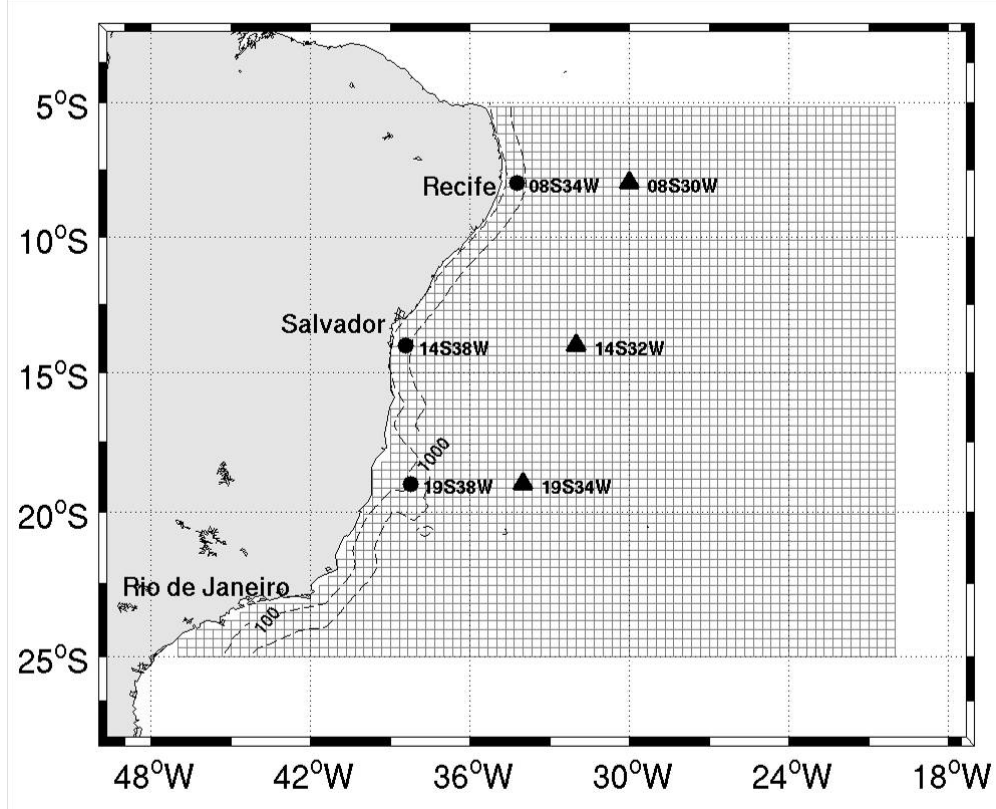


Figure 5.1. Model domain (dashed lines) with the PIRATA-SWE locations (filled triangles) and three sites located along the western boundary region closer to the Brazilian edge (filled circles). Near shore 100m and 1000m isobaths are plotted.

In three open boundaries (north, east and south) an active, implicit, upstream biased radiation condition connects the model solution to the surrounding ocean (Marchesiello et al., 2001). Horizontal Laplacian diffusivity inside the integration domain is zero, and a 12-point smooth increasing is imposed (up to $10^4 \text{ m}^2.\text{s}^{-1}$) in sponge layers near open ocean boundaries. The model equations are subjected to no-slip boundary conditions along the coastline. A basin scale seasonal hydrology derived from World Ocean Atlas 2005 WOA2005 database (monthly climatology at $1^\circ \times 1^\circ$ resolution) (Conkright et al., 2002) is used to infer thermodynamics (temperature and salinity) and geostrophic currents in the open boundaries. The oceanic circulation was forced at the sea surface by winds, heat and fresh water fluxes derived from the Comprehensive Ocean-Atmosphere Data

Set (COADS) monthly fluxes data at $0.5^\circ \times 0.5^\circ$ resolution (daSilva et al., 1994). The model runs from a state of rest for 10 years. The stability is achieved after a spin-up period of about one year. All the numerical results examined in this chapter correspond to averages for the last two years of simulation, except for the snapshots of high-frequency simulations (Section 5.3.1).

5.3 High-resolved climatological ROMS results

Due to its refined spatial resolution ($1/12^\circ$ in latitude and longitude; 40 vertical levels), I should expect the ROMS to resolve the meso-scale dynamics in the region, which isn't sufficiently allowed when OGCMs is used. Thus, as a preliminary test (Section 5.3.1), the high-resolution spatial model accuracy was evaluated by comparing two extreme seasonal model SST snapshots with examples of high-frequency SST patterns provided by satellite measurements. A second type of verification (Section 5.3.2) presented, was to validate the simulated annual cycle of temperature and heat content in the mixing layer depth (MLD). The PIRATA-SWE observations were then used for a rough local thermal evaluation of the model within the first 500m depth. As an early application of ROMS, a third type of interest (Section 5.3.3) is to use the simulated results in order to give insight to our knowledge of the seasonal variation of the main oceanic dynamics components which are at the origin of the annual SST change in that area. Finally, a fourth type of interest (Section 5.3.4) is to look at the yearly averaged oceanic transport simulated by ROMS across zonal sections at the three PIRATA buoy latitudes, as well as a fourth section along these buoys locations.

5.3.1 Instantaneous SST evaluation

The SST patterns for the two mid-month September and March, *i.e.* during two extreme seasonal conditions, is presented as the first illustrations of the model simulation. These figures show mainly a seasonal meridional change in SST along the South Atlantic western boundary. The so-called South Atlantic Warm Pool (SAWP), marked by high SST values ($> 27^{\circ}\text{C}$), extends off the coastline from the equator to about 12°S during austral winter (*e.g.* September, Figure 5.2a) which only includes the region of the northern PIRATA buoy. Six months later, during austral summer (*e.g.* March, Figure. 5.2b), these high SST values invade the whole studied zone, and warmer waters now bathe the three PIRATA buoys. In connection with seasonal meridional extension, the SAWP pattern records seasonal zonal changes, with a more alongshore location during summer. The seasonal colder waters ($< 22^{\circ}\text{C}$) extension at the southern limit of the study domain follows the same meridional progression as the SAWP. These cold waters cross the southern limit of the studied domain during March. However, along the coastline, they remain stationary south of 16°S during all the year (Ikeda & Stevenson, 1978; Carbonel, 2003). It is also noted, as illustrated by these figures, that ROMS succeeds in resolving meso-scale dynamical processes such as frontal structures or filaments.

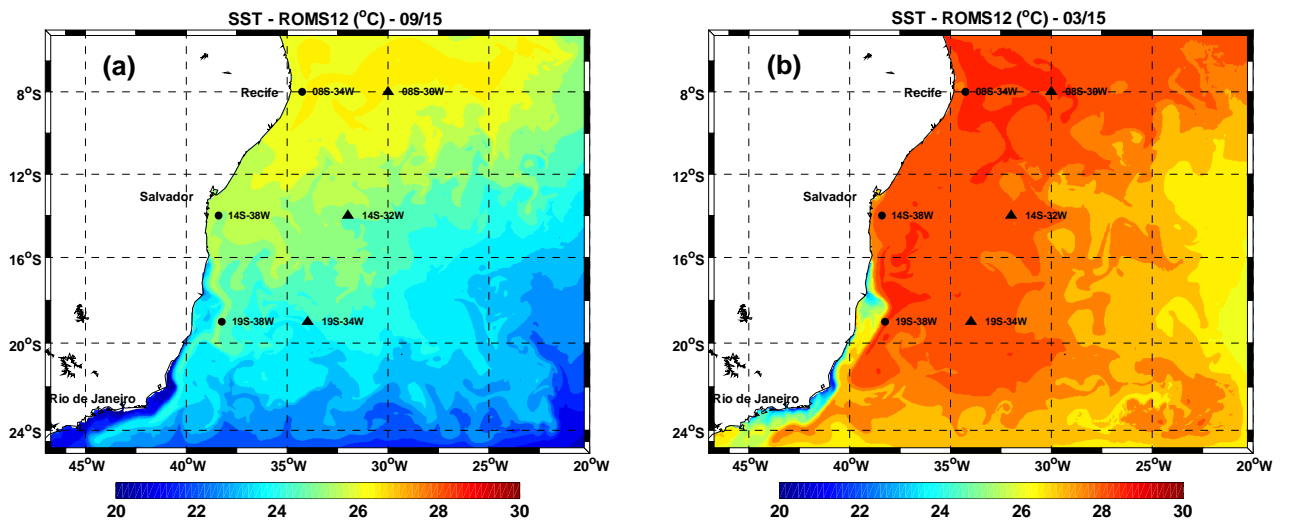


Figure 5.2. Horizontal distribution of SST obtained from ROMS in mid-September (a) and mid March (b). PIRATA-SWE locations (filled triangles) and three sites located along the western boundary region closer to the Brazilian edge (filled circles).

These phenomena, which are particularly visible at the frontier between warm and cold waters on the ROMS results (Figures. 5.2a,b) when using a $1/12^\circ$ resolution ($= 9.25$ km), also appear (slightly more diffuse) in two examples of daily observed SST by satellite also using 9,25 km resolution (*GODAE High Resolution Sea Surface Temperature Pilot Project - GHRSS-PP*, 2007): one in September 15, 2005 (Figures 5.3a), the other one in March 15, 2006 (Figure 5.3b). Due to several individual images used to estimate the satellite SST (process brought about cloud covers) the mesoscale structures seem damped when compared to the model instantaneous SST outputs.

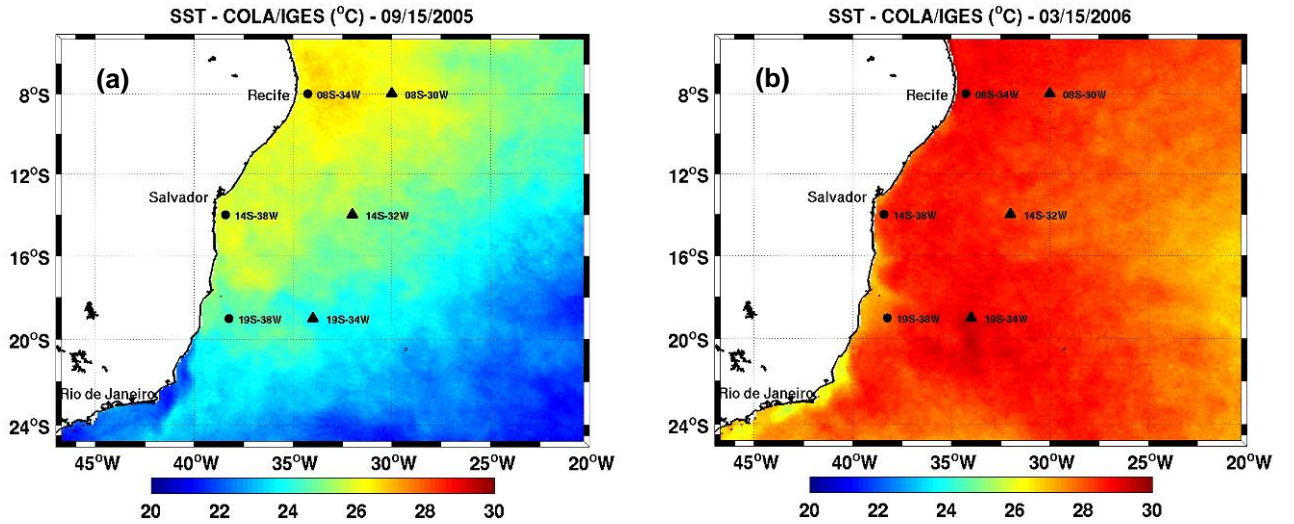


Figure 5.3. Horizontal distribution of SST obtained from observed satellite data on 15 September 2005 (a) and 15 March 2006 (b). PIRATA-SWE locations (filled triangles) and three sites located along the western boundary region closer to the Brazilian edge (filled circles).

5.3.2 Seasonal evaluation of the heat content

Figures 5.4a,b,c provide the seasonal variations of the 0-500m temperature for the three PIRATA-SWE locations ($08^\circ\text{S}-30^\circ\text{W}$, $14^\circ\text{S}-32^\circ\text{W}$ and $19^\circ\text{S}-34^\circ\text{W}$). These Hovmöller diagrams show the ROMS simulated temperature (dashed contours), superimposed by daily observed *in-situ* data (shaded colors) during the initial 2.5 year, approximately, recording of PIRATA-SWE network (September 2005 to February 2008). No-shaded parts

mean missing PIRATA values. A reasonable agreement between ROMS and PIRATA observations is noted, definitely more satisfactory than using an OGCM, even when forced by inter-annual surface fluxes (*e.g.* Nobre et al., 2008). ROMS reproduces the tightening of the thermocline for the most equatorial PIRATA site (08°S-30°W). The opposite situation, the relaxation of vertical gradient, occurs for the two southern sites.

Also of great interest is the apparent capacity of ROMS to simulate intraseasonal variations of the thermocline depth, which clearly occurs for the central and southernmost locations on the *in-situ* data within a 3-4 month periodicity. This is particularly evident on the 19°S-34°W site (Figure 5.4c). These observed variabilities can be partially explained in terms of ocean adjustment to disturbances in the buoyancy field due to the propagation of barotropic Kelvin waves. It causes vertical displacement of isopycnals and propagates with the coastal boundary on the left in the southern hemisphere. Keeping in mind that the present run is only forced by climatological fluxes, let us consider a promising accuracy of the intra-seasonal phenomena if ROMS is forced into inter-annual mode (showed in Chapter 6).

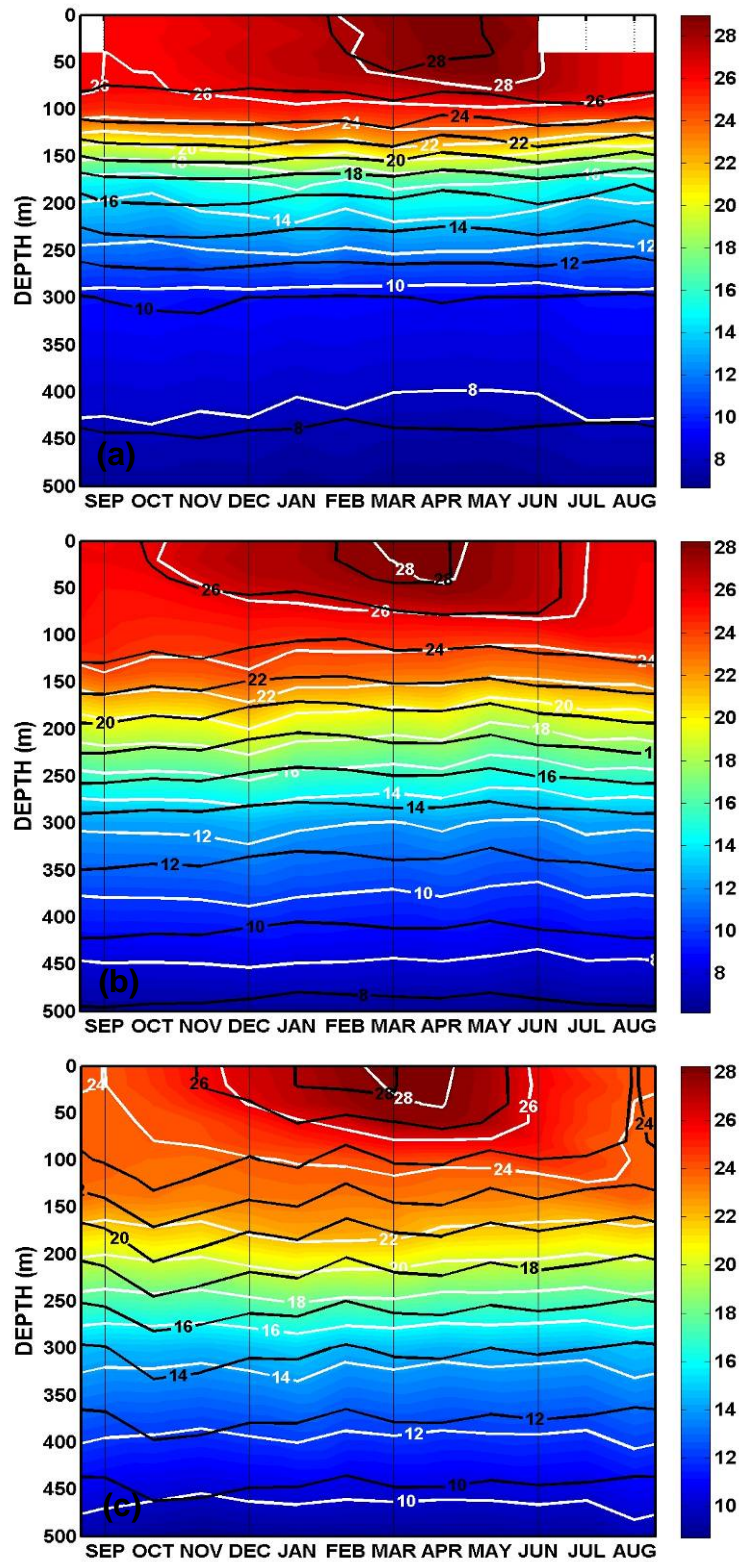


Figure 5.4. Comparison of the monthly mean vertical temperature distribution (°C) provided by ROMS (black dashed contours) with monthly mean for the period of September 2005 to February 2008 of the three PIRATA-SWE buoys (colour shading and white lines) extending from surface down to 500m. The four vertical black thin lines correspond to September 15th, December 15th, March 15th and June 15th. (a) 8°S-30°W; (b) 14°S-32°W; (c) 19°S-34°W.

Detailing the preceding discussion, monthly mean temperature profiles (0-500m) observed by PIRATA-SWE array during September, December, March and June (i.e. as related on Figures 5.4a,b,c) are compared to ROMS outputs for the same calendar months (Figures 5.5a,b,c,d). As shown previously, and though climatologically forced, the vertical distribution of the simulated temperature fairly agrees with the field measurements. In subsurface ($z > 100\text{m}$) the best resemblance ($\Delta < |0.5^\circ\text{C}|$) occurs for the PIRATA –SWE northernmost site ($8^\circ\text{S}-30^\circ\text{W}$) in March.

Such a small difference between model and observation is also noted, in December, for that site in the shallow (0-100m) and deeper (300-500m) waters, as well as for the $14^\circ\text{S}-32^\circ\text{W}$ site in the same month (December, Fig 5.5b). Larger differences ($\sim 1\text{-to-}2^\circ\text{C}$), noted below 200 m for the southern site ($19^\circ\text{S}-34^\circ\text{W}$) in March, for the two other sites for all months plotted, as well as upper 100m to $8^\circ\text{S}-30^\circ\text{W}$ in June, only, continue to be very acceptable considering that the ROMS here is running according to a climatological forcing. Of special interest is the very well reproduced MLD for the three PIRATA sites, whether during warm season ($\sim 20\text{-}30\text{m}$ in March), or cold season ($\sim 80\text{-}100\text{m}$ in September). SST values provided by the model are close to the PIRATA observations, except in September for the southern location, obviously subjected to larger inter-annual variability (see also Fig. 5.3a).

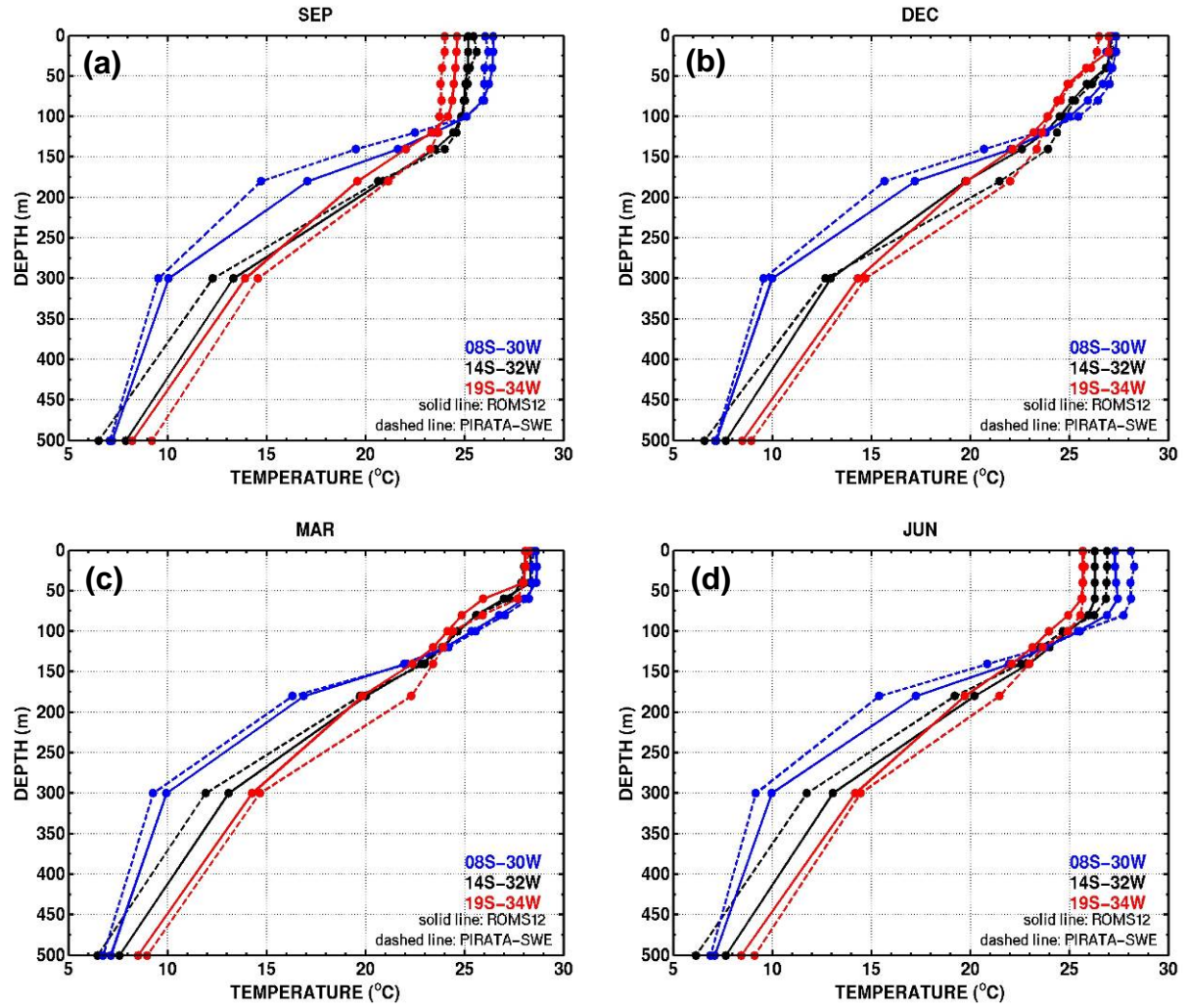
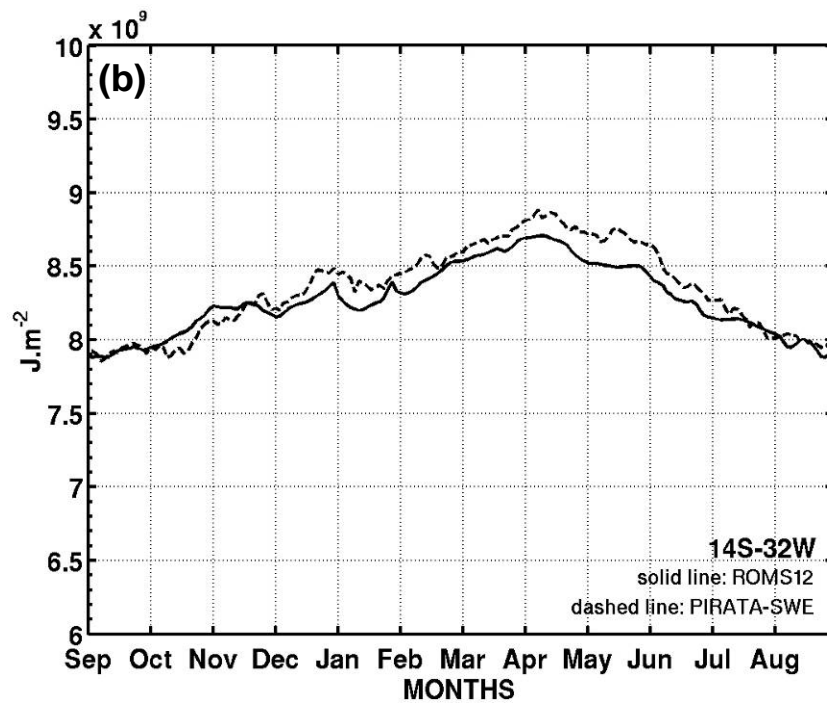
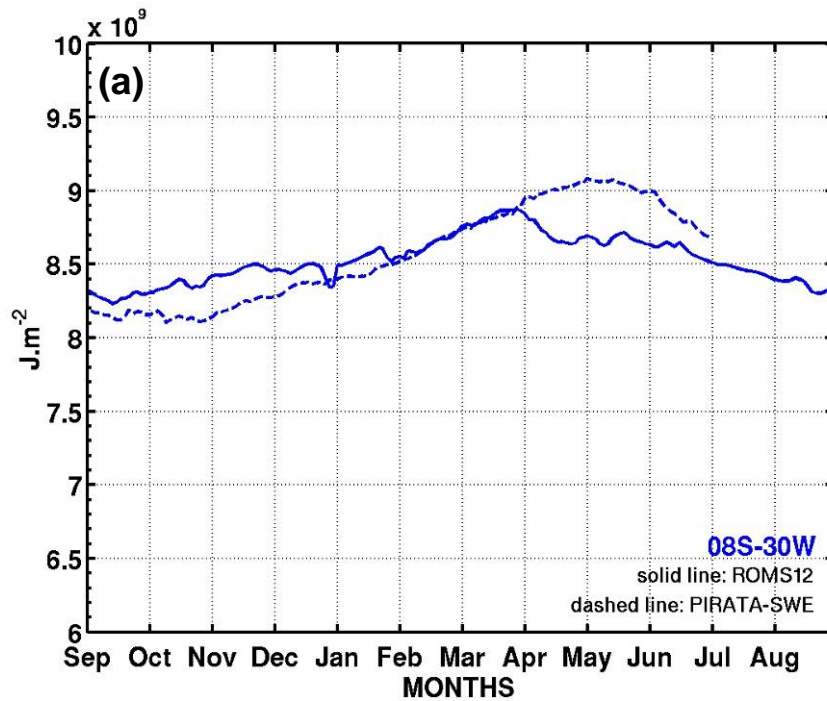


Figure 5.5. September (a), December (b), March (c) and June (d) monthly averaged vertical profiles of temperature 0-500m at the three PIRATA-SWE sites provided by climatic ROMS and by PIRATA monthly averaged profiles from September 2005 to February 2008



(Continue)

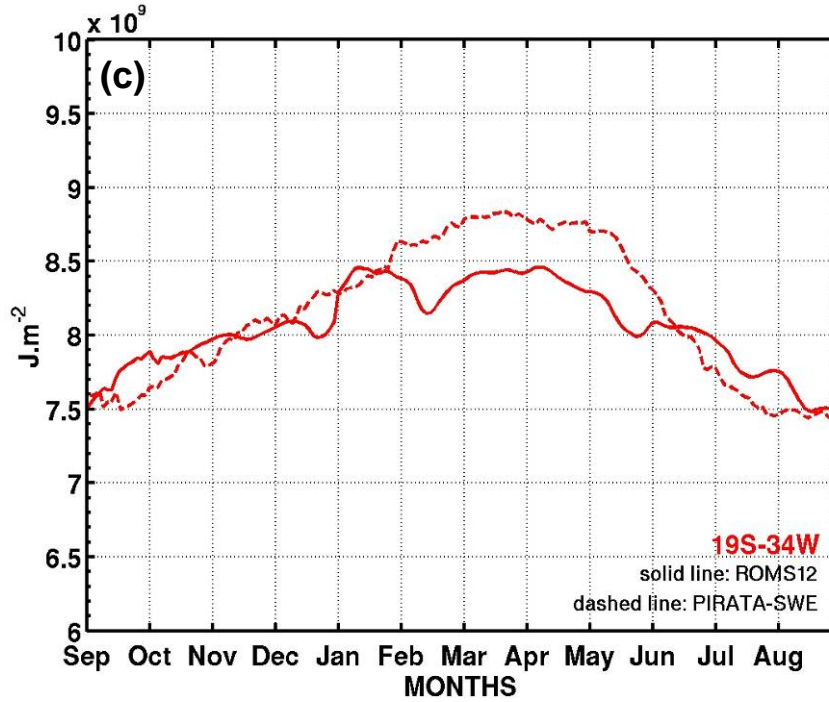


Figure 5.6. Comparison of temporal evolution of seasonal heat content in the mixed layer at 8°S-30°W (a), 14°S-32°W (b) and 19°S-34°W (c), provided by PIRATA *in-situ* observations (dashed line) and ROMS (solid line) for the period of September to August.

Seasonal evolutions of the heat content integrated inside the mixing layer (MLD defined in Appendix) are computed for the three PIRATA-SWE sites (Figure 5.6) according to the ROMS outputs (solid lines), and the *in-situ* PIRATA measurements from September 2005 to February 2008 (dashed lines). Like the previous discussion about the thermal profile comparisons (Figure 5.5), the agreement between simulation and observation here is also very satisfactory, especially for the site 14°S-32°W, *i.e.* the centre of the PIRATA-SWE array, where both observed and simulated curves take very similar shapes. The two largest differences ($\sim 4 \times 10^8 \text{ J.m}^{-2}$), both indicating a greater observed value of heat content *vs.* the climatological simulation, are noted from February to June for the southern site, and from April to June for the northern site.

5.3.3 Oceanic dynamics vs. atmospheric forcing

After checking that ROMS approach is capable of reproducing the ocean thermodynamics in the study region, ROMS results was used to test the relative influence of the ocean dynamics *vs.* the atmospheric forcing for settling the seasonal variation of the mixing layer temperature. For that, the three PIRATA sites are now focused, adding three other locations with the same latitudes as those of PIRATA sites, but along the Brazilian coast (see Figure 5.1).

Considering the local heat budget inside the mixing layer, the different components of the temperature equation can be written as:

$$\underbrace{\frac{\partial T}{\partial t}}_{\text{LOCAL CHANGE}} + \underbrace{U_j \frac{\partial T}{\partial x_j} + \frac{\partial(\overline{u'_j T'})}{\partial x_j}}_{\text{OCEAN (ADVECTION+DIFFUSION)}} - \underbrace{\Phi_T}_{\text{HEAT FLUX}} = 0 \quad (5.1)$$

where U_i is the mean velocity, T (or SST) is the temperature of MLD, and Φ_T is the total heat flux used to force the ROMS (Marchesiello et al., 2003).

Temporal changes of the three terms on the left of Eq. 1 (in °C/Month), as well as T (in °C), have been monthly integrated through MLD, and are presented in Figure 5.7 for the three sites of PIRATA-SWE and the three coastal locations. A first overview indicates that the main seasonal behaviors of the dynamics are very similar in the whole domain, though we note somewhat larger amplitudes in higher latitudes than in equatorial areas, and along the coastline rather than in the open ocean. Highest T (dotted black curves) values are centered around March (from 28.50°C in the northern locations, to 27.75°C in the southern locations), and coldest T values are centered around August-September (from 26.25°C in the north, to 24.00°C in the south). The seasonal change of temperature is roughly of sinusoidal type, except in the southern coastal site (Figure 5.7e), located at the eastern limit of the coldest waters (see Figures 5.2a,b), where T undergoes a rapid reduction of half degree in November-December, thus slowing down the

thermal increase between minimum ($\sim 24.8^{\circ}\text{C}$) in July-August and maximum ($\sim 28.0^{\circ}\text{C}$) in February-March. As related on Eq. 5.1 the local changes in T (continuous black curves on Figure 5.7) results from the combination of net atmospheric forcing (“FLUX” in red) and net oceanic balance (“ADV+DIFF” in blue). In agreement with previous works (*e.g.* Carton & Zhou, 1997), and except for the location 19°S - 38°W , which shall be discussed hereafter, local variations of T are mainly driven by the atmospheric forcing in the sense that positive (negative) values of $\frac{\partial T}{\partial t}$ generally occur during positive (negative) values of “FLUX”. It is however interesting to note that, as opposed to what was generally thought until now for this region, the net oceanic contribution evolves according to an amplitude of the same order of magnitude (until $3^{\circ}\text{C}/\text{Month}$, peak-to-peak) rather than the seasonal variations of atmospheric forcing.

The time duration of positive values of “FLUX”, occurring mainly from August-September to March-April, (*i.e.* when the South Hemisphere is warmer), is significantly longer than the duration of negative occurrences in May-June-July, *i.e.* when the sun is at its northern position. These time durations are slightly modulated according to latitude: close to equator the “FLUX” is positive during a longer period (~ 8 -9 months), while in the south of the study domain, positive and negative periods tend to be of equal duration (~ 6 months). Another characteristic is that the positive values of “FLUX” are generally of larger amplitude than the negative values.

Consequently, in order to maintain the local equilibrium of $\frac{\partial T}{\partial t}$ (a longer duration associated with larger amplitudes) positive “FLUX” must thus be compensated by an inverse net oceanic contribution during the same periods. In fact, “ADV+DIFF” opposes to atmospheric forcing “FLUX” most of the time, with larger and longer negative values during the period August-September to March-April, and shorter and weaker positive values during the remainder of the year, centered around June. Additional analyses carried out from individual oceanic components (not shown here), and confirmed by results from another recent study (Servain & Lazar, personal

communication), brings some additional information: the cooling of the mixing layer by oceanic effect noted here in the whole region comes primarily from a mixing by vertical diffusion between MLD water and deeper colder waters, while the warming by oceanic effect mainly comes from horizontal advection and lateral diffusion.

Let us take a closer look at the 19°S-38°W site, in the southern studied region. It is positioned in a complex region, where the interaction between southward Brazil Current and Vitoria-Trindade ridge, during the austral summer, may induce the formation of cyclonic thermocline eddies, which trap cold waters from an extending upwelling regime north of Cabo Frio (Castelão et al., 2004; Campos, 2006).

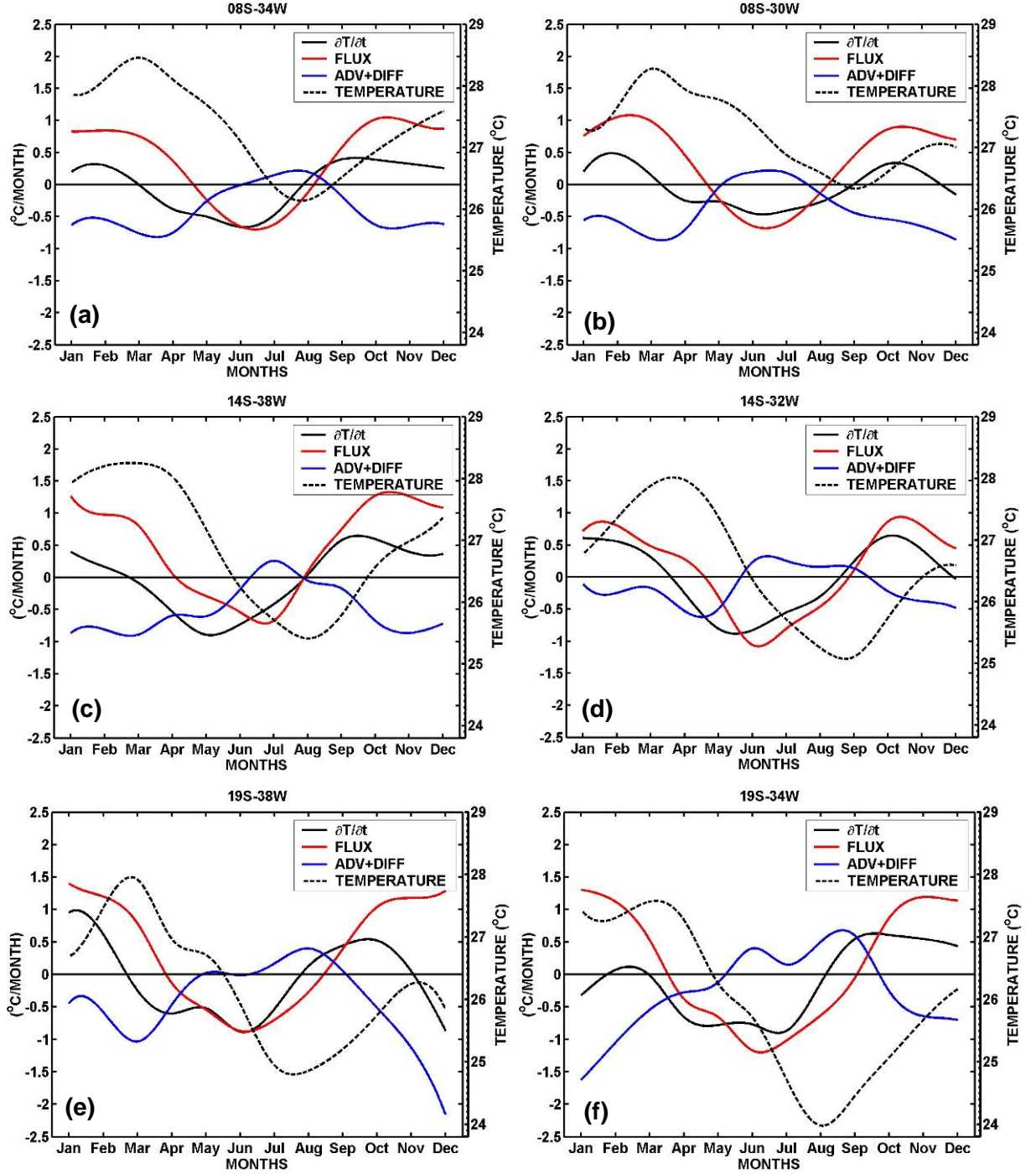


Figure 5.7. Seasonal evolution of SST ($^{\circ}\text{C}$) (black dashed line), atmospheric (red line) and oceanic (blue line) contributions to the local change of SST ($^{\circ}\text{C}/\text{Month}$) (black continuous line) provided by ROMS at 8°S-34°W (a), 8°S-30°W (b), 14°S-38°W (c), 14°S-32°W (d), 19°S-38°W (e) and 19°S-34°W (f) locations.

5.3.4 Mass transports across sections

Mean (yearly averaged) meridional current and transport values obtained from the ROMS simulation along zonal sections (0-1500m) at 8°S, 14°S and 19°S (*i.e.* the latitudes of the three PIRATA-SWE buoys) are presented in Figure 5.8a,b,c. A fourth section (Figure 5.8d) provides current and transport information within the 0-600m across this mooring track. Three density levels are indicated on the plots. The $\sigma_t = 24.5 \text{ kg.m}^{-3}$ separates the upper Tropical Surface Water (TSW) from the upper thermocline waters. The $\sigma_t = 26.8 \text{ kg.m}^{-3}$ (at about 150 m depth) is the lower level of the water supplying the EUC (Schott et al., 1998). The $\sigma_t = 32.15 \text{ kg.m}^{-3}$ (at about 1100 m depth) indicates the lower boundary of the upper warmer waters as well as the lower boundary of the Antarctic Intermediate Water (AAIW). Below 1100 m depth we found the North Atlantic Deep Water (NADW) extending to about 4000 m depth ($\sigma_t = 45.9 \text{ kg.m}^{-3}$). This is the layer where the Deep Western Boundary Current (DWBC) transports southward cold waters from the North Hemisphere.

The zonal sections (Figures 5.8a,b,c) show a clear representation of the NBUC-NBC skirting the coastline from 100 to 1000m, with a northward transport increasing from 5.8 Sv at 19°S to 17.4 Sv at 8°S. The site 8°S-34°W is located above the core of the NBUC which is situated at about 50 km from the coast, at 180-to-500 m depth approximately (Silveira et al., 1994; Schott et al., 2002; Stramma et al., 2003; Schott et al., 2005). These results have been detected from field measurements. Stramma & England (1999) showed from hydrographic data that the SEC bifurcation latitude is 16°S in near surface layer (top 100m), 20°S in the layer (100-500m) and 26°S in the AAIW (500-1200m). Wienders et al. (2000) also used hydrographic data to indicate that SEC bifurcation latitude is 14°S at the surface, 24°S in the (400-500m) layer and around 26°S-28°S in the AAIW.

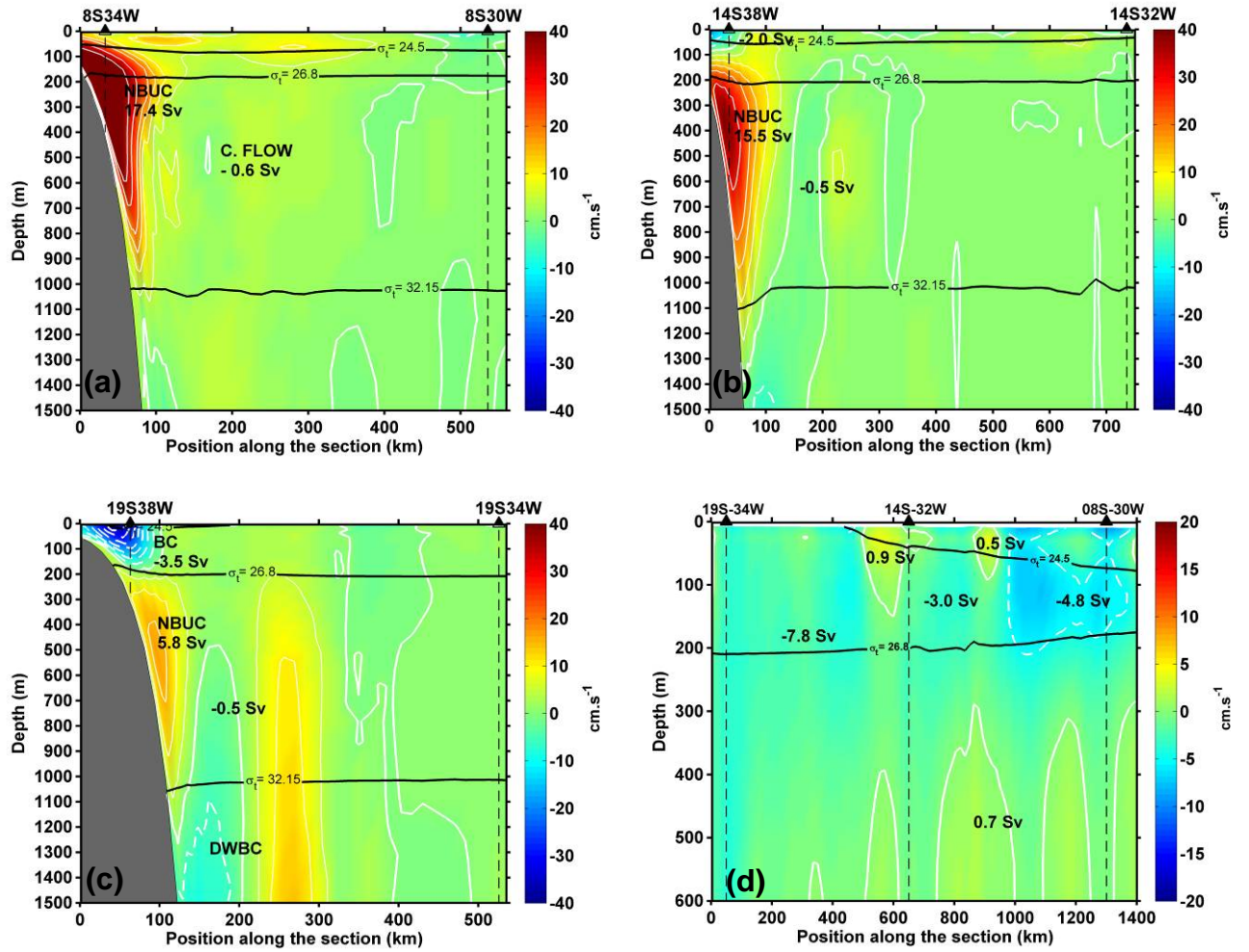


Figure 5.8. Mean annual volume transport averaged across three zonal sections at 8°S (a), 14°S (b) and 19°S (c), and across the section along the PIRATA-SWE array (d). Positive (negative) values indicated by solid (dashed) white lines correspond to northward (southward) currents (panels 8a, 8b, and 8c), while positive (negative) values indicated by solid (dashed) white lines for the section along the PIRATA array correspond to eastward (westward) currents (panel 8d). The three horizontal solid black lines indicate the 24.5, 26.8 and 32.15 sigma-t values (in kg.m-3).

The ROMS results also agree with the numerical findings of Harper (2000), Malanotte-Rizzoli et al. (2000) and Rodrigues et al. (2007), indicating a poleward depth increasing of the SEC bifurcation along the Brazilian edge, as well as its seasonal variability: the SEC bifurcation reaches its southernmost position in July and its northernmost position in November (not shown here).

The flowing southward BC, confined to the shallow and near shore part of the Brazilian continental slope, is especially recognizable on the 19°S section (Figure 5.8c). These numerical results were observed in previous

studies. Miranda & Castro (1981) identified the BC at 19°S as a surface narrow current (~ 75 km) limited to upper 500 m depth. Evans et al. (1983) indicate that BC is still confined and organized above the continental shelf at 20.5°S. The World Ocean Circulation Experiment (WOCE) current-moorings measurements obtained at 19°S pointed out a BC confined to the upper 200 m depth, with a mean southward velocity of approximately 15 cm.s⁻¹ (Müller et al., 1998).

The current and transport section along the PIRATA-SWE array (Figure 5.8d) allows us to have an idea of how the southern part of the SEC extends before reaching the western continental boundary. Indeed, we may note a succession of more powerful westward systems (one core with 4.8 Sv, from 50 to 200 m depth, and with a 300-400 km width) and less powerful eastward systems (each one with a core less than 1.0 Sv, from 0 to 100 m depth, and with a width lower than 100 km). Let us note however that the most important westward transport of 7.8 Sv shallower 600 m between 19°S-34°W and 14°S-32°W PIRATA sites has large extension with small velocity intensity values across the section. Elsewhere in the deeper ocean the E-W transport given by the model results is relatively weak.

According to ROMS simulation, the annual-mean westward transport between 8°S-30°W and 19°S-34°W for the SEC is 15.6 Sv for the upper 600 m, which is in good agreement with observations and previous numerical studies. For instance, Wienders et al. (2000) estimated a westward transport of 21.5 Sv for the SEC within the SACW layer between 7.5°S to 20°S, while the hydrographic data of Stramma (1991) showed a westward SEC transport of about 20 Sv for this same region. Furthermore the recent numerical simulations of Rodrigues et al. (2007) indicated an annual-mean westward SEC transport between 6°S and 22°S (along the meridian 30°W) of 18 Sv.

Chapter 6

6. Interannual high-resolution regional ocean dynamics simulation in the Southwestern Tropical Atlantic

Inside this area there is a complex current system of great importance from an oceanographic point of view, being a key driver for regional climate. A high resolution ocean model has been adapted for the simulation of this system, and it is now forced with interannual data sets to be compared with PIRATA observations. It should be helpful in obtaining a better knowledge of this oceanic system, its dynamic equilibriums and evolutions. The goal here is to analyse the accuracy of a versatile new generation state-of-the-art Regional Ocean Modeling System (ROMS) to reproduce some aspects of intra-seasonal to interannual ocean dynamics and heat contents in the region of the southernmost extension of the westward SEC.

6.1. The high-resolved interannual ROMS approach

The case study presented here involves the open ocean area near the NE Brazilian coast. The integration domain, bathymetry and boundary conditions are imposed as presented in the previous chapter. Changes were made in assimilation of geostrophic currents induced on lateral boundaries, based on a daily-mean (2005-2007) hydrography scale and currents derived from OGCM-ECCO (<http://ecco.jpl.nasa.gov/>). At sea surface these changes were based on daily-mean (2005-2007) wind stress by QuickSCAT (Liu, 2002), combined with monthly-averaged heat and fresh water fluxes derived from COADS (da Silva et al., 1994).

6.2 Thermal structure in Southwestern tropical Atlantic

6.2.1. Instantaneous SST evaluation of interannual simulation

After establishing kinetic energy, in order to validate the numerical results, the model accuracy was evaluated by comparing daily SST surface maps derived from the ROMS model to daily infrared SSTs derived from the *GODAE High Resolution SST Pilot Project* (GHR SST-PP, 2007).

This comparison was done for two different scenarios: September 15th 2005, which corresponds to the austral winter time, and March 15th 2006, which corresponds to the austral summer time (Figure 6.1). The satellite-derived SST maps have a horizontal resolution of 9.25 km. A full description of the GHR SST-PP can be found on the GHR SST-PP web site at <http://www.ghrsst-pp.org>.

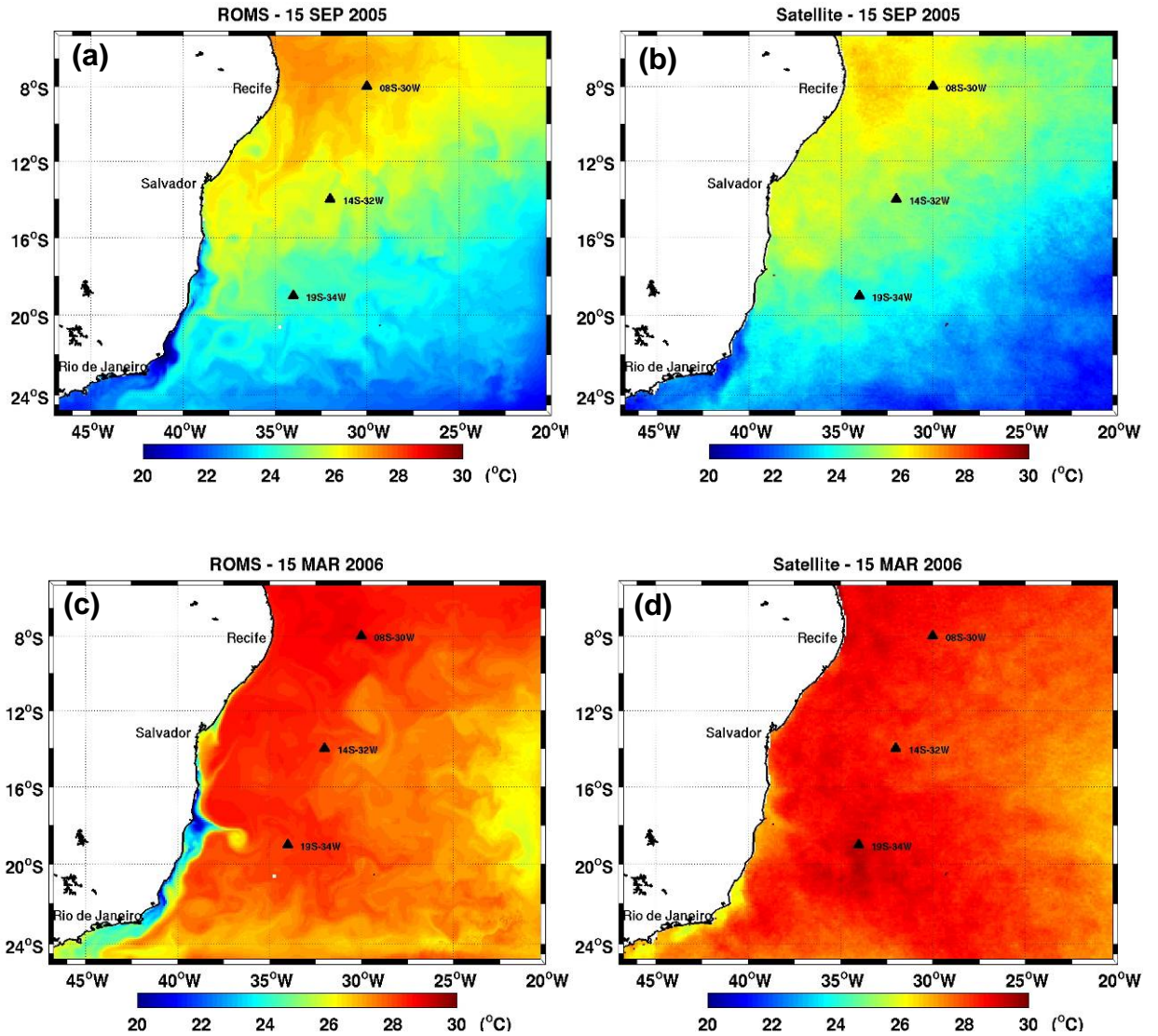


Figure 6.1. Comparison between ROMS-derived SST (a and c) and GHRSSST-PP-derived SST (b and d) for September 15th 2005 and March 15th 2006.

In the region of interest, the model and daily SST satellite patterns are consistent, showing a distinct meridional seasonal change along the South Atlantic western boundary. The so-called Southwestern Atlantic Warm Pool (SAWP) (Huang et al., 1995; Nobre et al., 2005), which is marked by high SST values ($> 27^{\circ}\text{C}$), extends off the South American coastline from the equator to about 12°S on September 15th, 2005, including the northern part of the PIRATA-SWE (Figures 6.1a, b). Six months later, on March 15th, 2006, these high SST values invade the whole area of study, and warmer waters are observed at the three PIRATA buoy sites (Figures. 6.1c, d). Besides its

meridional seasonal migration, the SAWP pattern also records seasonal zonal changes with a more eastward extension during the summer, especially in the northern part. The seasonal spreading out of cold waters ($< 22^{\circ}\text{C}$) in the open ocean in the southern limit of the study domain follows the same meridional progression as that observed for the SAWP. These cold waters are advected off the southern limit of the study area in March.

Besides the fact that the model accurately reproduces the satellite-derived SST overall, it also resolves the mesoscale dynamical processes quite well, including frontal structures, meanders and local upwelling regions. For instance, the cold water filaments observed in the model outputs for March 15th, 2006 in the vicinity of the Abrolhos Bank (Lat. $17\text{--}18^{\circ}\text{S}$ – Long. $38.5^{\circ}\text{--}39.5^{\circ}\text{W}$) and the Vitória-Trindade Ridge (Lat. 20°S – Long. $34\text{--}38^{\circ}\text{W}$) are good indicators of observed and modeled upwelled waters and mesoscale cyclonic structures previously documented in this area (Schmid et al., 1995; Campos, 2006). Indeed, the modeled SST is especially efficient compared to the satellite-derived SST estimates along the coastline where the infrared retrievals may be cloud-contaminated. Although the horizontal resolution of the model and the GHRSSST-PP SST product are almost the same (~ 10 km), the fine mesoscale surface structures evident in the model results seem to be smoothed in the infrared SST maps. This is probably due to the fact that several individual images and infrared products are combined and used to estimate the SST. For example, it does not seem random that higher differences between satellite and modeled SST are present in late austral summer close to the coastal region between 16°S and 22°S (Figures 6.1c, d); this is a well-known cloudy area under the influence of the atmospheric South Atlantic Convergence Zone – SACZ (Chaves and Nobre, 2004; De Almeida et al., 2007).

6.2.2. Seasonal (2005-2007) evaluation of the subsurface temperature and mixed layer depth

In this second set of model evaluations, samples of local time series of the vertical distribution of temperature given by ROMS are directly compared to the first available two-year period dataset provided by PIRATA-SWE. Figure 6.2a,b,c primarily shows the simulated and observed variations of the 0-500 m temperature profile (Sep 2005-Jun 2007) for the three PIRATA-SWE locations (08°S-30°W, 14°S-32°W and 19°S-34°W). The modeled temperature is represented by black contours (for a two-day period), while the PIRATA temperature appears as white contours (also for a two-day period), and shaded colors (daily). Vertical interpolations were processed on the PIRATA data when only one out of three consecutive temperature sensors along the moored line was dysfunctional. That was the case for the first 50 m level at the 08°S-30°W mooring site from the 10th of November 2006 to the end of June 2007, as well as for the levels below 180 m at the 19°S-34°W mooring from the 3rd of November 2006 to the end of June 2007. Missing values are represented by blank areas. ROMS reproduces well the tightening of the thermocline for most of the northernmost PIRATA-SWE site (08°S-30°W, Figure 6.2a), and the relaxation of the vertical gradient for the two southernmost sites (Figure 6.2b, c). In terms of the seasonal cycle within the mixed layer, the simulated and observed cores of the warmest (>28°C for the near equatorial site, >26°C for the two other sites) shallow waters (0-75 m) occur within the same period of the year. There are, however, a few episodic discrepancies between ROMS and the PIRATA-SWE data in the levels including the thermocline and the layer depths from ~75 to ~200 m for the northernmost site, and from ~100 to ~250 m or even more for the other two sites. For most of these differences, the 26°-to-16°C isotherm depths given by the model are shallower than the PIRATA-SWE observations, extending from a few meters (*e.g.*, the northern site) to a few tens of meters (*e.g.*, the 20°C isotherm depth for a few episodes in central and southern sites). This indicates a relatively permanent cold bias in the model for these depths, which can vary from 0.8°C at 08°S-30°W to more than 2°C at 19°S-34°W at the most. These discrepancies are probably due to the model's difficulty in

accurately reproducing the ventilation of subducted lower-thermocline waters coming from the subtropical South Atlantic Ocean. For the lower levels (*e.g.*, ~16°-to-12°C isotherms) the model again becomes generally consistent with the observations.

The PIRATA-SWE data clearly show intraseasonal variations of the thermocline depth within a 3-4 month periodicity, especially for the central and southernmost locations (Figure. 6.2b, c). This observed variability can be partially explained in terms of an ocean adjustment to disturbances in the buoyancy field due to the propagation of Tropical/Kelvin-Helmholtz instability waves (Proehl, 1996; Polito and Cornillon, 1997; Jochum et al., 2004). These disturbances cause vertical displacement of the isotherms and propagate equatorward keeping the coastal boundary to the left in the southern hemisphere. Of great interest here is the apparent capacity of ROMS to generate such variability in the temperature profile (see the black lines on Figure 6.2b,c around the 20°C isotherm depth), even if simulated and observed fluctuations are not always in phase.

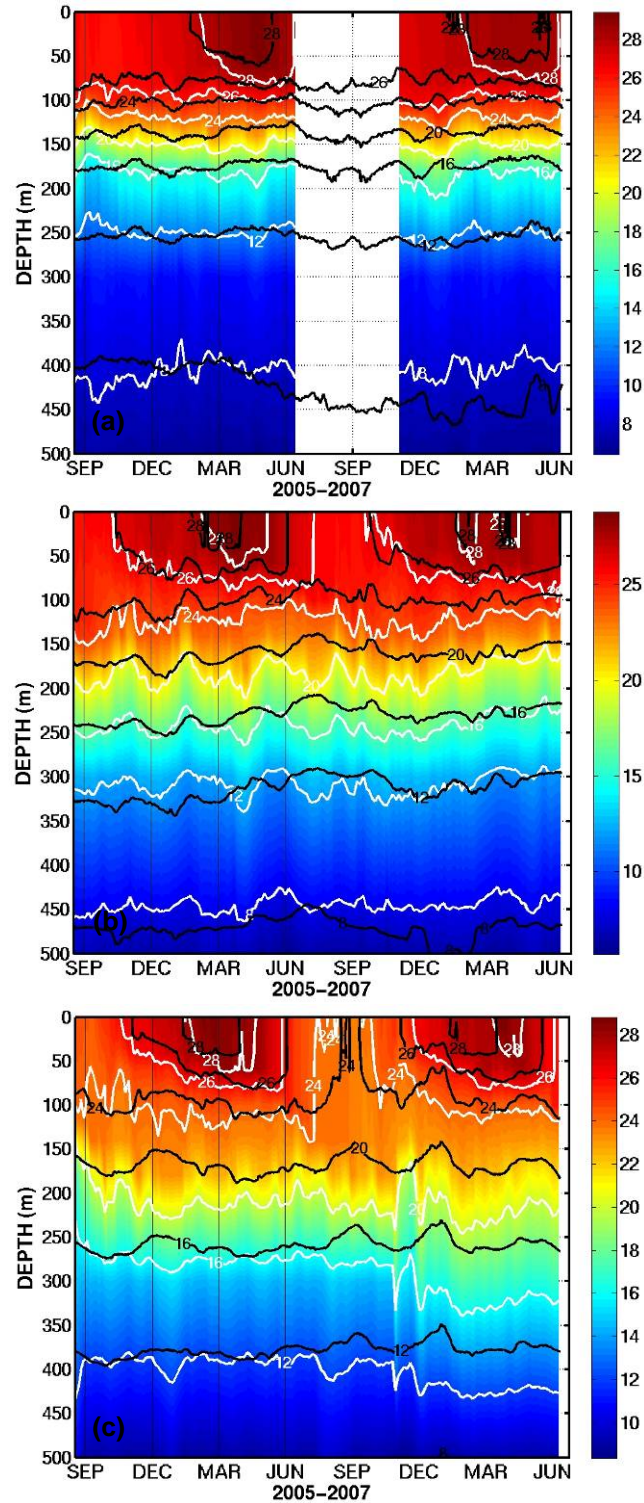


Figure 6.2. Comparison between simulated and observed temperature (°C) variations for the upper 500m from September 2005 to June 2007 for the three PIRATA-SWE locations at (a) 08°S-30°W, (b) 14°S-32°W and (c) 19°S-34°W. Model-derived temperature is represented by black contours and the PIRATA-SWE observed temperature appears as white contours and shaded colors.

In order to gain better insight into the preceding discussion, four selected monthly mean temperature profiles (0-500 m), computed from ROMS outputs, are compared to the observational data derived from the three PIRATA-SWE moorings for the same months (Figure 6.3), *i.e.* September 2005, December 2005, March 2006 and June 2006. For most of the 12 temperature profiles (also marked by vertical black lines on Figure 6.2), the model and observations are in good agreement. This is especially the case during the first two months (September and December 2005), where a cold bias, such as those previously discussed, occurs in September 2005 at 14°S-32°W within 100-250 m, and in December 2005 at 19°S-34°W within 50-300 m. Other examples of limited negative biases are observed in March and June 2006 at these same depths.

We conclude this subsection with an evaluation of the temporal evolution of the mixed layer depth (MLD) for both the model runs and the observations. Following Sprintall and Tomczak (1992), we computed the MLD in terms of temperature and density steps (see the Appendix for details). Note that for these calculations, the number of available levels for the modelled temperature and salinity is 20 for the first 300 meters, *i.e.* two (five) times the temperature (salinity) number of levels of the PIRATA-SWE data for the same depth. Figure 6.4 shows the simulated and observed temporal evolutions of the MLD from September 2005 to July 2007 according to the ROMS outputs (solid lines) and the *in-situ* PIRATA-SWE measurements (dashed lines). The ROMS-derived MLD *vs.* the PIRATA-SWE-derived MLD shows a similar pattern between the model and the observations with a few discrepancies that are more pronounced at the 8°S-30°W mooring site.

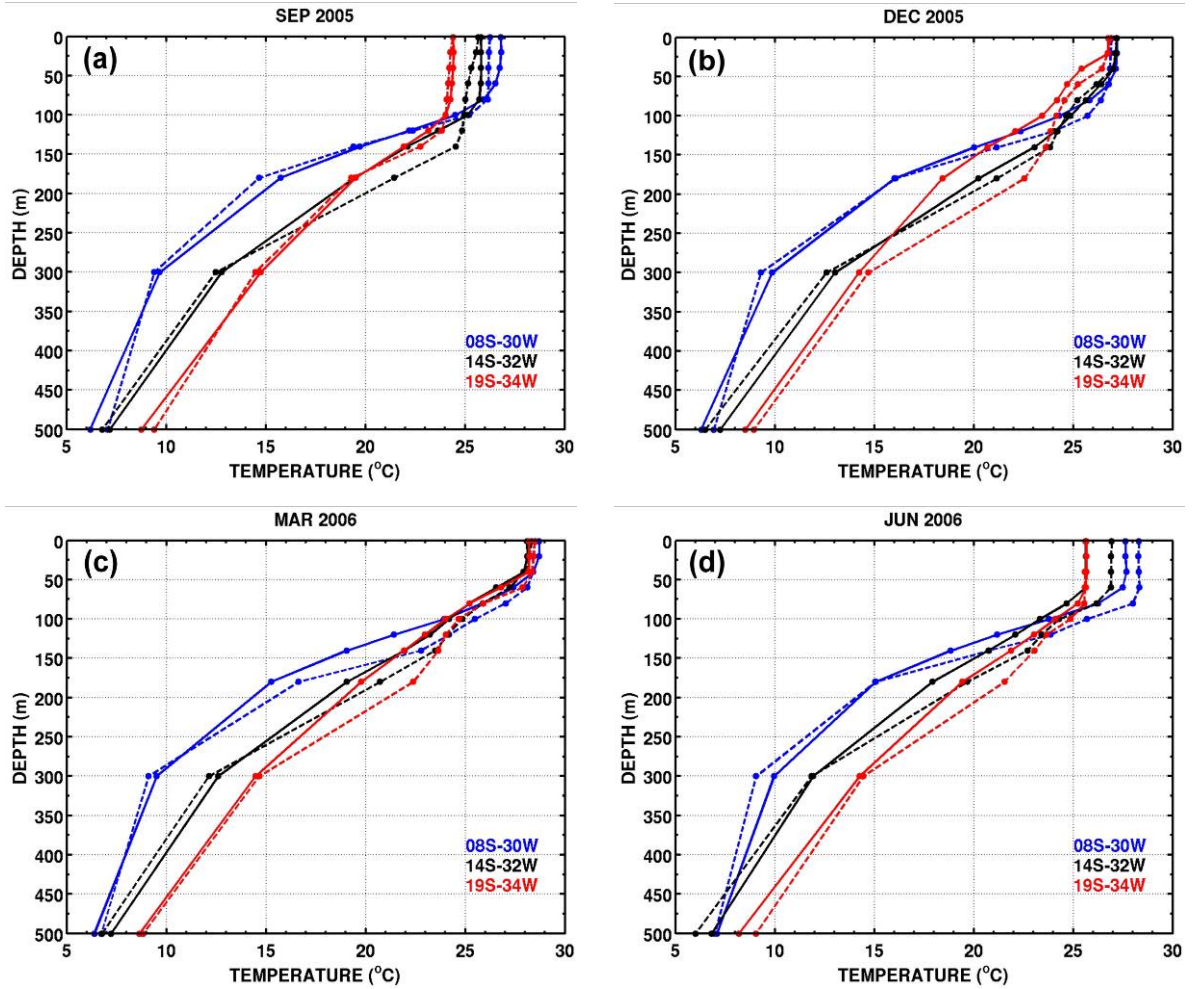


Figure 6.3. Comparison of monthly averaged vertical profiles of temperature for the first 500m between the PIRATA-SWE in-situ observations (dashed line) and the ROMS simulation (solid line) for: (a) September 2005, (b) December 2005, (c) March 2006 and (d) June 2006. Colours are associated to each PIRATA-SWE buoy: 08°S-30°W (blue), 14°S-32°W (black) and 19°S-34°W (red).

The calculated cross-correlation coefficients between observed and modelled MLD signals are 0.65 (8°S-30°W), 0.45 (14°S-32°W) and 0.71 (19°S-34°W) (95% confidence level and 321 degrees of freedom). The cross-correlation coefficient is a measurement of similarity between the signals. Quite good agreement is evident and the observed and simulated MLD curves have similar shapes, ranging from small values (~30-60 m) during the austral summer, to large values that reach up to 100 m at the end of the austral winter. Note that the PIRATA-SWE-derived MLD was not plotted at 19°S-34°W from 10 May to 11 November 2006 due to missing salinity observations in the upper level. Perhaps the largest difference for the MLD estimation between ROMS and in-situ data is noticed here at the 08°S-30°W

site (Figure 6.4a). Indeed, even if the seasonal evolutions are in phase, the simulated MLD is generally systematically shallower (from 0 to about 30 m) than the observational data. This feature is already visible in Figure 6.2, where the ROMS 26°C isotherm depth at 08°S-30°W is always significantly shallower. The systematic underestimation of the MLD at 08°S-30°W seems to be related to the difficulty in estimating observational MLD. The vertical measurements of salinity on the ATLAS moorings are presently limited to only four levels (1, 20, 40, and 120 m) within the upper layer (see section 2.2 on Chapter 2). Another reason for this discrepancy can be related to the use of climatological heat flux to forcing surface layer. One way to investigate this last hypothesis is through a series of case studies to check the model's sensitivity to different forcings.

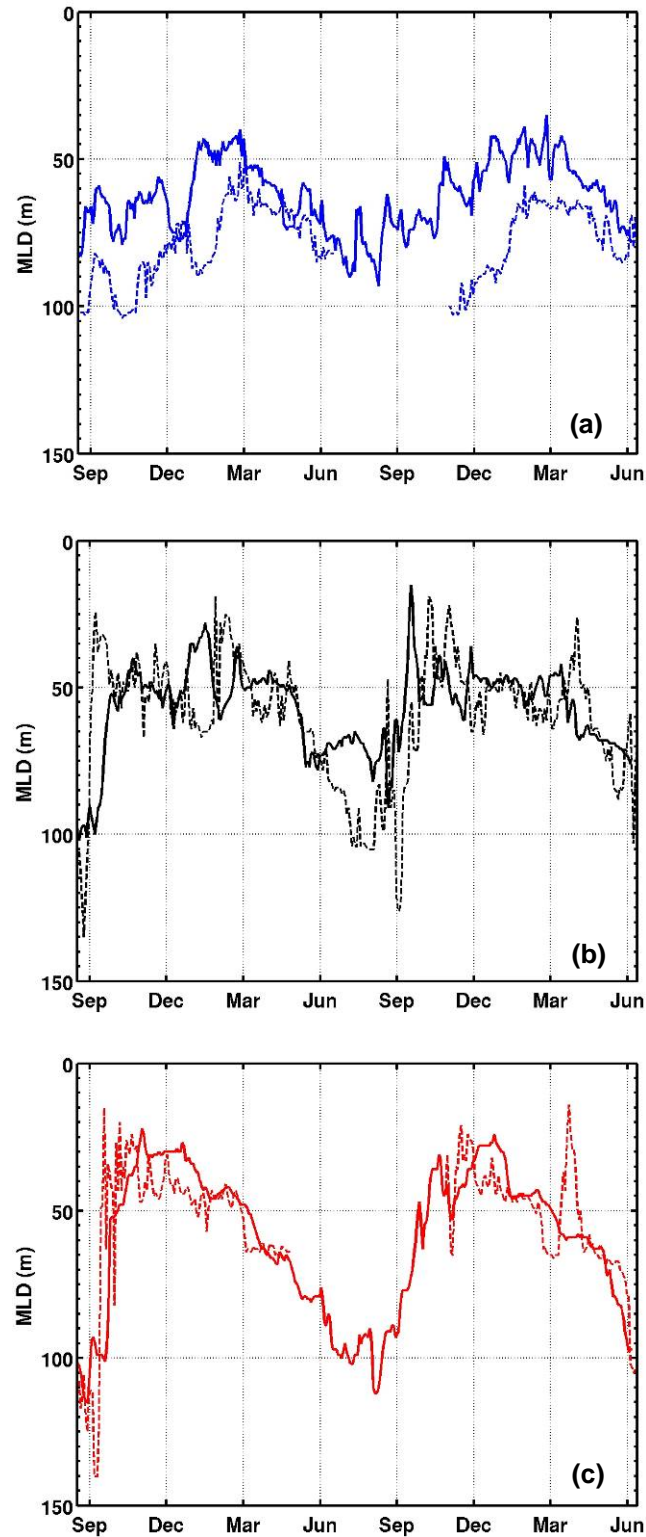


Figure 6.4. Comparison of temporal evolution of seasonal mixed layer depth (MLD) at: (a) 8°S-30°W, (b) 14°S-32°W and (c) 19°S-34°W, provided by PIRATA-SWE in-situ observations (dashed line) with ROMS (solid line) for the period of September 2005 to June 2007.

6.3. Transport and pathways in the Southwestern tropical Atlantic

6.3.1. Meso-scale activity in the Southwestern tropical Atlantic

The averaged (2005-2007) simulated Sea Surface Height (SSH) and the derived surface Eddy Kinetic Energy (EKE) of the study area are presented in Figs. 6a-d. In these figures, the numerical results are compared to the AVISO Rio05 product for the same periods. Mean SSH was obtained from AVISO Rio05, combining hydrographic data, surface drifters velocities, altimetry and a geoid model (Rio and Hernandez, 2004). Simulated and measured surface Eddy Kinetic Energy (EKE) were calculated from SSH gradients with a similar temporal sampling.

The ROMS-simulated boundary systems (Figures 6.5a and 6.5b, respectively) bear good resemblance to those of AVISO Rio05 data (Figs. 6.5c and 6.5d). The similarity of the isocontours as well as the eddy-induced structures along the BC is particularly strong. The highest values are greater than $50 \text{ cm}^2 \text{ s}^{-2}$, found in cSEC and NBUC/BC areas; this holds for both AVISO Rio05 and ROMS. In general, observations show stronger meso-scale activities in the Southwestern tropical Atlantic boundary as compared to the ROMS simulation, but the geographic patterns are similar. It is possible to identify three common characteristic areas of high surface variability that are present in ROMS and AVISO Rio05 EKE charts. First, the near-shore BC patch south of 16°S , where meso-scale cyclonic structures are documented (Schmid et al., 1995; Campos, 2006). Second, along the Brazilian edge, north of Salvador, following the NBUC jet, and finally the zonal band close to the northernmost boundary of the integration domain ($5\text{-}6^\circ\text{S}$), where the central branch of the SEC develops (Lumpkin and Garzoli, 2005). Concerning the coastal region, SSH (and consequently EKE) maps indicate that the NBUC/BC proper is not well represented in AVISO Rio05 dataset. This is probably associated with the partial inability of the altimetry data to accurately capture part of the strong boundary current inertia near the coastline.

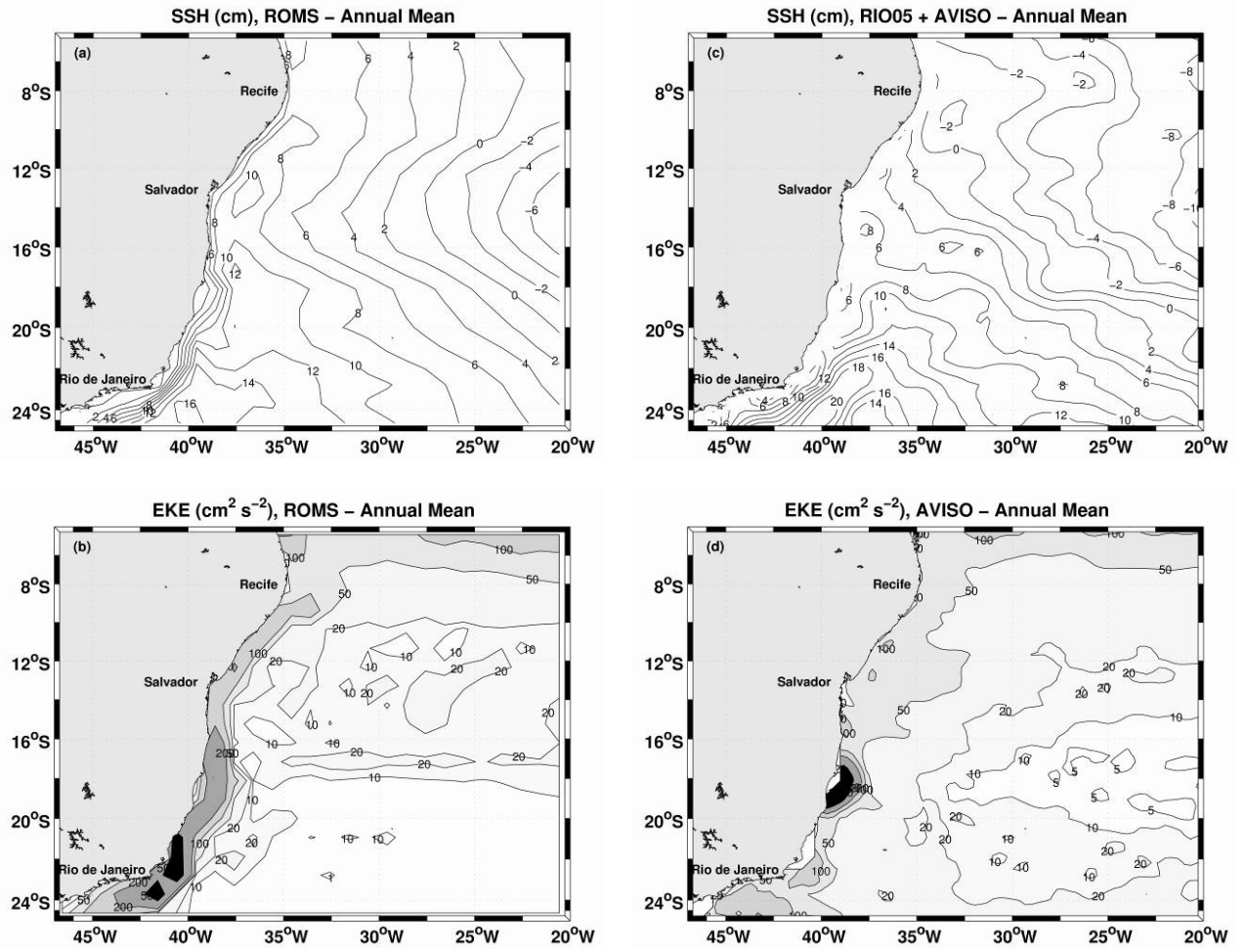


Figure 6.5. Averaged (2005-2007) SSH and EKE comparisons between ROMS simulations and AVISO Rio05 data: (a) ROMS - SSH (cm), (b) ROMS - EKE (cm² s⁻²), (c) RIO05+AVISO - SSH (cm) and (d) AVISO - EKE (cm² s⁻²).

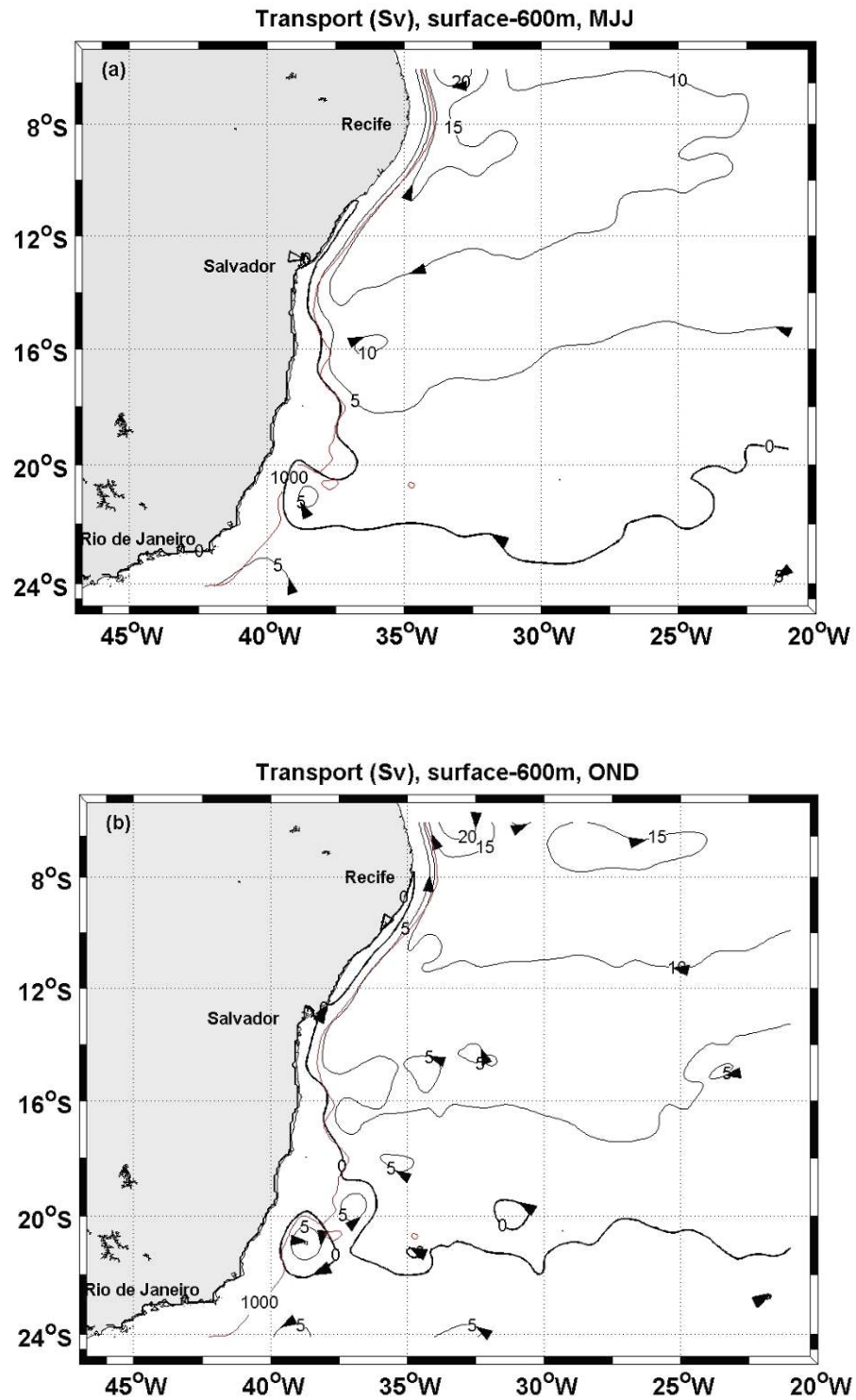


Figure 6.6. Transport function (Sv) for the modelled seasonal averaged (three months, 2005-2007) currents integrated from 600 m to the sea surface for a) MJJ and b) OND. The 1000 m isobath is represented by a red line.

6.3.2. Seasonal (2005-2007) variability of the sSEC/NBUC/BC system

The simulated volume transport in Sv ($1 \text{ Sv} = 10^6 \text{ m}^3 \text{ s}^{-1}$) of the sSEC/NBUC/BC system between the surface and 600 m is shown in Figure 6.6a, b for the averaged period of MJJ and OND (2005-2007), respectively. The first characteristic of ocean circulation expressed in Figure 6.6a, b is the inclination of the transport isolines during MJJ compared to the OND period. Indeed, during OND, when less intense SW trade winds are present, the transport lines west of 24°W approach the continent at more or less constant latitudes. In this case, the southern branch of the SEC, which carries 5 Sv, reaches the coast at about 16°S , while the transport isoline of 10 Sv approaches the land near 10°S . Even during MJJ, characterized by more intense action of the SW trades, the transport isolines of 5 and 10 Sv are clearly tilted in relation to the parallels, approaching the edge of the continental shelf at around 18°S and 14°S , respectively. Through these figures, we can also see a strengthening of the alongshore NBUC transport during the period in which the isolines reach the coast further south, with simultaneous weakening of the transport of BC to the south (MJJ, Figure 6.7a). The inverse situation is observed in Figure 6.6b (OND), when the bifurcation of sSEC occurs further north. In this case, the NBUC is weakened and the BC is intensified (see also Figure 6.10a-b).

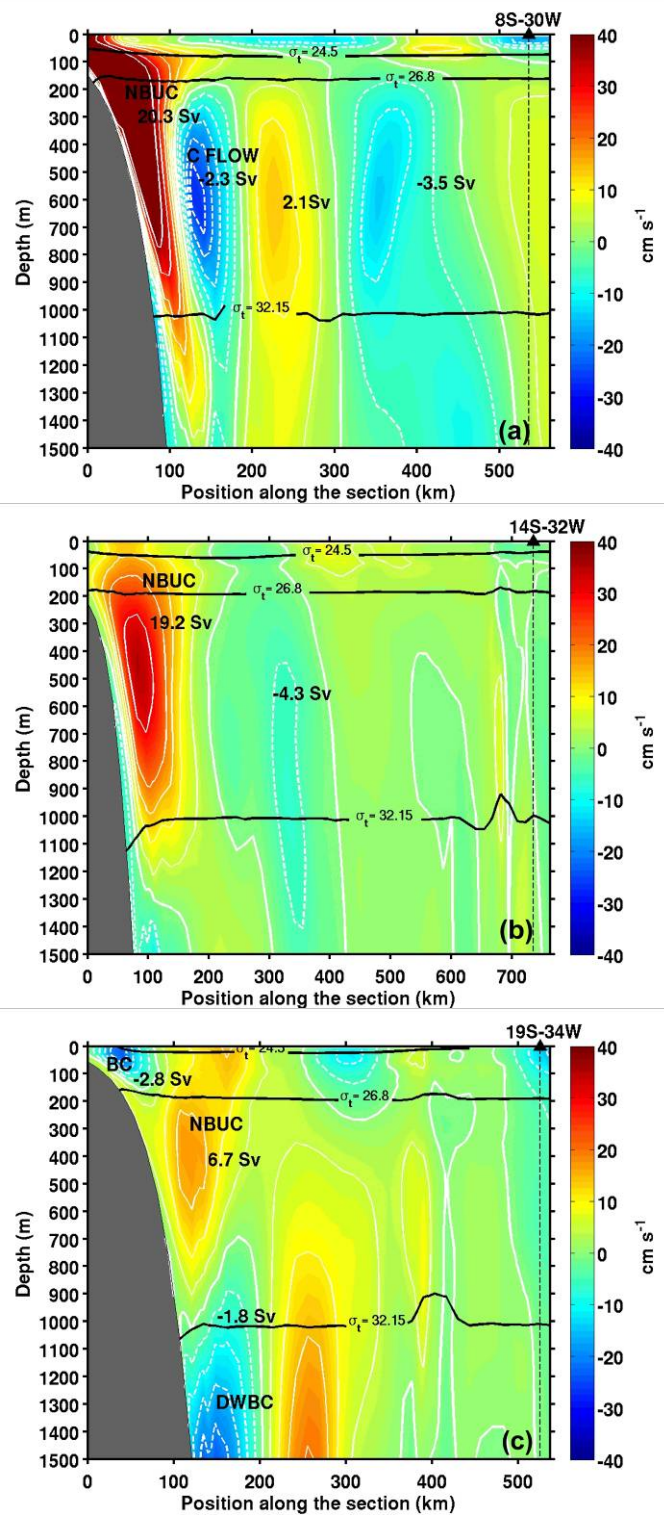


Figure 6.7. Model simulation of meridional current and transport values averaged from September 2005 to July 2007 along zonal sections (0-1500 m) at: (a) 8°S, (b) 14°S and (c) 19°S. Positive (negative) values indicated by solid (dashed) lines correspond to northward (southward) currents.

Meridional current and transport estimates averaged for the period of September 2005 to July 2007 are presented here along zonal sections (0-1500 m) at 8°S, 14°S and 19°S, which correspond to the latitudes of the three PIRATA-SWE buoys (Figure 6.7a-c). Three σ_t levels are selected according to the local dynamics. The first sigma level ($\sigma_t = 24.5 \text{ kg m}^{-3}$) separates the upper Tropical Surface Water (TSW) from the upper thermocline waters. The second sigma level ($\sigma_t = 26.8 \text{ kg m}^{-3}$), which is located at about 150 m, is the lower level of the water supplying the EUC (Schott et al., 1998). The third one ($\sigma_t = 32.15 \text{ kg m}^{-3}$), which corresponds to ~1000 m, indicates the lower boundary of the upper warmer waters as well as the lower boundary of the Antarctic Intermediate Water (AAIW). Below a depth of 1100 m, we found the North Atlantic Deep Water (NADW) extending to about 4000 m. This is the layer where the Deep Western Boundary Current (DWBC) transports southward cold waters from the northern hemisphere.

The zonal mean sections in Figure 6.7a-c show a clear representation of the NBUC skirting the coastline from 100 to 1000 m, with a northward transport increasing from 6.7 Sv at 19°S to 20.3 Sv at 8°S. Along the latitude of 8°S, the core of the NBUC is located about 50 km from the coast, at approximately 50-to-600 m depth (Fig. 8a), and between 250-to-650 m depth at 14°S (Fig. 8b) and at 19°S (Figure 6.7c). Still, in the first 1500 m, the presence of a mean southward flow east of the lower NBUC is observed from the model transects at 8°S and 14°S (*i.e.* 150 and 350 km from the coast, respectively), suggesting a continuous offshore recirculation branch at depths between 200-1400 m. The southward transports of 2.3 Sv at 8°S and 4.3 Sv at 14°S (Figure 6.7a, b) were also found in the LADCP measurements and EOF analysis performed by Schott et al. (2005) and Schuckmann (2006), who found mean representative values of -5.2 ± 4.9 and -4.1 ± 3.7 Sv at 5°S (ship sections) and 11°S (ship sections + mooring array), respectively. There are three possible explanations for the origin of this flow. One could be the deflection of zonal currents. However, no evidence of a southward deflection has been reported in the literature for these currents, because the South

Equatorial Undercurrent and the Southern Intermediate Countercurrent transport stays practically constant between 35°W and 28°W (Schott et al., 2005). A second explanation for this southward flow located east of the NBUC is an inflow from the east as part of the deep cSEC, which deflects southward before reaching the Brazilian coast, and thus forms an offshore counterflow (hereinafter referred as CFLOW) to the deep NBUC. Furthermore, the flow could be explained by a retroflection of the deep NBUC just a little bit north of the northeastern tip of Brazil to supply the southward offshore flow across 5°S, identified in the high resolution (1/12°) MICOM model simulation (Schott et al., 2005). In order to investigate these hypotheses, we plotted in Fig. 6.8 the annual averaged (2005-2007) meridional current (cm s^{-1}) and transport (in Sv) obtained by ROMS for: (a) the along zonal section (0-1500 m) at 7°S, and (b) the depth range of 200-1000 m, where southward CFLOW is stronger (see Fig. 6.7a and b). Despite the proximity of the northern boundary to the integration domain (and as a consequence, of the influence of the numerically-imposed sponge layer condition between 5-6°S), our modeling results plead in favor of the second case mentioned above, *i.e.*, that the offshore counterflow to the deep NBUC is fed by the southernmost limb of the deep cSEC.

Further east of the CFLOW (-2.3 Sv) shown in Figure 6.7a, we can distinguish two main current systems, one to the north with a corresponding transport of 2.1 Sv from 200 to 300 km away from the coast, and another to the south (-3.5 Sv) located between 300 and 500 km from the shoreline. These meridional offshore cores were also found by Schott et al. (2005) between the 9°S and 11°S transects.

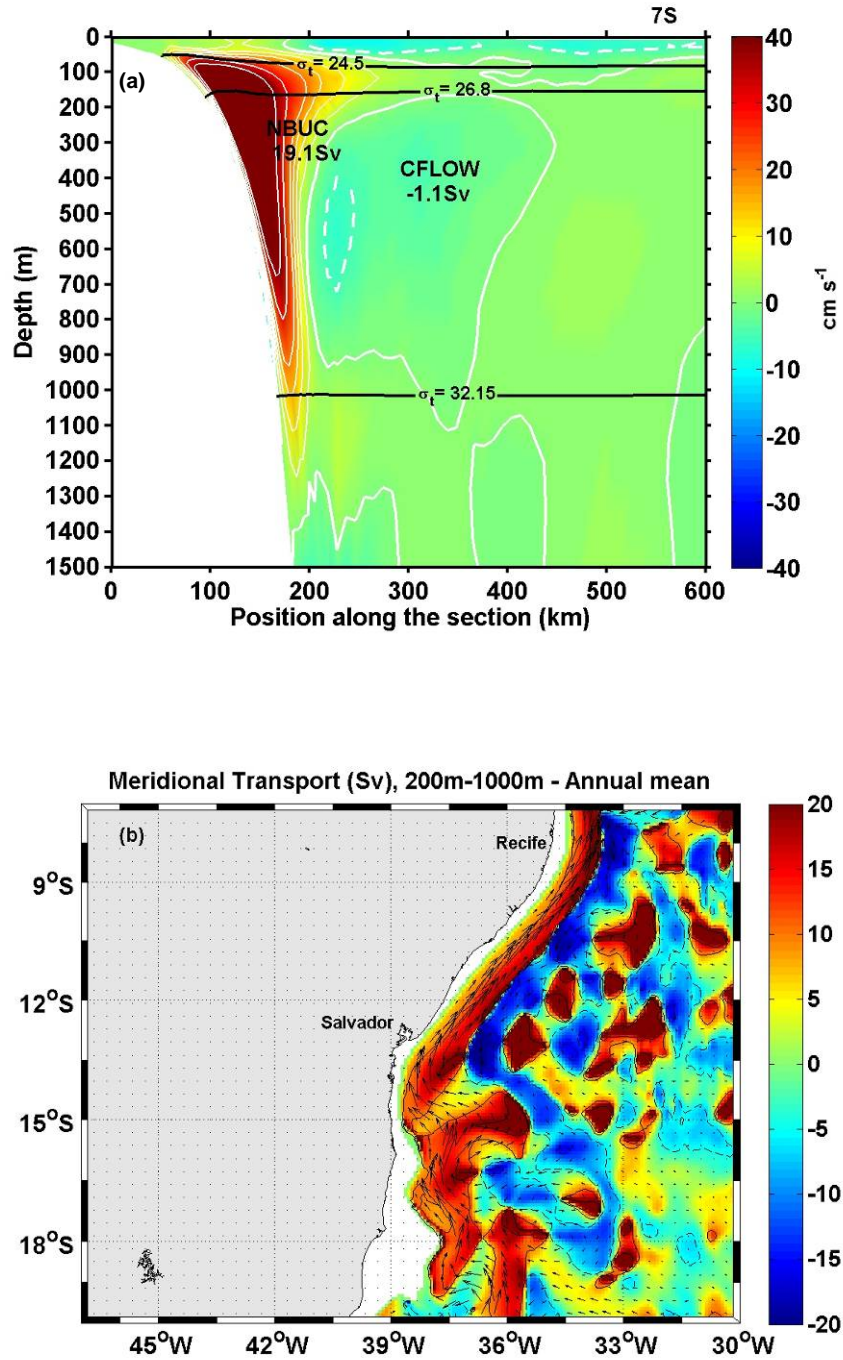


Figure. 6.8. Annual averaged (2005-2007) meridional current (cm s^{-1}) and transport (in Sv) obtained by ROMS for: (a) the along zonal section (0-1500 m) at 7°S. Positive (negative) values indicated by solid (dashed) lines correspond to northward (southward) currents, (b) the depth averaged range 200-1000 m, where CFLOW is stronger

The southward-flowing BC, confined to the shallow and near-shore part of the Brazilian continental slope, is especially recognizable at the 19°S section with a mean transport of -2.8 Sv and meridional velocities ranging from 10 to 20 cm s⁻¹ (Figure 6.7c). Miranda and Castro (1981) identified the BC at 19°S as a surface narrow current (~ 75 km) limited to the upper 500 m. Evans et al. (1983) indicate that the BC remains confined and organized as a coherent flow above the continental shelf at 20.5°S. The World Ocean Circulation Experiment (WOCE) current-mooring measurements obtained at 19°S show a BC confined to the upper 200 m depth, with a mean southward velocity of approximately 15 cm s⁻¹ (Müller et al., 1998). The mean cross-shore section at 19°S obtained here from the 2005-2007 simulations (Figure 6.7c) confirms the presence of a southward BC tight flow (less than 100 km) limited to the top 200 m. At 19°S east of the NBUC flow (6.7 Sv), one can find the upper part of the DWBC transporting cold waters southward (1.8 Sv) above $\sigma_t = 32.15 \text{ kg m}^{-3}$ (Fig. 6.7c).

In our simulation, the sSEC bifurcation reaches its southernmost position in MJJ and its northernmost in OND, which corresponds respectively to the months of July (southernmost) and November (northernmost) found in the climatological runs of Rodrigues et al. (2007). Furthermore, a time variation of the model outputs indicates (Figure 6.9) that the NBUC system strengthens around May 2006 and May 2007, *i.e.* when the sSEC bifurcation reaches its southernmost position, while the BC transport is decreasing at that time until May 2006, when it is practically null. On the other hand, maximum southward BC transports are verified during January 2006 as well as in January 2007 and March 2007, just after the period when sSEC bifurcation reaches its lowest latitudes, with a minimum northward NBUC flow in December 2005 and October/December 2006 (Figure 6.9).

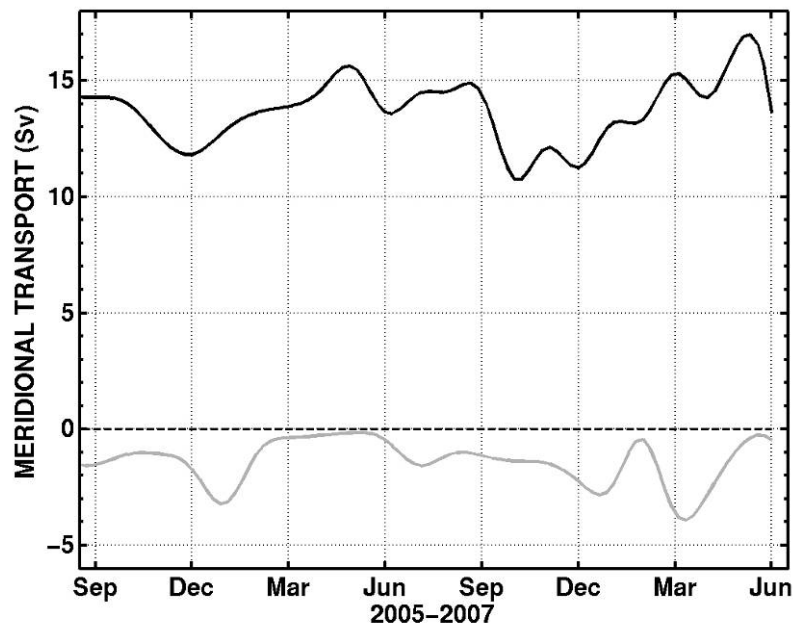


Figure. 6.9. Interannual variability of the North Brazil Undercurrent (NBUC) transport along 8oS (from the surface to 400 m), and Brazil Current (BC) transport along 19oS (from the surface to 400 m), obtained from ROMS simulations for the period of September 2005 to July 2007. Positive (negative) values indicated by the black (gray) line correspond to northward (southward) transports.

The depth dependence of the sSEC bifurcation latitude is abridged in Figure 6.10a, b. In these figures, the sSEC bifurcation is represented by a white line, where the averaged (2005-2007) MJJ and OND meridional velocity (spatially averaged within a 1° longitude band off the Brazilian coast) is zero. The white areas in Figure 6.10a-b represent the Vitória-Trindade Ridge and Abrolhos Bank. ROMS also agrees well with the numerical findings of Harper (2000), Malanotte-Rizzoli et al. (2000) and Rodrigues et al. (2007), indicating a poleward depth increase of the sSEC bifurcation along the Brazilian coastline. Averaged MJJ results in Figure 6.10a show that the bifurcation varies from near the surface at 13°S to 500 m depth at the model boundary at 24°S . During this period, the NBUC is strengthened and the BC weakened. In contrast, the OND averaged results indicate that the bifurcation shifts southward from 8°S at the surface layers to 20°S at 500 m depth, when a weaker NBUC and stronger BC are observed (Figure 6.10b). This southward deepening of sSEC bifurcation along the shoreline results in

a similar poleward depth increase of the NBUC cores, as verified in the 8°S, 14°S and 19°S transects (Figures 6.7a-c). These numerical results have also been detected in field measurements. Stramma and England (1999) and Rodrigues et al. (2007) showed from hydrographic data that the SEC bifurcation takes place at 14-16°S in a near-surface layer (top 100 m), then at 14-20°S in the layer between 100-500 m, and at 21-26°S in the AAIW (500-1200 m). Wienders et al. (2000) also used hydrographic data to indicate that the SEC bifurcation latitude is 14°S at the surface, 24°S in the 400-500 m layer and around 26°S-28°S in the AAIW. More recently, the annual mean dynamic height and geostrophic flow charts generated by Rodrigues et al. (2007) from CTD and bottle data (Curry, 1996) confirmed the poleward shift of the sSEC with increasing depth.

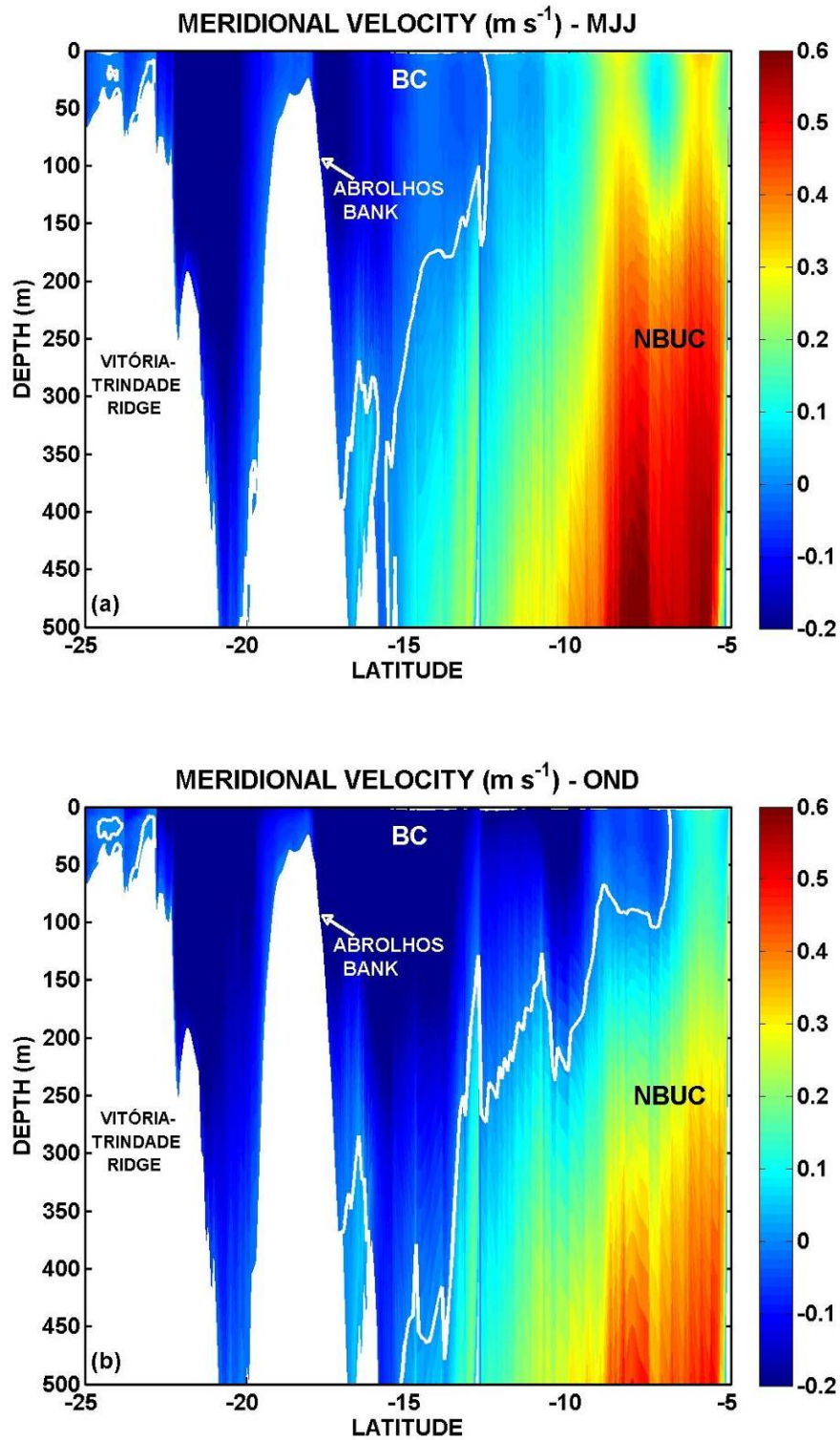


Figure. 6.10. Seasonal averaged (three months, 2005-2007) meridional velocity (m s^{-1}) obtained from the ROMS simulation for a) MJJ and b) OND. The velocities are averaged within a 1° longitude band off of the Brazilian coast. The white line is the contour of zero velocity that represents the bifurcation of the sSEC. The white areas represent the Vitoria-Trindade Ridge and Abrolhos Bank.

6.3.3 Coupling westward sSEC and wind stress

The zonal current and transport averaged from September 2005 to July 2007 along the PIRATA-SWE array indicate how the southern part of the SEC extends before reaching the western continental boundary (Figure 6.11a). Indeed, we note a complex succession of more powerful westward systems. From south to north, we find two near-surface cores of -8.5 and -2.9 Sv, corresponding to the broad and relatively weak sSEC westward flow between 10°S and 19.5°S (Stramma, 1991; Stramma and Schott, 1999; Lumpkin and Garzoli, 2005). More to the north, in the vicinity of the northern PIRATA mooring, a third westward core of 2.8 Sv surfaces as the southernmost part of the cSEC (Lumpkin and Garzoli, 2005). ROMS results also point out a less powerful near-surface eastward core of 1.25 Sv located between sSEC and cSEC. Other subsurface narrow eastward circulations may reach the whole water column between 200 and 1200 m depth (not fully shown in Fig. 6.11a).

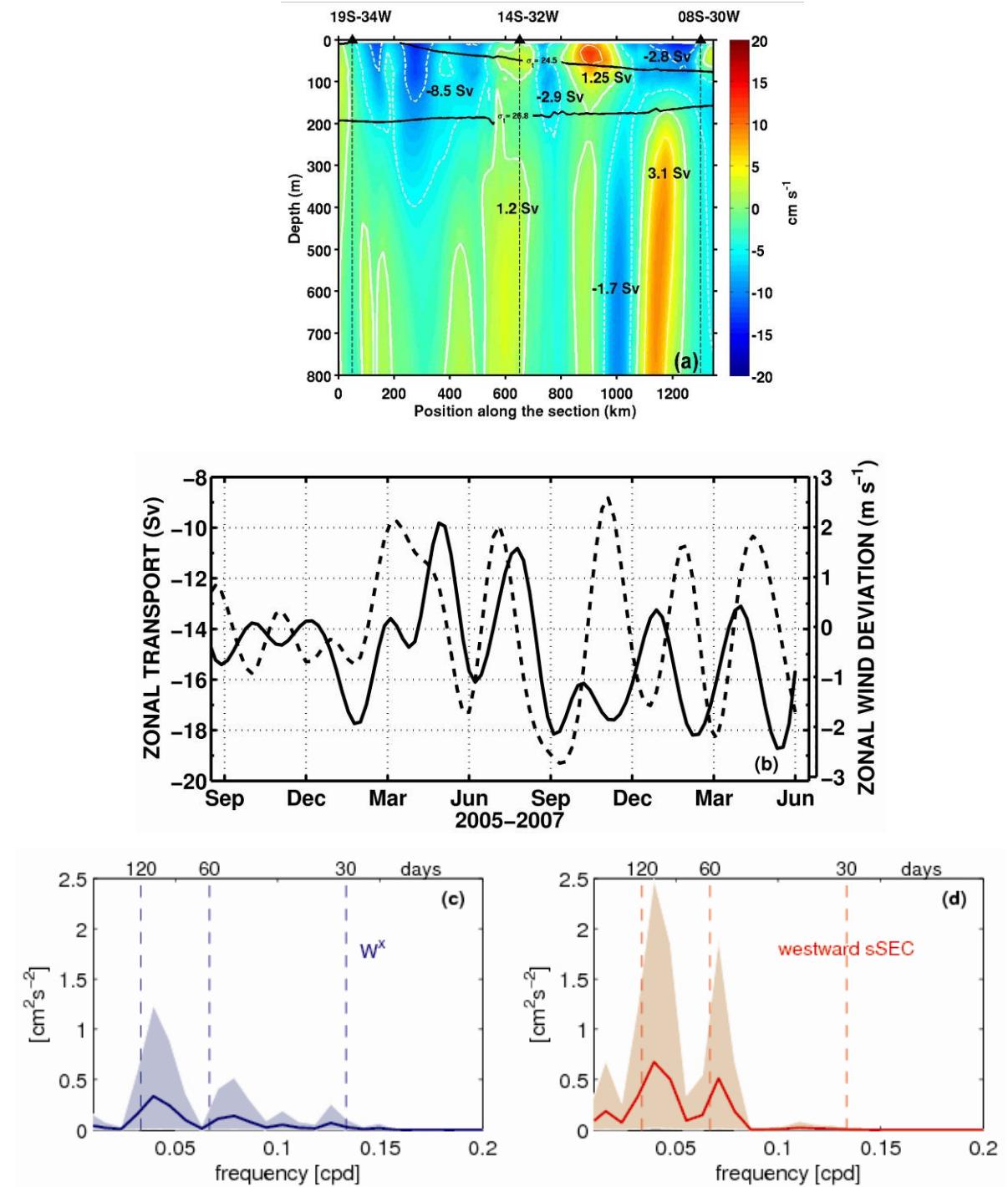


Figure 6.11. (a) Mean annual volume transport averaged across the section along the PIRATA-SWE array between 8°S–30°W and 19°S–34°W. Positive (negative) values indicated by the solid (dashed) lines correspond to eastward (westward) currents. The two horizontal solid black lines indicate the 24.5 and 26.8 sigma-t values (in kg m⁻³), respectively. (b) Time evolution (Sep. 2005–June 2007) of the westward SEC transport (0–400 m depth) obtained from ROMS simulations along the PIRATA-SWE array (solid line), and the QuickSCAT zonal wind speed anomalies over the model domain (dashed line). The variance spectra for: (c) the zonal wind, and (d) westward sSEC transport. The confidence levels are indicated by shaded areas in both spectra.

According to this ROMS simulation, the mean westward transport between 8°S-30°W and 19°S-34°W, corresponding to the sum of the sSEC and cSEC, is -14.9 Sv for the upper 400 m, which agrees well with previous observations and numerical studies. For instance, the hydrographic data used by Stramma (1991) showed a westward SEC transport of about -20 Sv along 30°W for the upper 500 m comprised between 3°S and 19°S. Furthermore, the recent climatological simulations of Rodrigues et al. (2007) indicate an annual mean westward SEC transport between 6°S and 22°S of -15 Sv along the 30°W meridian and down to 400 m. These authors found maximum SEC transports during JFM of about -15.6 Sv, and minimum flows of -14.0 Sv during MJJ. From September 2005 to July 2007, monthly-averaged westward transport (0-400 m depth) obtained from the ROMS simulation across the PIRATA-SWE moorings (Fig. 6.11b), shows large interannual and intraseasonal variability. The weakest westward transport (~10-11 Sv) is noted in mid-2006, while the strongest westward SEC transport (~18-19 Sv) occurs in February 2006, and three times from September 2006 to June 2007. The time evolution (Sep. 2005-Jun. 2007) of the QuickSCAT zonal wind speed anomalies over the model domain is also plotted in Figure 6.11b. Since the mean zonal wind for this region is negative, a positive difference indicates weaker westward zonal winds than the mean, while negative deviation values indicate monthly averaged winds greater than the mean for the simulation period. Positive zonal wind anomalies are associated with a decrease in the upper transport of SEC, with time lags between zero and two months. These values occur in April 2006, July 2006, November 2006, February 2007 and April 2007 (Figure 6.11b). Minimal SEC transports are observed in May 2006, August 2006, January 2007 and April 2007. On the other hand, the negative zonal wind anomalies in Figure 6.11b (December 2006, January 2006, August 2006, September 2006, January 2007 and March 2007), are followed by an increase in the SEC transport, which is observed in February 2006, September 2006, February 2007 and April 2007. In Figure 6.11c-d the zonal wind speed anomalies over the model domain are correlated with westward sSEC transport (0-400 m depth) obtained from the ROMS simulation across the PIRATA-SWE (Sep. 2005 to

Jun. 2007). Since the interest here is in the seasonal signals, a 30-180 day band-pass filter was applied to both the atmospheric and the modeling data to be compared. For the cross-correlation field, the variance-preserving spectra are constructed for the area with higher cross-correlation. The confidence levels are indicated by shaded areas in both spectra. The spectral analysis points out the signal periodicity of both datasets. The calculated maximum cross-correlation between zonal wind and westward transport is 0.51. The spectral analyses show two dominant signals at approximately 90 and 50 day periods for both zonal wind speed and sSEC transport (Figure 6.11c and d, respectively). In addition to seasonal effects, these ocean signals may also represent the westward propagation of Rossby waves, as evidenced in the mooring measurements and analyses of Schott et al. (2005) and Schuckmann (2006).

Chapter 7

7. Regional biogeochemical modelling in the Southwestern tropical Atlantic

In the oligotrophic regions of the ocean, the supply of inorganic nutrients in the euphotic layer may limit the concentration of microalgal biomass, the rate of phytoplankton growth, or both (Marañón et al., 2000). Several mechanisms have been proposed to explain the formation and maintenance of the deep chlorophyll maximum (DCM), which is an oceanographic feature of tropical and subtropical oceans. Higher in-situ growth at the nutricline rather than in the upper mixed layer, and acclimation of phytoplankton to low irradiance, has been suggested (Cullen, 1982) as the cause of DCM formation on subtropical gyres.

Early reports of low productivity in the subtropical gyres (Steeman-Nielsen and Jansen, 1957; Thomas, 1970; Eppley et al., 1973) have been considered to be in error due to methodological deficiencies (Fitzwater et al., 1982). Nevertheless, recent work carried out in oligotrophic regions, using new techniques (Malone et al. 1993; Letelier et al. 1996), presents a large range in the rates of phytoplankton production and growth inside these areas. In fact, this controversy will be maintained, while the lack of

knowledge on temporal and spatial variability in the biology of open ocean still exists (Marañón et al., 2000). Consequently, any uncertainties in the productivity estimates in these areas will have significant effects on the prediction of global biogeochemical models (Marañón et al., 2000). On the other hand, there are few studies on the physical processes related with DCM formation inside the Southwestern tropical Atlantic. Montes (2003) suggests that the support of nutrient inside the euphotic zone, in the Southwestern tropical Atlantic, is maintained by diffusion process in nutricline basis. In this chapter, we use a coupled physical-biogeochemical modelling approach to increase the knowledge of physical processes that contribute to the formation of DCM, and investigate their seasonal variability related with SEC/NBUC/BC system current.

7.1 The coupled ROMS approach

The ROMS version used in this chapter was previously presented in Chapter 3. This modelling was based on physical approach of climatological forcings at the Southern tropical Atlantic grid (Figure 7.1) adopted in Chapter 5. The initial condition to start the biogeochemical model was obtained from WOA2005 (Conkright et al., 2002) for nutrient and from seasonal and annual SeaWifs data (Penven et al., 2008; O' Reilly et al., 1998) for Chlorophyll a, phytoplankton and zooplankton concentrations inside the euphotic layer.

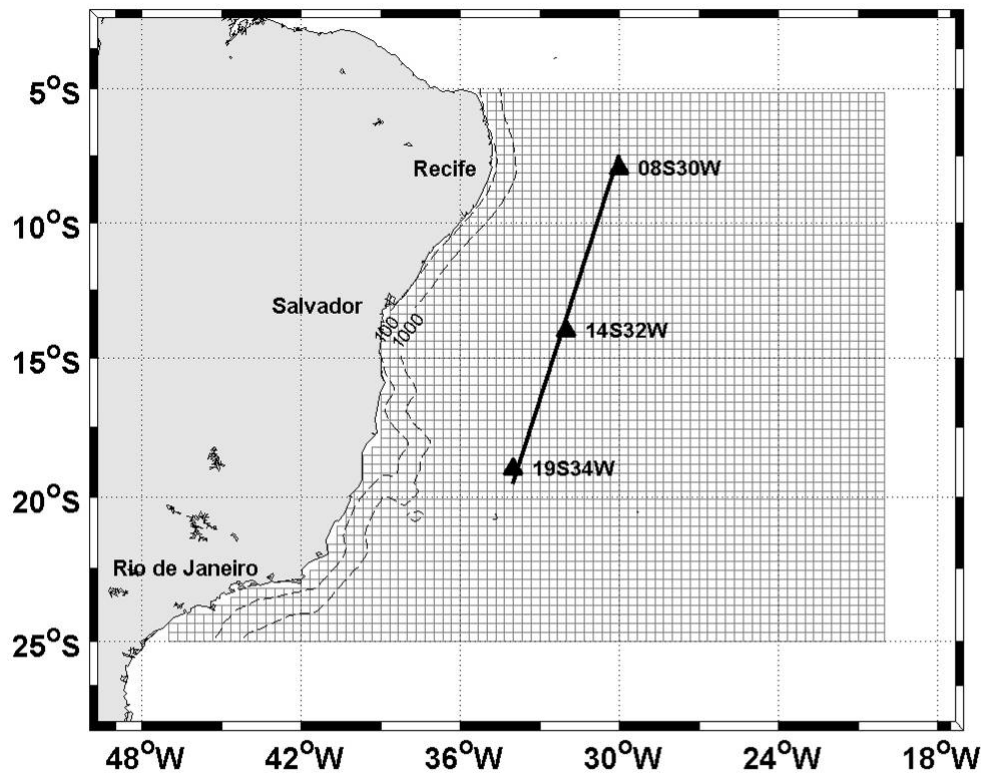


Figure 7.1. Model domain (dashed gray lines) with the PIRATA-SWE locations (filled triangles). Section along three PIRATA-SWE sites (solid lines). Thin dashed lines are 100m and 1000m isobaths, respectively.

7.2 Evaluation of simulated and satellite Chlorophyll *a* data

As a preliminary test to validate the numerical results, the model accuracy was evaluated by comparing monthly mean of chlorophyll *a* surface maps derived from the ROMS model to monthly averaged 2001-2006 daily SeaWiFS Chlorophyll *a* data. This comparison was done for two different scenarios: November, which corresponds to the austral spring (Figure 7.2a,c), and July, which corresponds to the austral winter (Figure 7.2b,d).

In the region of subtropical gyre, the model and SeaWiFS results are consistent, showing a low concentration of chlorophyll *a* in these two months that correspond to oligotrophic areas (Figures. 7.2a, c and 7.2b,d). However the bloom caused by upwelling on the south Brazilian coast is not in phase with SeaWiFS maps. The higher concentrations along the coast occur in July to SeaWiFS (Figure 7.2b) as the ROMS result indicates in November. It suggest that constant primary production and growth rates does not

represent locally the near coast upwelling. Furthermore, along the north boundary (5°S) ROMS indicates concentrations of chlorophyll *a* that does not agree with satellite images. These vortices with blooms discrepancies indicates that boundary conditions applied on NCPZD model can take more influence inside domain that the thickness of relaxation layer of open boundaries, mainly at north boundary.

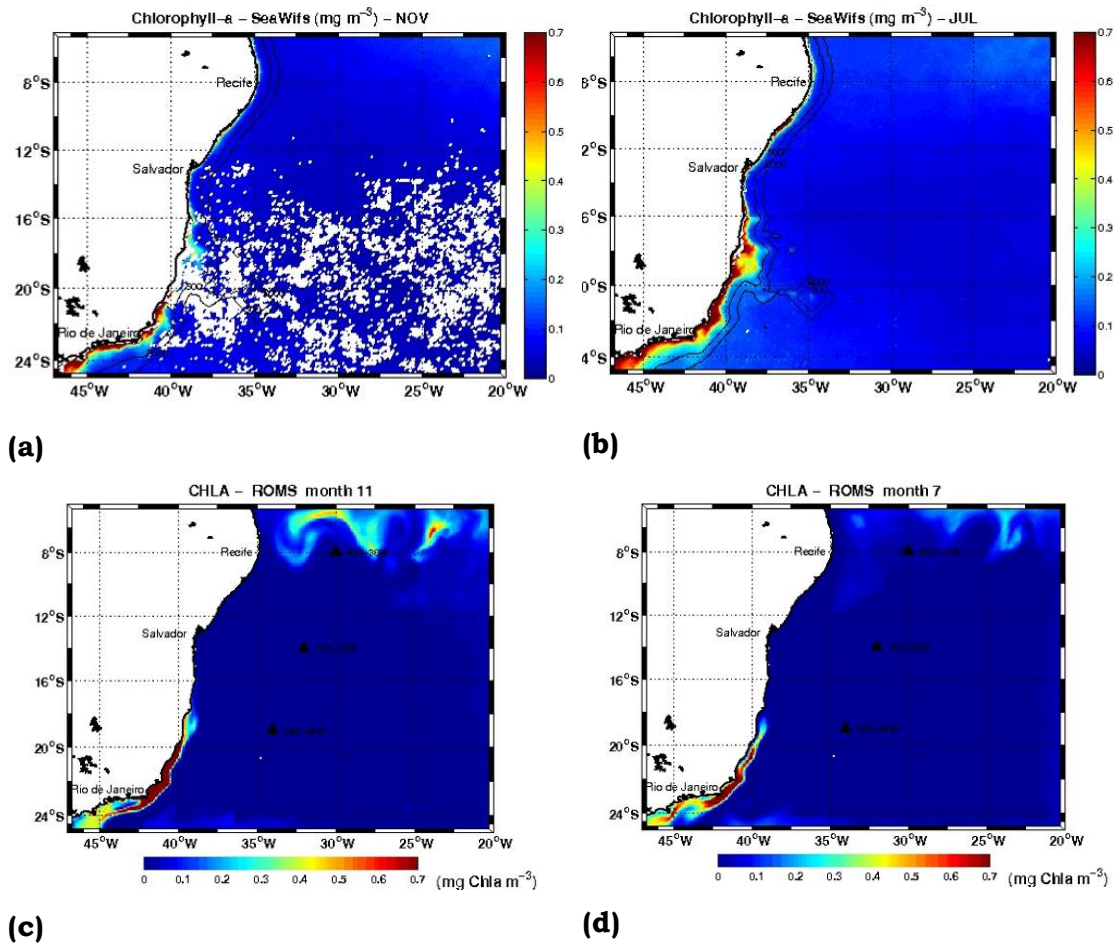


Figure 7.2. Chlorophyll *a* distribution on surface to SeaWifs on: a) November b) July and ROMS results on: c) November d) July

7.3 Salinity intrusion causes and implications

Figure 7.3a presents monthly averaged results of simulated salinity to Maximum Salinity Waters (MSW, hereinafter) values of salinity (salt concentration > 37.5) occur south of 14°S , a region inside the subtropical gyre, with high surface salty waters. At mid-latitude the negative fresh water balance is the main process that contributes to the increase in salinity by high evaporation rates and low rain quantity. Furthermore, the surface forced wind that transports surface waters masses to north are weaker in November than in July. This holds the spreading towards the north of these waters. Figure 7.3b shows an intrusion of MSW between 50 and 110 meters until it reaches near 10°S . The equatorward transport of MSW is due to wind driven circulation (Rodrigues et al., 2007). It transfers surface MSW of subtropical gyre to lower latitudes. This presented result also suggests that the subduction of MSW (finger) and northward spreading, in July, is associated with the presence of lower density tropical water ($\sigma_t < 24.8$) at low-latitudes in the SAWP region. The seasonal variability of MSW along this section causes the occurrence of isohaline layer shallower (deeper) than the isothermal layer in November (July). This has been studied, in the tropical ocean, since the Meteor research cruises in 1936 (Defant, 1961). The barrier layer (BL), which is located between the halocline and the thermocline (Lukas and Lindström, 1991), may isolate the upper isohaline layer from the cold and rich nutrient waters.

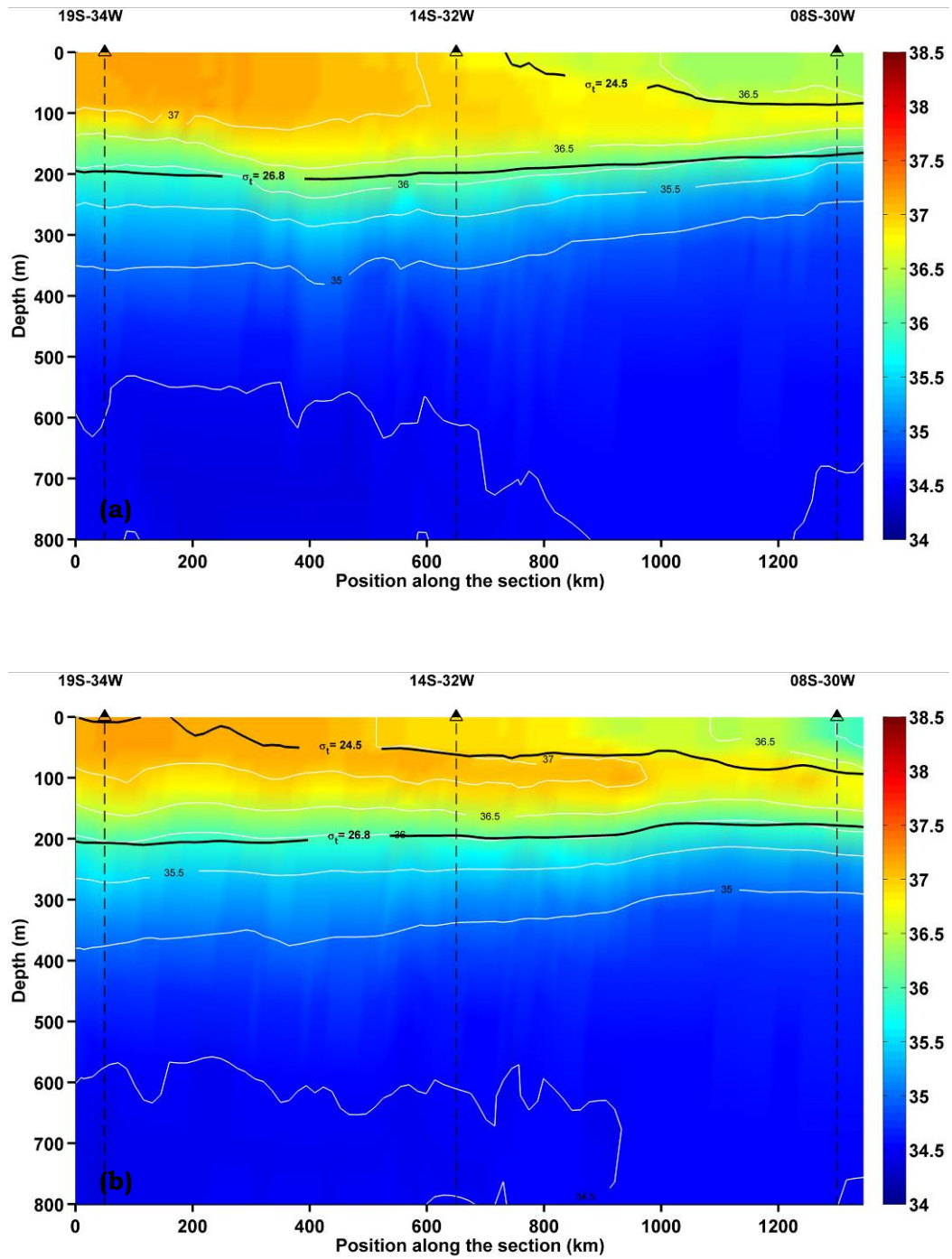


Figure 7.3. Vertical salinity distribution of ROMS along PIRATA-SWE sites on: a) November b) July.

7.4 Seasonal Nitrate concentration

The monthly averaged nitrate results of the biogeochemical model in November and July (Figures 7.4a,b respectively) shows that there doesn't exist great differences between nitrate distributions along this section. Although, small differences that appears in the inclination of nutricline between 14°S and 8°S, following the 36.5 isoline of salinity, shows best agreement with Marañón et al. (2000) results of south subtropical gyre. This small nutricline displacement to a deeper level between the two northern PIRATA-SWE sites, in July, showing more nutricline establishment, may be caused by intrusion of surface and poor nutrient MSW, which comes from mid-latitudes and subducts until it reaches near 10°S (Figure 7.3b). The presence of a null concentration line along the section around $\sigma_t=26.8$, July (Figure 7.4b), indicates that the subduction of poor nutrient MSW, may decrease the nutrient support on upper layers. Besides, in July (austral winter) intensified trade winds, in this region, causes enlargement MLD. On the other hand, in November (Figure 7.4a) at late austral spring, a small and shallow thermocline appears between 19°S and 14°S, due to more intensities of heat flux and weaker trade winds, the null line of nitrate concentration almost disappears. However, low concentrations still are achieved along the MLD. This agrees with Montes (2003) results, suggesting that the major source of nutrients comes from deeper rich nutrient water by diffusion processes.

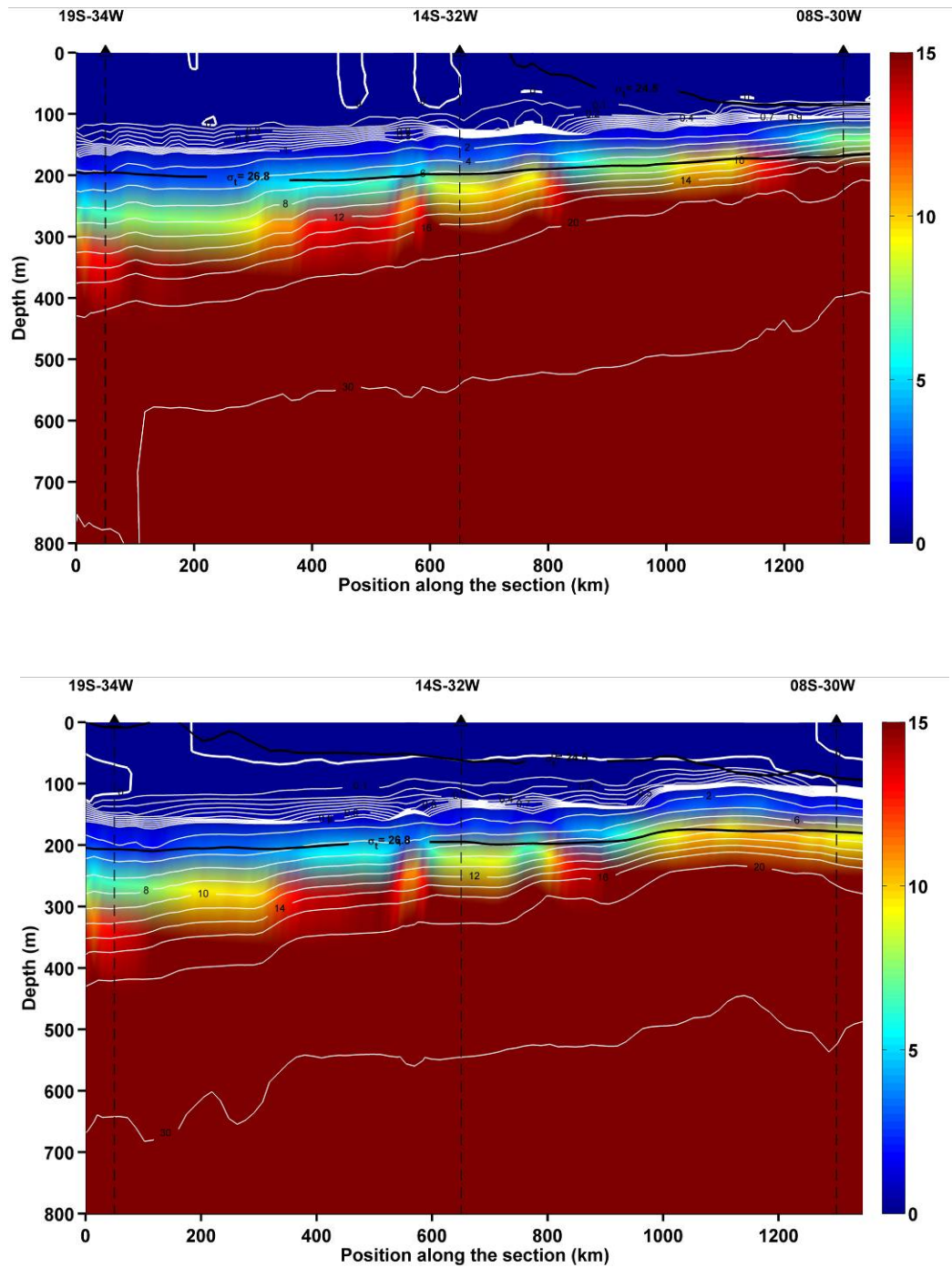


Figure 7.4. Vertical nitrate distribution of ROMS along PIRATA-SWE sites on: a) November b) July.

Chapter 8

8. Conclusions and perspectives

The tropical South Atlantic is a region of complex links between climatic variability of the sea surface temperature (SST) and its heat content in upper layers to an atmospheric convective system as precipitation on the adjacent continent. The main goal of this thesis was to investigate the seasonal and intraseasonal variability of mass and heat transport in two different regions of the South Tropical Atlantic: the equatorial band and the Southwestern tropical Atlantic. In order to achieve the proposed goal, a new generation state-of-the-art ROMS was applied to reproduce the dynamic of these

systems.

Numerical transports and currents results were compared to ocean measurements obtained from oceanography cruises. These comparisons suggest that the climatological modeling approach employed here reproduces the main features of the zonal circulation observed from field measurements. For example, numerical currents and transports distributions showed, in Chapter 4, a very neat distinction between eastward and westward flows along the equator. The model stressed the presence of a EUC core with velocities reaching 0.8 m.s^{-1} , occupying a deeper position in August (80-110 m depth) and shallower in March (50-80 m depth). The transport of EUC ranged from 7.9 Sv (March, at the 15°W cross-equatorial section) to 15 Sv (August, at 25°W). These numerical findings are confirmed by the sea measurements and analysis of Stramma et al (2003), Giarolla et al. (2005) and Brandt et al. (2006). The westward flows of the SECc and the SECn were also well represented by this approach. The transport of SECc ranged from -2.8 Sv (August, at 15°W) to -12 Sv (March, at 25°W), while the SECn intensity ranged from -1.9 Sv (August, at 25°W) to -11.9 Sv (March, at 15°W). Closer to the African shore, the seasonal variation of the equatorial currents transport along the 5°W section shows highest values of the EUC and GC in the period April–August, and lowest values occurring in the period September–March. On the other hand, the SEC seasonality presents inverse standards, i.e., weaker SECc and SECn transports in April–August and stronger westward flows during the period September–March. The thermal structure of the upper 500 m obtained in simulations was compared with PIRATA Program dataset measured at the equatorial moorings. Special

interest can be seen in the very well reproduced MLD for the equatorial PIRATA sites. In particular, the upwelling induced shallower MLD verified by the eastern buoys during austral winter and late spring. The Hovmöller diagrams indicated that the vertical distribution of the simulated temperature agrees with field measurements. Best agreement between model and sea measurements is achieved close the surface on the western part of the Atlantic basin (PIRATA sites 35°W and 23°W). Larger differences (~ 1 to 3°C) are noted between 100 and 300 m for eastern PIRATA sites (10°W and 0°W) in austral winter. The reduced flow in zonal currents observed (and numerically reproduced) in August is associated to the intensification of the equatorial upwelling mechanism in the eastern basin (Stramma and Schott, 1999). These authors also remind us that an equatorial upwelling and downwelling exist on the equatorial currents system but where it takes place exactly is an unsolved question. It seems to be a next interesting research step to be explored with the numerical simulation approach. The seasonal evolution of the Southwestern Atlantic Warm Pool (SAWP) – Cold Tongue system was accurately represented on simulation. This is a very important modelling issue since the eastern part of the Brazilian Northeastern Region is subject to the effects of equatorial easterly atmospheric waves emanating from convection over Africa. The generalized flooding conditions over the coast of this region are observed when pulses of easterly waves encounter warmer SST in the SAWP area (Nobre et al., 2004). These results are very encouraging. The ROMS seems to be capable of reproducing the main features of the mean EUC/NECC/GC and SECc/SECn at different sections along the equator. The verified model adjustment to offshore field data is

promising. For example, these results can be extensively used in the future as boundary conditions for smaller-scale sea modelling, for evaluating the remote influences of the open ocean forcing over the dynamics of the still little studied oceanic islands in the northeastern Brazilian waters.

In Chapter 5, a climatological modelling brings new insights to Oceanic terms (advection + diffusion) responsible for the seasonal evolution of the heat budget inside the upper ocean mixed layer (MLD), which was calculated from numerical outputs and compared with the atmospheric forcing balance. Local illustrations of these results are given for the PIRATA-SWE sites and along the western Atlantic Ocean boundary. It is confirmed that the atmospheric surface fluxes are the main forcing mechanism acting on the heat budget in upper ocean mixing layers. Nevertheless the oceanic contribution is also very important, and can compensate the atmospheric forcing effect in the southern part of the study region. During practically all year, the oceanic component acts as an inversed contribution of the atmospheric forcing. During the warm season, that corresponds for instance (*i.e.* positive effect of the atmosphere) to a relatively strong cooling of the mixing layer mainly by vertical diffusion through the thermocline from colder deeper waters, and, during the cold season (*i.e.* negative effect of the atmosphere) to a weaker warming of the surface waters, mainly by horizontal advection.

These ROMS outputs, in this region, confirm the extreme complexity of the oceanic circulation in this area. Along the virtual track represented by the three PIRATA moorings (about 1400 km), we highlighted no less than six westward currents and four eastward currents on a yearly average. Although

the annual net mass transport across this PIRATA track is normally directed towards the west (18.8 Sv for the upper 600 m, in agreement with early estimations), that indicates that it will not be possible to perform any geostrophic computations using only the density profiles measured by the PIRATA sites. This implies that a continuous observation of the ocean dynamics in this area will be necessary to implement the PIRATA network with other better adapted systems.

Chapter 6 presents the use of ROMS forced by interannual boundary conditions in order to investigate the intraseasonal and interannual variability in the southwestern Atlantic for the 2005-2007 period. After checking that ROMS makes it possible to capture correctly the meso-scale phenomena illustrated by instant SST patterns, numerical temperature values, issued from ROMS simulation, were compared to vertical profiles obtained by the first two years of available data from the recent deployed PIRATA-SWE buoys. Comparison between simulated temperature and *in-situ* temperature data are in good agreement for the first 500 m ocean layer.

These ROMS outputs confirm the extreme complexity of the oceanic circulation in this area. This is obviously the case along the western continental boundary where many alongshore currents coexist and can interact. The interannual numerical results indicate a close relationship between SEC and the western boundary currents flowing along the Brazilian edge. When the sSEC bifurcation reaches its southernmost position (MJJ), the northward NBUC transport is stronger (May 2006, May 2007) and the BC transport decreases. Otherwise maximum southward BC flows are verified during January 2006 and January/March 2007, with minimum

northward NBUC flows in December 2005 and October/December 2006, during the period when sSEC bifurcation reaches its lowest latitudes (OND).

Along the section delineated by the PIRATA-SWE moorings, we highlighted the existence of three strong near surface westward currents alternated by two weak eastward currents on a yearly average. Although the annual net mass transport across this PIRATA track is usually westward (14.9 Sv for the upper 400 m), this indicates that geostrophic computations using only the density profiles measured by the three PIRATA-SWE sites are somewhat misfit. This situation is worsened because the vertical measurements of salinity on the ATLAS moorings are presently limited to only four levels within the 0-120 m upper layer. This implies that for a continuously observation of the ocean dynamics in this area it will be necessary, not only to upgrade the vertical sampling of the PIRATA-SWE network, but, to also certainly implement other adapted systems.

The evaluation of this high resolution regional ocean simulation shows the capability of the model in reproducing the known ocean dynamics in the region and their variability. One can note that it has been achieved on a relatively long period and as a free run (i.e. without the need of artificially restoring the model solution towards observations). Hence, we can analyze now this model solution to rigorously diagnose the dynamical balances and the eddy dynamics.

Chapter 7 presents results of an ecological model that runs coupled with the Climatological ROMS, as set in Chapter 5. Evaluation of monthly mean chlorophyll a between simulated and SeaWifs satellite data on two

different months shows that the model can reproduce main features of primary production in an oligotrophic area limited by nutrients support, where small oscillation in this support can produce high difference in results. The main contribution of this modelling to knowledge of biogeochemical processes around Southwestern tropical Atlantic occurs when this simulation is capable of representing a seasonal wind driven transport. That shows increases in subduction of MSW in July. This comes poor nutrient shallow waters to the thermocline basis. On other hand, small differences between nutrient distribution along nutricline in November and the maintenance of low primary production inside the euphotic zone along the year at the subtropical gyres, confirmed by Marañón et al. (2000), suggest that the vertical diffusion of nutrients acts to balance a deeper mixed layer and decreasing in light availability in July. The use of ROMS coupled with NCPZD could be used in the future as a useful tool to estimate the dispersion of the tuna eggs and larvae in the divergence of SEC (Mullon et al., 2002; Hugget et al., 2003).

A potential outcome of this thesis is the possibility of coupling the ROMS with a dynamically active regional atmospheric model, when SST, heat and freshwater fluxes are calculated from processes which couple both marine boundary layers. These studies are underway. The ROMS can be used with a higher resolution to resolve smaller scales, using improved turbulence closure schemes, or using better surface forcing or lateral boundary conditions. Using the nesting capability of ROMS (Penven et al., 2006), we could also explicitly resolve fast propagating signals across the whole Tropical Atlantic while addressing the coastal response in the

Southwestern region.

References

- Allen, J. S., 1980. Models of wind-driven currents on the continental shelf. *Annual Review of Fluid Mechanics* 12, 389 - 433.
- Arhan, M., Mercier, H., Boulès, B., Gouriou, Y., 1998. Hydrographic sections across the Atlantic at 7°30N and 4°30S. *Deep Sea Research I* 45, 829-872.
- Battisti, D. S., Hickey, B. M., 1984. Application of remote wind-forced coastal trapped wave theory to the Oregon and Washington coasts. *Journal of Physical Oceanography* 14, 887 - 903.
- Blaas, M., Dong, C. M., Marchesiello, P., McWilliams, J. C., Stolzenbach, K. D., 2007. Sediment-transport modeling on Southern Californian shelves: A ROMS case study. *Continental Shelf Research* 27, 832-853.
- Blanck, H. F., 1999. Using TOPEX Satellite El-Niño altimetry data to introduce thermal expansion and heat capacity concepts in chemistry courses. *Journal of Chemical Education* 76, 1635-1646.
- Blanke B., Arhan M., Madec G., Roche, S., 1999. Warm water paths in the equatorial Atlantic as diagnosed with a general circulation model. *Journal of Physical Oceanography* 29, 2753-2768.
- Boulès, B., Molinari, R. L., Johns, E., Wilson, W. D., Leaman, K. D., 1999a. Upper layer currents in the western tropical North Atlantic (1989–1991). *Journal of Geophysical Research* 104(C1), 1361–1375.
- Boulès, B., Gouriou, Y., Chuchla, R., 1999b. On the circulation in the upper layer of the western equatorial Atlantic. *Journal of Geophysical Research* 104, 21151–21170.
- Boulès B., Lumpkin, R., McPhaden, M. J., Hernandez, F., Nobre, P., Campos, E., Yu, L., Planton, S., Busalacchi, A. J., Moura, A. D., Servain, J., Trotte, J., 2008. The PIRATA Program: History, Accomplishments, and Future Directions. *Bulletin of the American Meteorological Society* 89, 1111-1125. doi: 10.1175/2008BAMS2462.1
- Brainerd, K. E., Gregg, M. C., 1995. Surface mixed and mixed layer depths.

- Deep-Sea Research I* 42, 1521-1543.
- Brandt P, Schott FA, Provost C, Kartavtseff A, Hormann V, Bourlès B and Fischer J. 2006. Circulation in the central equatorial Atlantic: Mean and intraseasonal to seasonal variability, *Geophysical Research Letters* 33, L07609, doi: 10.1029/2005GL025498.
- Brink, K. H., 1982. A comparison of long coastal trapped wave theory with observations off Peru. *Journal of Physical Oceanography* 12, 897 – 913.
- Brink, K. H., Stuart, D. W., Van Leer, J. C., 1984. Observations of the coastal upwelling region near 34°30'N off California: Spring 1981. *Journal of Physical Oceanography* 14, 378 – 391.
- Brink, K. H., 1989. Evidence for wind-driven current fluctuations in the western North Atlantic. *Journal Geophysical Research* 94, 2029 - 2044.
- Brink, K. H., 1991. Coastal-trapped waves and wind-driven currents over the continental shelf. *Annual Review of Fluid Mechanics* 23, 389 - 412.
- Camayo, R., Campos, E. J. D., 2006. Application of wavelet transform in the study of coastal trapped waves off the west coast of South America. *Geophysical Research Letters* 33, L22601, 1-5.
- Campos, E. J. D., Goncalves, J. E., Ikeda, Y., 1995. Water mass characteristics and geostrophic circulation in the south Brazil Bight - summer of 1991. *Journal of Geophysical Research* 100(9), 18537 - 18550.
- Campos, E. J. D., Piola, A. R., Miller, J. L., 1999. Water mass distribution on the shelf and shelf-break upwelling in the southeast Brazil Bight. *Annals of the 10th Symposium on Global Change Studies – American Meteorological Society*, 9 - 12.
- Campos, E. J. D., Velhote, D., da Silveira, I. C. A., 2000. Shelf break upwelling driven by Brazil Current cyclonic meanders. *Geophysical Research Letters* 27, 751 - 754.
- Campos, E. J. D., 2006. The equatorward translation of the Vitoria eddy in a numerical simulation. *Geophysical Research Letters* 33, L22607, doi:10.1029/2006GL026997.
- Carbonel, C. A. A. H., 2003. Modelling of upwelling–downwelling cycles caused by variable wind in a very sensitive coastal system. *Continental*

- Shelf Research* 23,1559-1578.
- Carton, J. A., Zhou, Z.,1997. Annual cycle of sea surface temperature in the tropical Atlantic Ocean. *Journal of Geophysical Research* 102, 27813-27824.
- Castelão, R. M., Campos, E. J. D., Miller, J. L., 2004. A modelling study of coastal upwelling driven by wind and meanders of the Brazil Current. *Journal of Coastal Research* 20, 662-671.
- Castelão, R. M., Barth, J. A., 2006. Upwelling around Cabo Frio, Brazil: The importance of wind stress curl. *Geophysical Research Letters* 33, L03602, 1 - 4.
- Castro Filho, B. M., 1985. Subtidal response to wind forcing in the South Brazil Bight during winter. Ph.D. Thesis. University of Miami, USA, 211pp.
- Castro, B. M., Miranda, L. B., 1998. Physical oceanography of the western Atlantic continental shelf located between 4° N and 34° S. In: Robinson, A. R. and Brink, K. H. *The Sea* 11. John Wiley, New York, 209-251.
- Cavalcanti, I. F. A., Kousky, V.E., 2003. Climatology of South American cold fronts. In: VII International Conference on Southern Hemisphere Meteorology and Oceanography, Wellington, New Zealand, 2003.
- Chaves, R., R., Nobre, P., 2004. Interactions between sea surface temperature over the South Atlantic Ocean and the South Atlantic Convergence Zone. *Geophysical Research Letters* 31, L03204. doi:10.1029/2003GL018647.
- Chelton, D. B., Schlax, M. G., Witter, D. L., Richman, J. G., 1990. Geosat altimeter observations of the surface circulation of the Southern Ocean. *Journal of Geophysical Research* 95(C10), 17877 - 17903.
- Church, J. A., Freeland, H. J., 1987. The energy source for the coastal trapped waves in the Australian coastal experiment region. *Journal of Physical Oceanography* 17, 289-300.
- Cirano, M., Campos, E. J. D., 1996. Numerical diagnostic of the circulation in the Santos Bight with COROAS hydrographic data. *Brazilian Journal of Oceanography* 44, 105-121.
- Cirano, M., Mata, M. M, Campos, E. J. D, Deiró, N. F. R., 2006. A circulação

- oceânica de larga-escala na região oeste do Atlântico Sul com base no modelo de circulação global OCCAM. *Brazilian Journal of Geophysics* 24(2), 209 – 230.
- Conkright, M. E., Locarnini, R. A., Garcia, H. E., O'Brien T. D., Boyer, T. P., C. Stephens, C., Antonov, J. I. ,2002. World Ocean Atlas 2001: Objective Analyses, Data Statistics, and Figures, CD-ROM Documentation, National Oceanographic Data Center, Silver Spring, MD.
- Cullen, J. J., 1982. The deep chlorophyll maximum: comparing vertical profiles of chlorophyll a. *Canadian Journal of Fisheries and Aquatic Sciences* 39 (5), 791-803.
- daSilva, A. M., Young, C. C., Levitus, S., 1994. Atlas of surface marine data 1994, Vol. 1, algorithms and procedures, NOAA Atlas NESDIS 6. U.S. Department of Commerce, NOAA, NESDIS, USA, 74 p.
- Davey, M., Huddleston, M., Sperber, K., Braconnot, P., Bryan, F. & coauthors, 2001. STOIC, a study of coupled model climatology and variability in tropical ocean regions. *Climate Dynamics* 18, 403-420.
- Defant, A., 1941. Die absolute Topographie des physikalischen Meeresniveaus un der Druckflächen, sowie die Wasserbewegungen im Raum des Atlantischen Ozean. Wissenschaftliche Ergebnisse Deutschen Atlantischen Expedition auf dem Forschungs und Vermessungsschiff. "Meteor" 1925-1927, 6(2), 191-260.
- Dengler, M., Schott, F. A., Eden C., Brandt, P., Fischer, J., Zantopp, R., 2004. Break-up of the Atlantic deep western boundary current into eddies at 8°S. *Nature* 432, 1018–1020.
- Enfield, D. B. and Allen, J. S., 1980. On the structure and dynamics of monthly mean sea level anomalies along the Pacific Coast of North and South America. *Journal of Physical Oceanography* 10, 557-578.
- Enfield, D. B., 1987. The Intraseasonal oscillation in eastern Pacific sea levels: How is it forced? *Journal of Physical Oceanography* 17, 1860 - 1876.
- Eppley, R. W., Renger, E. H., Venrick, E. L., Mullin, M. M., 1973. A study of plankton dynamics and nutrient cycling in the central gyre of the North Pacific Ocean. *Limnology and Oceanography* 18, 534-551.

- Evans, D. L., Signorini, S. R., Miranda, L. B., 1983. A note on the transport of the Brazil Current. *Journal of Physical Oceanography* 13, 1732-1738.
- Fennel, W., Lass, H. U., 2007. On the impact of wind curls on coastal currents. *Journal of Marine Systems* 68, 128-142.
- Fischer, J., Schott, F. A., 1997. Seasonal transport variability of the deep western boundary current in the Atlantic. *Journal of Geophysical Research* 102, 27751-27769.
- Fitzwater, S. E., Knauer, G. A., Martin, J. H., 1982. Metal contamination and its effect on primary production measurements. *Limnology and Oceanography* 27, 544-551.
- Foltz G., R., Grodsky, S., A., Carton, J., A., McPhaden, M., J., 2003. Seasonal mixed layer heat budget of the tropical Atlantic Ocean. *Journal of Geophysical Research* 108, 3146. doi:10.1029/2002JC001584.
- Ganachaud, A., 2003. Large-scale mass transport, water mass formation, and diffusivities estimated from World Ocean Circulation Experiment (WOCE) hydrographic data. *Journal of Geophysical Research* 108, L3213, doi:10.1029/2002JC001565.
- Garzoli, S. L., Garrafo, Z., 1989. Transports, frontal motions and eddies at the Brazil-Malvinas currents confluence. *Deep Sea Research* 36, 681-703.
- Giarolla E, Nobre P, Malagutti M and Pezzi LP. 2005. The Atlantic Equatorial Undercurrent: PIRATA observations and simulations with GFDL Modular Ocean Model at CPTEC. *Geophysical Research Letters* 32, L10617. doi:10.1029/2004GL022206.
- GODAE High Resolution Sea Surface Temperature Pilot Project - GHR SST-PP, 2007. <http://www.ghrsst-pp.org/>, on line dataset, 04 June 2007.
- Goes, M., Molinari, R., Silveira, I., Wainer, I., 2005. Retroreflections of the North Brazil Current during February 2002. *Deep Sea Research I* 52, 647-667.
- Goni, G. J., Baringer, M. O., 2002. Surface currents in the tropical Atlantic across high density XBT line AX08. *Geophysical Research Letters* 29, 2218. Doi:10.1029/2002GL015873.
- Gordon, A. L., 1986. Interocean exchange of thermocline water. *Journal of*

- Geophysical Research* 91, 5013-5046.
- Gordon, A. L., Greengrove, C. L., 1986. Geostrophic circulation of the Brazil-Falklands confluence. *Deep Sea Research I* 33, 573-585.
- Gould, R. W., 1987. The deep chlorophyll maximum in the world ocean: a review. *The Biologist* 66(1-4), 4-13.
- Grodsky, S. A., Carton, J. A., 2003. The intertropical convergence zone in the South Atlantic and the equatorial cold tongue. *Journal of Climate* 16, 723-733.
- Haidvogel, D. B., Arango, H. G., Hedström, K., Beckmann, A., Malanotte-Rizzoli, P., Shchepetkin, A. F., 2000. Model evaluation experiments in the North Atlantic basin: simulations in nonlinear terrain-following coordinates. *Dynamics Atmosphere and Oceans* 32, 239-281.
- Harper, S., 2000. Thermocline ventilation and pathways of tropical-subtropical water mass exchange. *Tellus* 52A, 330-345.
- Harrison, D. E., 1989. On climatological monthly mean wind stress and wind stress curl fields over the world ocean. *Journal of Climate* 2, 57-70.
- Hayes, S. P., L. J. Mangum, J. Picaut, A. Sumi, Takeuchi, K., 1991. TOGA-TAO: A moored array for real-time measurements in the tropical Pacific Ocean. *Bulletin of the American Meteorological Society* 72, 339-347.
- Huang, B., Carton, J. A., Shukla, J., 1995. A numerical simulation of the variability in the tropical Atlantic Ocean, 1980-88. *Journal of Physical Oceanography* 25, 835-854.
- Hugget, J. P., Freón, P., Mullon, C., Penven, P., 2003. Modelling the transport success of anchovy *Engraulis encrasicolus* eggs and larvae in the southern Benguela: The effect of spatio-temporal spawning patterns. *Marine Ecology Progress Series* 250, 247-262.
- Ikeda, Y., STEVENSON, M., 1978. Time series analysis of NOAA-4 sea surface temperature (SST) data TOGA-TAO: A moored array for real-time measurements in the tropical Pacific Ocean. *Remote Sensing of Environment* 7, 349-362.
- Jochum, M., Malanotte-Rizzoli, P., Busalacchi, A., 2004. Tropical instability waves in the Atlantic ocean. *Ocean Modelling* 7, 145-163.
- Jolliffe, I. T, 2002. Principal component analysis. Springer. New York.

- Kayano, M. T., Rao, V. B., Andreoli, R. V., 2005. A review of short-term climate variability mechanisms. *Advances in Space Research* 35, 843–851.
- Koné, V., Machu, E., Penven, P., Andersen, V., Garçon, V., Fréon, P., Demarcq, H., 2005. Modeling the primary and secondary productions of the southern Benguela upwelling system: A comparative study through two biogeochemical models. *Global Biogeochemical Cycles* 19, GB4021. doi:10.1029/2004GB002427.
- Large, W. G., McWilliams, J. C. & Doney, S. C., 1994. Oceanic vertical mixing: a review and a model with a nonlocal boundary layer parametrization. *Reviews in Geophysics* 32, 363-403.
- Lazar, A., Vintzileos, A., Doblas-Reyes, F., Rogel, P. & Delécluse, P., 2005. Seasonal forecast of tropical climate with coupled ocean-atmosphere GCMs: On the respective role of the atmosphere and the ocean model components in the drifting mean climate. *Tellus* 57, 387-397.
- Lee, S.,K. and Csanady, G.,T., 1999a. Warm water formation and escape in the upper tropical Atlantic Ocean: 1. A literature review. *Journal of Geophysical Research* 104, 29561-29571.
- Lee, S.,K. and Csanady, G.,T., 1999b. Warm water formation and escape in the upper tropical Atlantic Ocean: 2. A numerical model study. *Journal of Geophysical Research* 104, 29573-29590.
- Lemos, C. F., Calbete, N. O., 1996. Sistemas que atuaram no Brasil de 1987 a 1995. *Climanálise Especial*, Edição comemorativa de 10 anos. MCT/INPE-CPTEC.
- Letelier, R. M., Dore, J. E., Winn, C. D., Karl, D. M., 1996. Seasonal and interannual variations in photosynthetic carbon assimilation at Station ALOHA. *Deep-Sea Research II* 43, 467-490.
- Lett, C., Verley, P., Mullon, C., Parada, C., Brochier, T., Penven, P., Blanke, B., 2008. A Lagrangian tool for modelling ichthyoplankton dynamics. *Environmental Modelling & Software* 23, 1210-1214.
- Liu, W. T., 2002. Progress in scatterometer applications. *Journal of Oceanography* 58, 121-136.
- Lumpkin, R., Speer, K., 2003. Large-scale vertical and horizontal circulation

- in the North Atlantic ocean. *Journal of Physical Oceanography* 33, 1902-1920.
- Lumpkin, R., Garzoli, S. L., 2005. Near-surface circulation in the tropical Atlantic Ocean. *Deep Sea Research* 52, 495–518.
- Lutjeharms, J. R. E., Penven, P., Roy, C., 2003. Modelling the shear edge eddies of the southern Agulhas Current. *Continental Shelf Research* 23, 1099-1115.
- Malanotte-Rizzoli, P., Hedström, K., Arango, H. G., Haidvogel, D. B., 2000. Water mass pathways between the subtropical and tropical ocean in a climatological simulation of the North Atlantic. *Dynamics of Atmosphere and Oceans* 32, 331-371.
- Malone, T. C., Pike, S. E., Conley, D. J., 1993. Transient variations in phytoplankton productivity at the JGOFS Bermuda time series station. *Deep-Sea Res. I*, 40, 903-924
- Marañón, E., Holligan, P. M.; Varela, M., 2000. Basin-scale variability of phytoplankton biomass, production and growth in the Atlantic Ocean. *Deep-Sea Res. I*, v. 47, p. 825-857.
- Marchesiello, P., McWilliams, J. C., Shchepetkin, A., 2001. Open boundary conditions for long-term integration of regional oceanic models. *Ocean Modelling* 3, 1-20.
- Marchesiello, P., McWilliams, J. C. & Shchepetkin, A., 2003. Equilibrium structure and dynamics of the California Current System. *Journal of Physical Oceanography* 33, 753-783.
- Marchesiello, P., Lefevre, J., Penven, P., Lemarie, F., Debreu, L., Douillet, P., Vega, A., Derex, P., Echevin, V., Dewitte, B., 2008. Keys to affordable regional marine forecast systems. *La lettre trimestrielle Mercator Ocean* 30, 38-48.
- McCready, P., and Geyer, G.,R., 2001. Estuarine salt flux through an isohaline surface. *Journal of Geophysical Research* 106, 11629-11637.
- Meacham, S. P., 2000. Low-frequency variability in the wind-driven circulation. *Journal of Physical Oceanography* 30, 269-293.
- Messié, M., Radenac, M-H., 2006. Seasonal variability of the surface chlorophyll in the western tropical Pacific from SeaWiFS data. *Deep-Sea*

- Research I* 53, 1581-1600.
- Miller, J.R., 1976. The salinity effect on a mixed layer ocean model. *Journal of Physical Oceanography* 6, 29-35.
- Miranda, L. B., Castro, B. M., 1981. Geostrophic flow conditions of the Brazil Current at 19°S. *Ciência Interamericana* 22, 44-48.
- Miyama, T., McCreary Jr., J. P., Sengupta, D., Senan, R., 2006. Dynamics of biweekly oscillations in the equatorial Indian Ocean. *Journal of Physical Oceanography* 36, 827-846.
- Molinari, R., L., 1982. Observations of eastward currents in the tropical South Atlantic Ocean: 1978-1980. *Journal of Geophysical Research* 87, 9707-9714.
- Montes, M., J., F., 2003. Fatores que influenciam na produtividade dos oceanos: A importância do fluxo de difusão dos nutrientes para a biomassa do fitoplâncton na região oceânica do Nordeste brasileiro. PhD Thesis Universidade Federal de Pernambuco, Recife, Brazil, 198 p..
- Moore, J. K., Doney, S. C., Kleypas, J. A., Glover, D. M., Fung, I. Y., 2002. An intermediate complexity marine ecosystem model for the global domain. *Deep-Sea Research II* 49, 403-462.
- Moura, A., Shukla, J., 1981. On the dynamics of droughts in Northeast Brazil : Observations, theory, and numerical experiments with a general circulation model. *Journal of Atmospheric Science* 38, 2653-2675.
- Müller, T. J., Ikeda, Y., Zangenberg, N., Nonato, L. V., 1998. Direct measurements of the western boundary currents between 20°S-28°S. *Journal of Geophysical Research* 103, 529-543.
- Mullon, C., Cury, P. & Penven, P. ,2002. Evolutionary individual-based model for the recruitment of anchovy (*Engraulis capensis*) in the southern Benguela. *Canadian Journal of Fisheries and Aquatic Sciences* 59, 910-922.
- Murtugudde, R., Seager, R. & Busulacchi, A.,1996. Simulation of the tropical oceans with an ocean GCM coupled to an atmospheric mixed-layer model. *Journal of Climate*, 9:1795-1815.
- Nobre, P., Campos, E., Polito, P., S., Sato, O.,T., and Lorenzzetti, J. (with contribution by Robertson, I., Vianna, M., Servain, J., and Wainer, I.).

- 2004: PIRATA Western Extension Scientific Rational Report, INPE/CPTEC Special Report, Cachoeira Paulista, SP, Brazil.
- Nobre, P., Campos, E., Polito, P. S., Sato, O. T., Lorenzzetti, J. A., 2005. Brazilian proposal for a PIRATA-SW Extension. Scientific Rationale. 44 pp.
- Nobre, P., Campos, E., Servain, J. and Araujo, M., 2008. The PIRATA South-West Extension: Scientific motivation, Realization and Perspectives (in preparation).
- OGCM-ECCO - Estimating the Circulation and Climate of the Ocean, 2007. <http://ecco.jpl.nasa.gov/>, on line dataset, 12 September 2007.
- Ohlmann, J.C., Siegel, D.A., Gautier, C., 1996. Ocean mixed layer depth heating and solar penetration: A global analysis. *Journal of Climate* 9, 2265-2280.
- Olson, D. B., Podesta, G. P., Evans, R. H., Brown, O. B., 1988. Temporal variations in the separation of Brazil and Malvinas currents. *Deep Sea Research I* 35, 1971-1990.
- O'Reilly, J., E., Maritorena, S., Mitchell, B., G., Siegel, D., A., Carder, K, L., Garver, S., A., Kahru, M., McClain, C., 1998. Ocean color chlorophyll algorithms for SeaWiFS. *Journal of Geophysical Research*, 103(C11), 24937-24953.
- Penven, P., Roy, C., Colin de Verdière, A., Largier, J., 2000. Simulation and quantification of a coastal jet retention process using a barotropic model. *Oceanological Acta* 23, 615-634.
- Penven, P., Roy, C., Lutjeharms, J. R. E., Colin de Verdière, A., Johnson, A., Shillington, F., Fréon, P., Brundrit, G., 2001a. A regional hydrodynamic model of the Southern Benguala. *South African Journal of Science* 97, 472-476.
- Penven, P., Lutjeharms, J. R. E., Marchesiello, P., Roy, C., Weeks, S. J., 2001b. Generation of cyclonic eddies by the Agulhas Current in the lee of the Agulhas Bank. *Geophysical Research Letters* 27, 1055-1058.
- Penven, P., Debreu, L., Marchesiello, P., McWilliams, J. C., 2006. Application of the ROMS embedding procedure for the Central California Upwelling System. *Ocean Modelling* 12, 157-187.

- Penven P., Marchesiello P., Debreu L., Lefevre J., 2008. Software tools for pre- and post-processing of oceanic regional simulations. *Environmental Modelling and Software* 23(5), 660-662.
- Peterson R. G., Stramma, L., 1991. Upper-level circulation in the South Atlantic ocean. *Progress in Oceanography* 26, 1-73.
- Polito, P. S., Cornillon, P., 1997. Long baroclinic Rossby waves detected by TOPEX/POSEIDON, *Journal of Geophysical Research* 102, 3215–3235.
- Proehl, J., 1996. Linear instability of equatorial zonal flows. *Journal of Physical Oceanography* 26, 601–621
- Rao, V. B., de Lima, M. C., Franchito, S. H., 1993. Seasonal and inter-annual variations of rainfall over eastern Northeast Brazil. *Journal of Climate* 6, 1754-1763.
- Richardson, P., L., and McKee, T., K., 1984. Average Seasonal Variation of the Atlantic Equatorial Currents from Historical Ship Drifts. *Journal of Physical Oceanography* 14, 1226-1238.
- Rodrigues, R. R., Rothstein, L. M., Wimbush, M., 2007. Seasonal variability of the South Equatorial Current bifurcation in the Atlantic ocean: A numerical study. *Journal of Physical Oceanography* 37, 16-37.
- Schmid, C., Schafer, H., Podesta, G., Zenk, W., 1995. The Vitoria eddy and its relation to the Brazil Current. *Journal of Physical Oceanography* 25, 2532-2546.
- Schott, F. A., Stramma, L., Fischer, J., 1995. The warm water inflow into the western tropical Atlantic boundary regime, spring 1994, *Journal of Geophysical Research* 100, 24745–24760.
- Schott, F. A., Fischer, J., Stramma, L., 1998. Transports and pathways of the upper-layer circulation in the western tropical Atlantic. *Journal of Physical Oceanography* 28, 1904-1928.
- Schott, F. A., Brandt, P., Hamann, M., Fischer, J., Stramma, L., 2002. On the boundary flow off Brazil at 5-10oS and its connection to the interior tropical Atlantic. *Journal of Geophysical Research* 29. doi: 10.1029/2002GL014786.
- Schott, F., A., Dengler, M., Brandt, P., Affler, K., Fischer, J., Bourlès, B., Gouriou, Y., Molinari, R., L., and Rhein, M., 2003. The zonal currents

- and transports at 35°W in the tropical Atlantic. *Geophysical Research Letters* 30, 1349. doi:10.1029/2002GL016849
- Schott, F. A., Dengler, M., Zantropp, R., Stramma, L., Fischer, J., Brandt, P., 2005. The shallow and deep western boundary circulation of the South Atlantic at 50 – 110 S. *Journal of Physical Oceanography* 35, 2031–2053.
- Schuchmann, K., 2006. Intraseasonal variability in the southwestern and central tropical Atlantic ocean. PhD Thesis *Christian-Albrechts-Universität, Kiel, Germany*, 148 p..
- Servain J., Busalacchi, A., Moura, A., McPhaden, A., Reverdin, G., Vianna, M., Zebiak, S., 1998. A Pilot Research Moored Array in the Tropical Atlantic (PIRATA). *Bulletin of the American Meteorological Society* 79, 2019-2031.
- Shchepetkin, A. F., McWilliams, J. C., 1998. Quasi-monotone advection schemes based on explicit locally adaptive dissipation. *Monthly Weather Review* 126, 1541-1580.
- Shchepetkin, A. F., McWilliams, J. C., 2005, The regional oceanic modeling system (ROMS): a split-explicit, free-surface, topography-following-coordinate oceanic model, *Ocean Modelling* 9, 347-404.
- She, J., Klinck, J. M., 2000. Flow near submarine canyons driven by constant wind. *Journal of Geophysical Research* 105, 28671-28694.
- Silveira, I. C. A., Miranda, L. B., Brown, W. S., 1994. On the origins of the North Brazil Current. *Journal of Geophysical Research* 99, 22501-22512.
- Smith, W. H. F., Sandwell, D. T., 1997. Global seafloor topography from satellite altimetry and ship depth soundings. *Science* 277, 1957-1962.
- Spall, M.A., 1991. A diagnostic study of wind- and buoyancy- driven north Atlantic circulation. *Journal of Geophysical Research* 96, 18509-18518.
- Sprintall, J., Tomczak, M., 1990. Salinity considerations in the oceanic surface mixed layer. Ocean Sciences Institute Rep. 36, University of Sidney, 170 pp.
- Sprintall, J., Tomczak, M., 1992. Evidences of the barrier layer in the surface layer of the tropics. *Journal of Geophysical Research* 97, 7305-7316.
- Steeman-Nielsen, E., Jensen, E. A., 1957. Primary oceanic production, the autotrophic production of organic matter in the oceans. *Galathea Report*

- 1, 49-136.
- Stramma, L., Peterson, R. G., 1990. The South Atlantic Current. *Journal of Physical Oceanography* 20, 846–859.
- Stramma, L., 1991. Geostrophic transport of the South Equatorial Current in the Atlantic. *Journal of Marine Research* 49, 281-284.
- Stramma, L., Fischer, J. and Reppin, J., 1995. The North Brazil Undercurrent. *Deep Sea Research I* 42, 773-395.
- Stramma, L., England, M., 1999. On the water masses and mean circulation of the South Atlantic Ocean. *Journal of Geophysical Research* 104, 20863–20883.
- Stramma, L., Schott, F., 1999. The mean flow field of the tropical Atlantic Ocean. *Deep Sea Research* 46B, 279–303.
- Stramma, L., Fischer, J., Brandt, P., Schott, F., 2003. Circulation, variability and near-equatorial meridional flow in the central tropical Atlantic. In: *Interhemispheric Water Exchanges in the Atlantic Ocean*, G. J. Goni and P. Malanotte-Rizzoli, editors, Elsevier. B.V., pp 1-22.
- Stramma, L., Rhein, M., Brandt, P., Dengler, M., Böning, C., Walter, M., 2005. Upper ocean circulation in the western tropical Atlantic in boreal fall 2000. *Deep Sea Research* 52, 221–240.
- Talley, L. D., 2003. Shallow, intermediate, and deep overturning components of the global heat budget. *Journal of Physical Oceanography* 33, 530-560.
- Thomas, W. H., 1970. On nitrogen deficiency in tropical Pacific Ocean phytoplankton: photosynthetic parameters in rich and poor waters. *Limnology and Oceanography* 15, 380-385.
- Tsai, W. T., Spencer, M., Wu, C., Winn, C., Kellogg, K., 2000. SeaWinds on QuikSCAT: sensor description and mission overview. *Geoscience and Remote Sensing ;symposium, 2000. Proceedings. IGARSS 2000. IEEE 2000 International, vol.3, no., pp. 1021-1023 vol. 3, 2000.*
- Veleda, D. R. A., 2008. Seasonal and intraseasonal variability of the western boundary regime off the Eastern Brazilian Coast. PhD Thesis Universidade Federal de Pernambuco, Recife, Brazil, 198 p..
- Vintzileos, A., Delécluse, P. & Sadourny, R., 1999a. On the mechanisms in a tropical ocean-global atmosphere coupled general circulation model. Part

- I: Mean state and the seasonal cycle. *Climate Dynamics*, 15, 43–62.
- Vintzileos, A., Delécluse, P., Sadourny, R., 1999b. On the mechanisms in a tropical ocean-global atmosphere coupled general circulation model. Part II: Inter-annual variability and its relation to the seasonal cycle. *Climate Dynamics*, 15, 63–80.
- Weisberg, R., H., 1985. Equatorial Atlantic velocity and temperature observations: February–November 1981. *Journal of Physical Oceanography* 15, 533–543.
- Wienders, N., Arhan, M., Mercier, H., 2000. Circulation at the western boundary of the south and equatorial Atlantic. *Journal of Marine Research* 58, 1007–1039.
- Woodruff, S., Diaz, H. F., Elms, J. D., Workey, S. J., 1998. COADS release 2 data and metadata enhancements for improvements of Marine Surface Flux Fields. *Physics and Chemistry of the Earth* 23, 517–526.
- Zhang, H. M., Bates, J. J., Reynolds, R. W., 2006. Assessment of composite global sampling: sea surface wind speed. *Geophysical Research Letters* 33, L17714: 1–5.